METHOD OF CALCULATING RETROREFLECTOR-ARRAY TRANSFER FUNCTIONS

DAVID A. ARNOLD

(NASA-CR-157932) METHOD OF CALCULATING RETROREFLECTOR-ARRAY TRANSFER FUNCTIONS (Smithsonian Astrophysical Observatory) 166 p HC A08/MF A01 CSCL 20F
N79-24821
Unclas
G3/74 22091

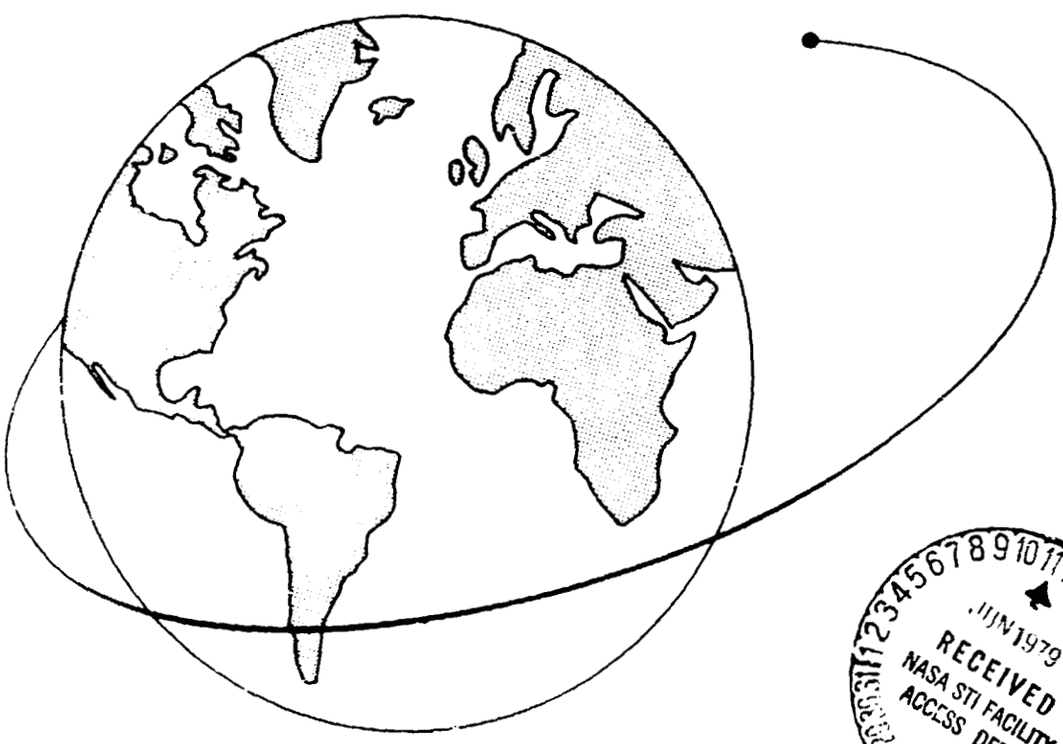

JUN 1979
RECEIVED
NASA STI FACILITY
ACCESS DEPT.

Smithsonian Astrophysical Observatory
SPECIAL REPORT 382

METHOD OF CALCULATING RETROREFLECTOR-ARRAY TRANSFER FUNCTIONS

David A. Arnold

TABLE OF CONTENTS

		Page
	ABSTRACT	vii
1	INTRODUCTION	1
2	BASIC RETROREFLECTOR PROPERTIES	3
	2.1 Retroreflection	3
	2.2 Angle of Incidence on Back Faces	3
	2.3 Symmetry of Incident and Reflected Rays	4
	2.4 Equal Path Length for All Rays	4
	2.5 Range Correction for Optical Path Length	6
	2.6 Input and Output Apertures	9
	2.7 Tube Analogy	12
	2.8 Masking and Recession	13
	2.9 Multiple Apertures	15
	2.10 Multiple Retroreflection	16
	2.11 Dihedral-Angle Offsets	18
	2.11.1 Effect of refraction on beam divergence	23
	2.11.2 Beam spread at normal incidence	24
	2.11.3 Phase gradients due to dihedral-angle offsets	25
	2.12 Six Sectors	26
3	ACTIVE REFLECTING AREA	29
	3.1 Circular Retroreflector	29
	3.2 Triangular Retroreflector	32
	3.3 Hexagonal Retroreflector	40
	3.4 Cutoff Angles for Total Internal Reflection	50
4	POLARIZATION	57
	4.1 Transmission across a Dielectric Boundary	58
	4.2 Reflection from a Dielectric Boundary	60
	4.2.1 Ordinary reflection	60
	4.2.2 Total internal reflection	61

TABLE OF CONTENTS (Cont.)

Page

4.3 Reflection from a Metal Surface 62

4.3.1 Perfect metal 62

4.3.2 Real metal 62

4.4 Polarization State of Each Sector 63

5 DIFFRACTION. 69

5.1 Diffraction Integral. 69

5.1.1 Fraunhofer diffraction. 70

5.1.2 Modified Fraunhofer formulas 72

5.2 Calculation of Diffraction Patterns from an Array of Phases 73

5.3 Diffraction Integral for a Trapezoid. 75

5.3.1 Factorization of the diffraction integral 80

5.3.2 Reverse order of integration 83

5.4 Diffraction Integral for an Arbitrary Shape 84

5.5 Diffraction Pattern of a Cube Corner 87

5.5.1 Diffraction pattern of triangular and hexagonal retro-reflectors 88

5.5.1.1 Vertices of the active reflecting area for a triangular retroreflector 89

5.5.1.2 Vertices of the active reflecting area for a hexagonal retroreflector 95

5.5.1.3 Vertices of a sector 101

5.5.1.4 Intersection of two line segments 102

5.5.1.5 Integration limits for a sector 105

5.5.2 Diffraction pattern of a circular reflector. 105

5.5.2.1 Airy pattern 106

5.5.2.2 Ellipse geometry 107

5.5.2.3 Intersection of a line and an ellipse 110

5.5.2.4 Slope of an ellipse. 111

5.5.2.5 Order of integration over y and z variables. . 112

5.5.2.6 Numerical and analytical parts of integration 113

5.5.2.7 Second-order numerical integration. 114

5.6 Symmetry of Cube-Corner Diffraction Patterns 114

TABLE OF CONTENTS (Cont.)

Page

6 RAYLEIGH DISTRIBUTION 117

6.1 Factors Modifying the Rayleigh Distribution 118

6.2 Guidelines for the Application of the Rayleigh Distribution. 118

7 ARRAY TRANSFER FUNCTION 119

7.1 Retroreflector-Array Coordinate System 119

7.2 Coordinate System of the Incident Beam and the Observer. 121

7.3 Coordinate System for the Diffraction Pattern of Cube Corners . . 121

7.4 Conversion between the Coordinate Systems of the Incident Beam and the Retroreflector. 122

7.5 Transmitted Pulse 127

7.6 Position of the Retroreflector along the Line of Sight 128

7.7 Incoherent Return. 129

7.8 Coherent Return. 132

7.8.1 Calculation shortcuts 136

7.8.2 Relation of coherence to diffraction. 137

7.8.3 Coherent variations 138

7.8.4 Mean value of coherent quantities 139

7.8.5 Coherent variations versus pulse length. 141

7.9 Half-Maximum Range Correction 141

7.10 Pulse Spreading by Array versus Pulse Length 142

7.11 Range Equation and Gain Function. 145

7.12 Velocity Aberration 148

7.13 Variation of the Transfer Function within the Diffraction Pattern . 149

8 RETROREFLECTOR-POSITION CALCULATIONS 151

8.1 Calculation of Retroreflector Positions and Orientations 151

8.2 Orientation with Respect to a New Pole 154

8.3 Condensing Large Arrays for Coherent Calculations. 156

8.4 Shadowing 157

8.4.1 Geos 157

8.4.2 Peole 158

9 ACKNOWLEDGMENTS 161

10 REFERENCES 163

ABSTRACT

This report presents methods for computing the properties of the reflection from a cube-corner array when it is illuminated by a laser pulse. Such information is useful in the design of satellite retroreflector arrays and ground tracking equipment as well as in the analysis of the data obtained. The methods derived include the effects of coherent interference, diffraction, polarization, and dihedral-angle offsets. Considerable space is devoted to deriving expressions for the diffraction pattern and active reflecting area of various types of retroreflectors.

METHOD OF CALCULATING RETROREFLECTOR-ARRAY TRANSFER FUNCTIONS

David A. Arnold

1. INTRODUCTION

The work described in this report was begun as part of the Lageos study program (formerly called Cannonball) supported by grant NGR 09-015-164 from the National Aeronautics and Space Administration (NASA). The laser ranging accuracies proposed for the Lageos satellite required the development of a transfer function to relate the observed return pulses to the center of mass of the satellite. Preliminary transfer-function analyses done for the Lageos retroreflector array are presented in Weiffenbach (1973). The development of the techniques and computer programs has been continued under NASA grants NGR 09-015-196 and NGR 09-015-002. Transfer functions computed for most of the retroreflector-equipped satellites now in orbit have been published (Arnold, 1972, 1974, 1975a,b, 1978). This report documents the techniques and equations used in calculating the transfer functions presented in those references. Transfer-function analyses have also been done for some of the retroreflector satellites at Goddard Space Flight Center (Felsentreger, 1972; Fitzmaurice, 1977; Minott, 1972, 1974a,b; 1976, 1978; Plotkin, 1964; Regardie, 1976). Since the optical properties of the cube corners are of primary importance, a large part of this report is devoted to reviewing the basic properties of cube corners, deriving analytical expressions for the active reflecting area of various cube-corner designs, and developing methods for computing the diffraction pattern of these retroreflectors. The diffraction calculation for a circular reflector employs numerical integration over one of the variables in the surface integral.

This work was supported in part by grants NGR 09-015-164, NGR 09-015-196, and NGR 09-015-002 from the National Aeronautics and Space Administration.

Expressions for the incoherent and coherent returns from an array are presented. The phases of the reflections from individual cube corners are chosen by use of a pseudo random-number generator. Statistics on the variation of the properties of the return pulse due to coherent interference are derived by computing many coherent returns.

The last section outlines the method of computing the position and orientation of each cube corner in an array in which design data are used.

2. BASIC RETROREFLECTOR PROPERTIES

2.1 Retroreflection

A retroreflector consists of three mutually perpendicular reflecting surfaces. Let the reflecting surfaces be the xy, yz, and zx planes (Figure 1). A light ray incident on one of the surfaces, such as the xy plane, has the component of the velocity vector normal to that plane, the z component, reversed. After reflection from the three surfaces, all components of the velocity vector are reversed and the ray has been retroreflected.

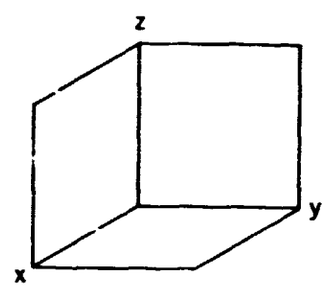

Figure 1. Basic retroreflector.

2.2 Angle of Incidence on Back Faces

Each of the three orthogonal reflecting surfaces in a cube corner reverses the component of the light's velocity vector normal to that surface. Since the magnitude of the velocity vector is not changed by any of the reflections, it follows that the angle of incidence of the beam with a particular face must be a constant independent of the order in which the reflections occur. Therefore, the angle of incidence on a given face is equal to the angle the incident beam makes with each face. This property is particularly useful when determining the cutoff angles for total internal reflection in uncoated cube corners.

2.3 Symmetry of Incident and Reflected Rays

The vertex of a retroreflector is halfway between the lines defined by the incident and the reflected rays. In a two-dimensional retroreflector (Figure 2), $\overline{OC}$ is constructed through the vertex parallel to the incident ray $\overline{AB}$ and the reflected ray $\overline{DE}$. By the law of reflection, $\alpha_1 = \alpha_2$ and $\beta_1 = \beta_2$, and by construction, $\alpha_1 = \alpha_3$ and $\beta_1 = \beta_3$. Therefore, $\overline{BC} = \overline{OC}$ and $\overline{OC} = \overline{CD}$ because the triangles are isosceles. Since $\overline{BC} = \overline{CD}$, the line $\overline{OC}$ is halfway between the incident and the reflected rays. The same diagram is equally valid in three dimensions since the third reflection reverses the component of the velocity perpendicular to the paper and does not alter the angle of the lines in this perspective. The above proof is the same for any pair of axes; thus, the line $\overline{OC}$ must be in the same plane as $\overline{AB}$ and $\overline{DE}$ and halfway between them.

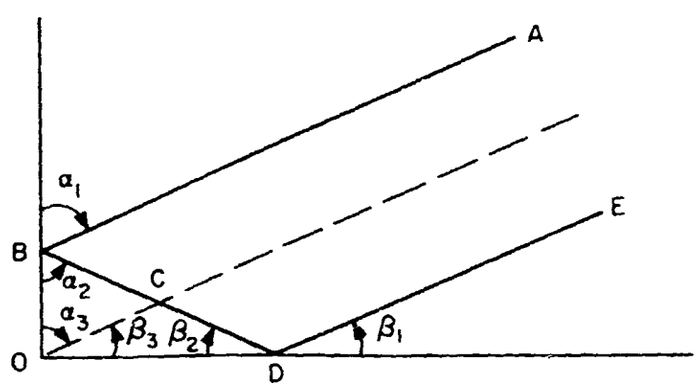

Figure 2. Two-dimensional retroreflector.

2.4 Equal Path Length for All Rays

The distance traveled by all rays is the same as the distance traveled by the ray that goes to the vertex. In Figure 3, $\overline{BG}$ is constructed parallel to $\overline{CE}$, so $\overline{CB} = \overline{DH} = \overline{EG}$. Also, $\overline{CD} = \overline{OD} = \overline{DE}$, as shown previously. Therefore, the path B–C–E–G is equal to the distance $\overline{HO} + \overline{OH}$.

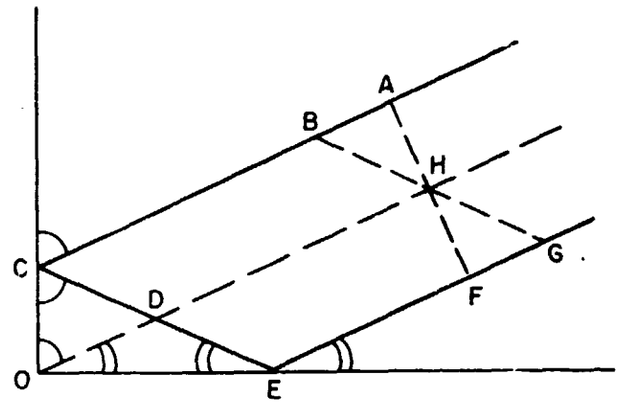

Figure 3. Path length for a two-dimensional retroreflector.

$\overline{AF}$ is constructed perpendicular to the incident and reflected rays and is a phase front. Since $\overline{AB} = \overline{FG}$, the path A–C–E–F equals B–C–E–G. The equalities above also hold for the horizontal and vertical components of all the line segments. Since this is true for any pair of axes, the three-dimensional distance traveled by all rays from the phase front is the same. This proof works for either a hollow reflector or a solid one whose face is perpendicular to the light beam.

If the reflector is made of a dielectric whose face is flat, the optical path length for all rays is also constant. In Figure 4, $\overline{BF} \perp \overline{OI}$ and $\overline{AG} \perp \overline{IH}$. As shown before, the path B–C–E–F equals the distance $\overline{JO} + \overline{OJ}$. Since $\overline{FG}$ is twice $\overline{JI}$, the path B–C–E–G equals $\overline{IO} + \overline{OI}$. Outside the dielectric, $\overline{AB}$ is twice $\overline{HI}$, so $\overline{AB} = \overline{HI} + \overline{IH}$. These relations hold for both the horizontal and the vertical components of the distances. Since a similar proof exists for any pair of axes, the three-dimensional optical path length for all rays is the same as the optical path length of the ray that travels to the vertex. If the front surface and the back reflecting faces are not optically flat, or if the angles between the reflecting faces are not exactly 90°, the optical path length will be different for different rays.

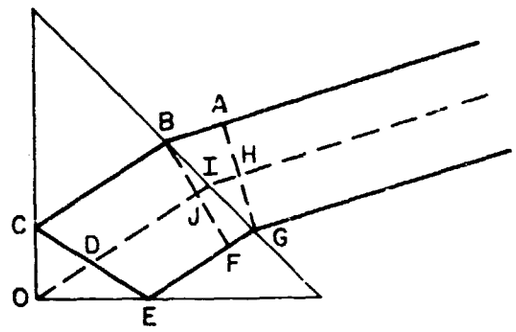

Figure 4. Solid two-dimensional retroreflector.

2.5 Range Correction for Optical Path Length

The range measured by timing a laser pulse reflected from a hollow cube corner is the range to the vertex of the reflector. If the retroreflector consists of a dielectric, such as fused quartz, then it is necessary to correct for the slower velocity of the light beam in the dielectric. The optical path length is n times the geometrical path length, where n is the index of refraction. If the length of the retroreflector from the vertex to the center of the front face is L, the optical path length in the cube corner at normal incidence is nL. The difference between the optical and the geometrical path length is $nL - L = L(n - 1)$. The range measured to a solid cube corner at normal incidence is greater than the range measured to a hollow cube corner by $L(n - 1)$. The range correction will vary with the incidence angle of the beam on the front face of the cube corner. It is a little simpler to calculate the correction from the center of the front face of the reflector than from the vertex.

The correction factor ΔR is the difference between the optical path length $n\overline{OB}$ and the distance $\overline{AC}$ (see Figure 5); that is,

$$\Delta R = n\overline{OB} - \overline{AC} \quad . \tag{2-1}$$

The length of the reflector is $L = \overline{OA}$. The incidence angle is i and the refracted angle is r. From Figure 5, we see that

$$\overline{OB} = \frac{L}{\cos r} \quad . \tag{2-2}$$

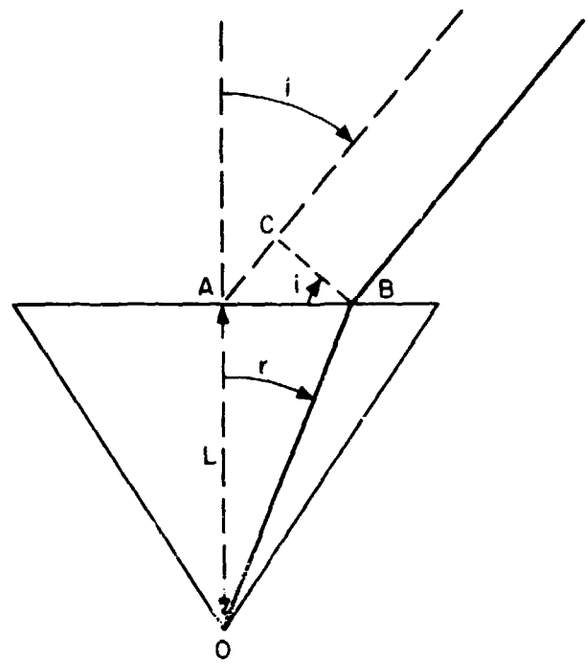

Figure 5. Optical path length in a retroreflector.

Using Snell's law,

$$\frac{\sin i}{\sin r} = n \quad ,$$

we get

$$\sin r = \frac{\sin i}{n} \quad ,$$

from which we can write

$$\cos r = \sqrt{1 - \sin^2 r}$$

$$= \sqrt{1 - \frac{\sin^2 i}{n^2}}$$

$$= \frac{1}{n} \sqrt{n^2 - \sin^2 i} \quad .$$

Substituting this into equation (2-2) yields

$$\overline{OB} = \frac{L}{\cos r}$$

$$= \frac{nL}{\sqrt{n^2 - \sin^2 i}} \quad . \tag{2-3}$$

From Figure 5,

$$\overline{AC} = \overline{AB} \sin i$$

$$= L \tan r \sin i$$

$$= L \frac{\sin r}{\cos r} \sin i$$

$$= \frac{L \sin i/n}{(1/n)\sqrt{n^2 - \sin^2 i}} \sin i$$

$$= \frac{L \sin^2 i}{\sqrt{n^2 - \sin^2 i}} \quad . \tag{2-4}$$

Substituting equations (2-3) and (2-4) into equation (2-1), we get

$$\Delta R = n\overline{OB} - \overline{AC}$$

$$= \frac{n^2 L}{\sqrt{n^2 - \sin^2 i}} - \frac{L \sin^2 i}{\sqrt{n^2 - \sin^2 i}}$$

$$= \frac{L}{\sqrt{n^2 - \sin^2 i}} (n^2 - \sin^2 i)$$

$$= L \sqrt{n^2 - \sin^2 i} \quad .$$

The correction with respect to the vertex can be expressed as follows:

$$\Delta R' = \Delta R - L \cos i$$

$$= L\sqrt{n^2 - \sin^2 i} - L \cos i$$

$$= L\left(\sqrt{n^2 - \sin^2 i} - \cos i\right) .$$

2.6 Input and Output Apertures

As shown in Section 2.3, the retroreflected ray leaves along a line on the opposite side of the vertex from the incident ray. Figure 6a shows the retroreflector from the direction of the incident beam; a ray incident at point A will be retroreflected from point B, which is an equal distance on the other side of the vertex O. Similarly, point C moves to point D. For any shaped retroreflector face, the shape of the retroreflected beam can be constructed by moving each point on the outline of the face an equal distance on the other side of the vertex. Figure 6b shows the result for a triangular retroreflector at normal incidence. The solid line, the shape of the retroreflector face, is called the input aperture, and the dotted line, giving the outline of the retroreflected beam, is the output aperture. The overlap of the two figures is the active reflecting area. Any ray that is incident outside the overlap region will not be retroreflected, since the symmetry of the incident and the reflected rays would require that the last reflection occur at a point outside the cube corner.

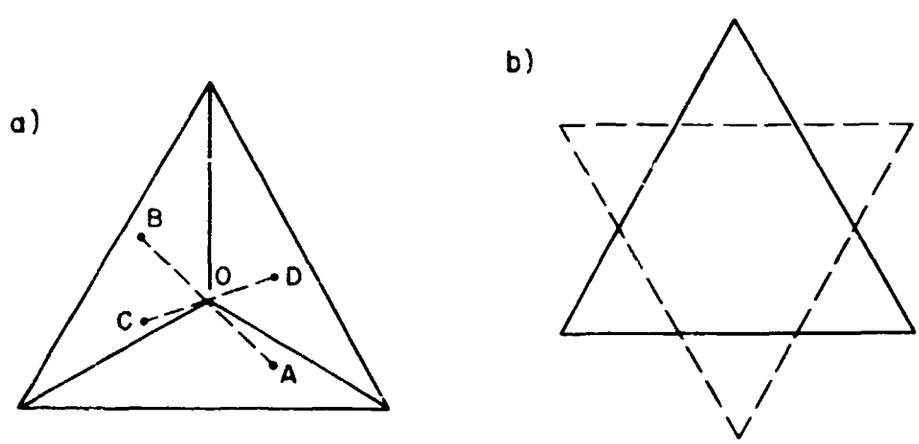

Figure 6. a) Method of constructing the output aperture; b) triangular input and output apertures.

When the incident beam is not at normal incidence, the vertex as viewed from the direction of the beam is not in the center of the aperture. When the output aperture is constructed, it is also off center, so the intersection of the two figures giving the active reflecting area is decreased. Figure 7 depicts this effect for a square aperture. At normal incidence, the apertures coincide, while at an oblique angle of

Figure 7. Displacement of the input and output apertures in the plane of the front face.

incidence, the centers of the input and the output apertures are separated by some distance $\overline{OO'}$. The separation of the apertures can be calculated from the incidence angle, as shown in Figure 8. The ray A incident on the center of the input aperture is retroreflected as ray A′. The distance D between the points of intersection of A and A′ with the front face is

$$D = 2L \tan \phi' \quad ,$$

where ϕ' is the angle between the rays and the symmetry axis of the cube corner. The separation is given in the plane of the front face of the retroreflector. As viewed from the angle ϕ', this distance is $D \cos \phi'$. If the cube corner consists of a solid dielectric, then the separation as viewed from the incidence angle ϕ is $D \cos \phi$. The angles ϕ and ϕ' are related by Snell's law,

$$\frac{\sin \phi}{\sin \phi'} = n \quad .$$

Similarily, the intersection of the input and output apertures as computed in the plane of the front face will be smaller by the factor $\cos \phi$ when viewed from the direction of the incident beam.

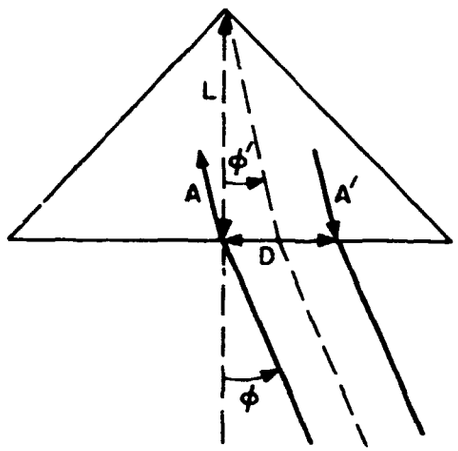

Figure 8. Separation of input and output apertures.

In general, the direction of the incident beam is given by the two angles θ and ϕ, where ϕ is measured from the normal to the front face and θ is the azimuth angle around the normal. The input and output apertures separate along the line given by the projection of the incident beam onto the front face (see Figure 9).

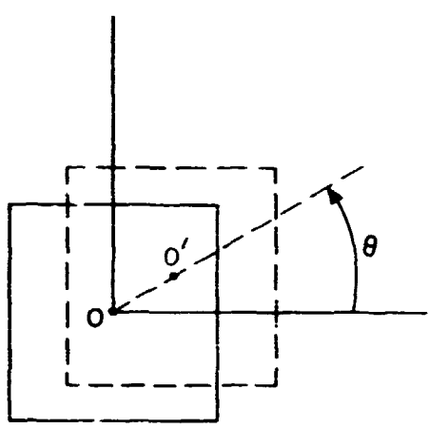

Figure 9. Direction of separation of the input and output apertures.

In summary, the active reflecting area for a retroreflector when illuminated by a beam whose direction is given by the angles θ and ϕ is the intersection of the input and output apertures in the plane of the front face multiplied by $\cos\phi$. The separation of the apertures is along the plane of incidence, the separation being $2L \tan\phi'$ in the plane of the front face.

2.7 Tube Analogy

Instead of thinking of both the input and the output apertures as being in the plane of the front face of the retroreflector, we can visualize the active reflecting area by considering the apertures as the openings at either end of a tube. In fact, when looking into a retroreflector, it appears as though the output aperture is an equal distance in back of the vertex from the input aperture. In this representation, the output aperture is constructed by taking each point on the input aperture and moving it an equal distance on the opposite side of the actual position of the vertex, as shown in Figure 10. This technique is similar to the model of cube-corner phenomena given in Eckhardt (1971).

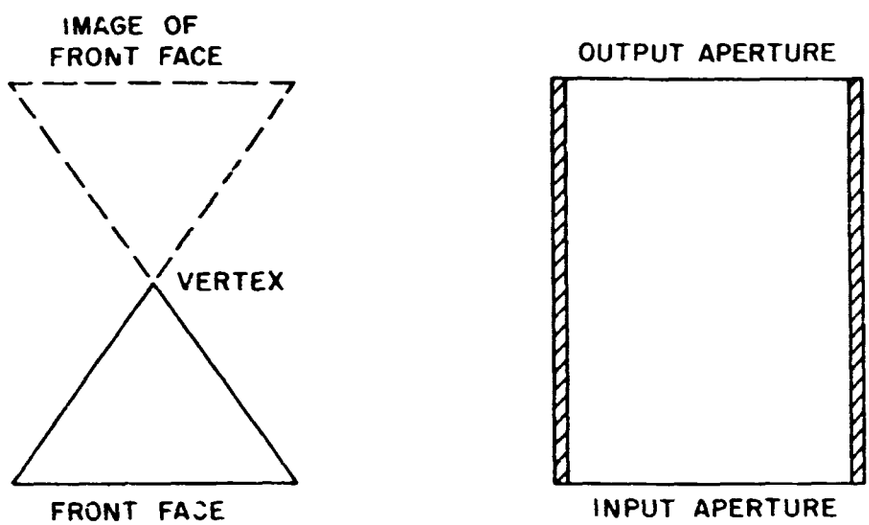

Figure 10. Tube analogy for input and output apertures.

The space seen by looking through the tube from various angles is the active reflecting area for that incidence angle. The analogy holds for a solid cube corner by filling the tube with a dielectric (Figure 11). The active reflecting area for a solid reflector is larger than that of a hollow one at off-normal incidence because the rays are bent into the cube corner.

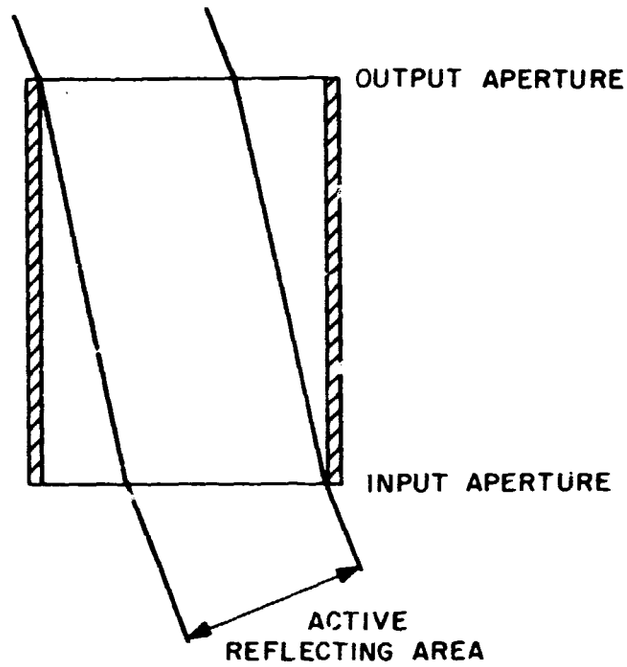

Figure 11. Solid-cube-corner tube analogy.

2.8 Masking and Recession

By means of a variety of techniques, the active reflecting area of a cube corner can be made to decrease more rapidly as the incidence angle departs from the normal to the front face. The tube analogy is perhaps the best way to visualize the effect of these techniques. If the cube corner is made narrower while keeping the length from vertex to face constant, the reflecting area is decreased directly at normal incidence and the cutoff angle (the angle beyond which there is no retroreflected signal) is smaller as measured from normal incidence. The same effect could be achieved by masking the front face by the same amount. Figure 12 shows both techniques.

If a hollow reflector is recessed in a cavity of the same shape as the face, the effect is the same as changing the width-to-length ratio, as was done in the two previous techniques. If a solid cube corner is recessed, the effect is somewhat more complicated. The wall of the container shadows the face of the reflector at an oblique incidence angle. Since refraction occurs at the dielectric boundary, the displacement

D of the input and output apertures is the sum of two terms. As shown in Figure 13, D is given by

$$D = 2(R \tan \phi + L \tan \phi') \quad ,$$

where R is the amount of recession, and ϕ and ϕ' are the angles of the beam before and after refraction, respectively.

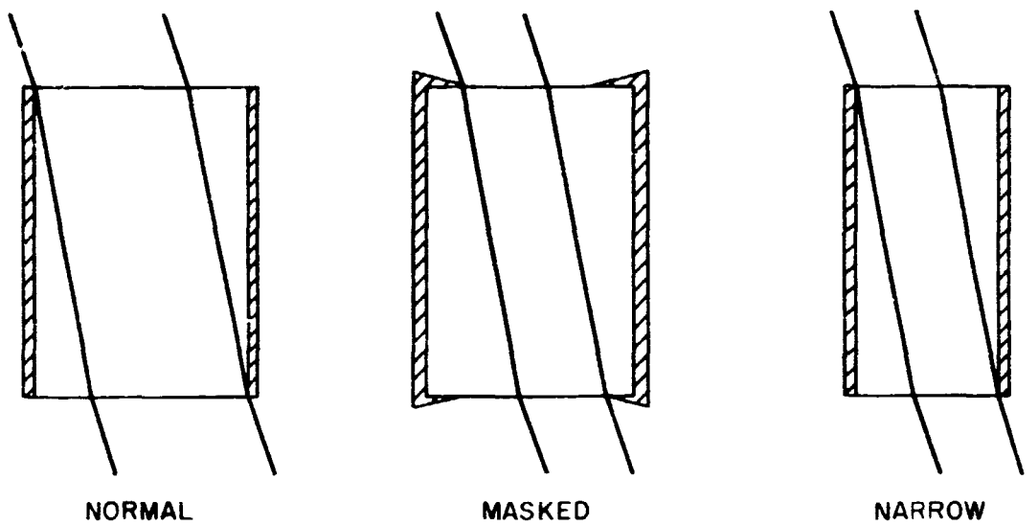

Figure 12. Effect of reducing the width-to-length ratio.

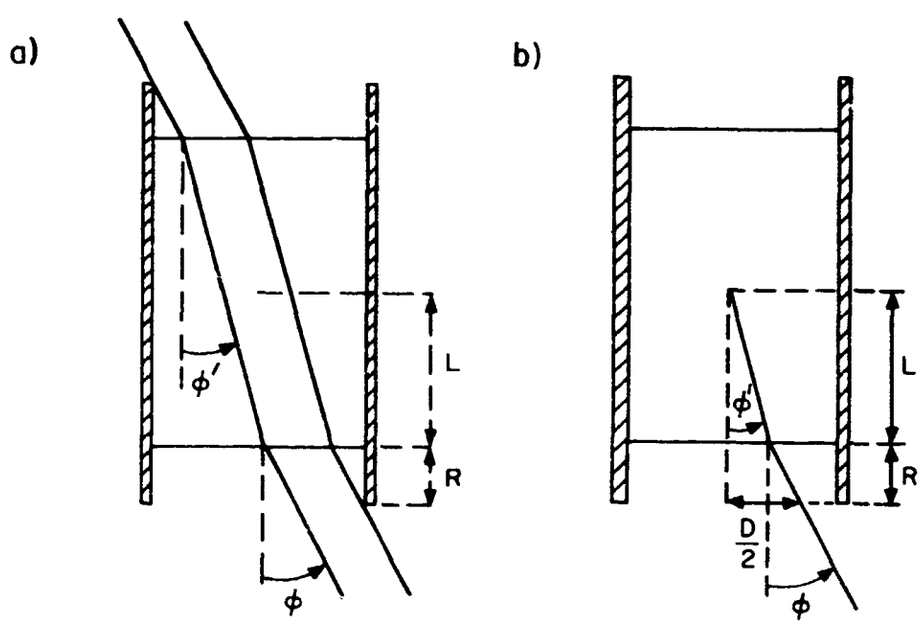

Figure 13. Recessed solid cube corner.

2.9 Multiple Apertures

The technique of masking can be used to produce pairs of apertures on a retroreflector. If half the aperture of a cube corner is covered (Figure 14), there will be

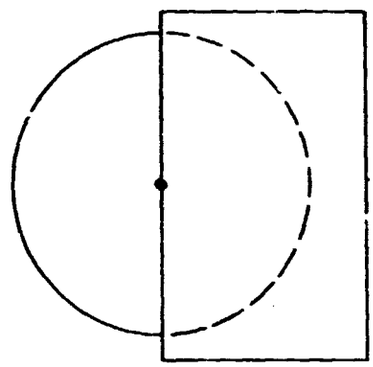

Figure 14. Half-covered retroreflector.

no effective reflecting area. Rays entering the open left half of the retroreflector must exit on the right side by the principle of the symmetry of the incident and reflected rays about the vertex. If holes are made in the mask on the right side of the aperture, rays entering the holes will exit from the open left half and those entering the left half exactly opposite the holes will exit from the holes. Thus, pairs of apertures can be produced, as shown in Figure 15. Figure 15 has the mask covering slightly more than half the aperture, in order that a line will not be opened up in the center if the cube corner is slightly misaligned. The problem of alignment is also the reason for not having matching holes in a mask that covers the entire aperture. Corresponding apertures would not be exactly opposite each other except at normal incidence.

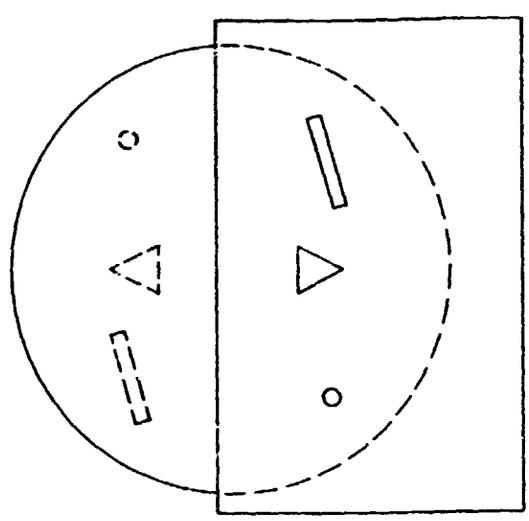

Figure 15. Pairs of apertures.

2.10 Multiple Retroreflection

In a solid cube corner, a partial reflection occurs at the front face both as the light enters the cube corner and as it leaves. The light reflected on entrance is not in the retroreflection direction except at normal incidence. The light reflected back into the cube corner as the beam is leaving can give rise to multiply retroreflected beams. The contribution of these multiple retroreflections is negligible, largely because the reflection coefficient is small. Except at normal incidence, the active reflecting area decreases for each successive reflection, and only every other beam leaving the cube corner is in the correct direction.

At normal incidence, the [illegible]ction coefficient is

$$R = \left(\frac{n-1}{n+1}\right)^2 .$$

For n = 1.46, [illegible] = 0.035. The path of multiply retroreflected rays according to the tube analogy is drawn in Figure 16.

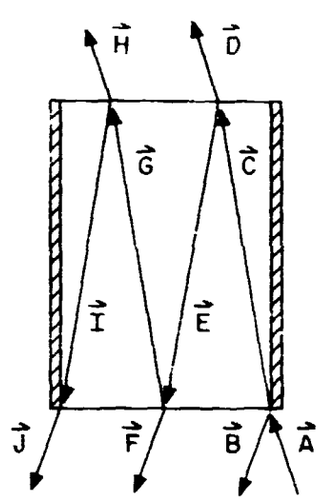

Figure 16. Multiple retroreflection.

Figure 17 shows the widths and positions of the various input and output apertures and active reflecting areas for a square cube corner.

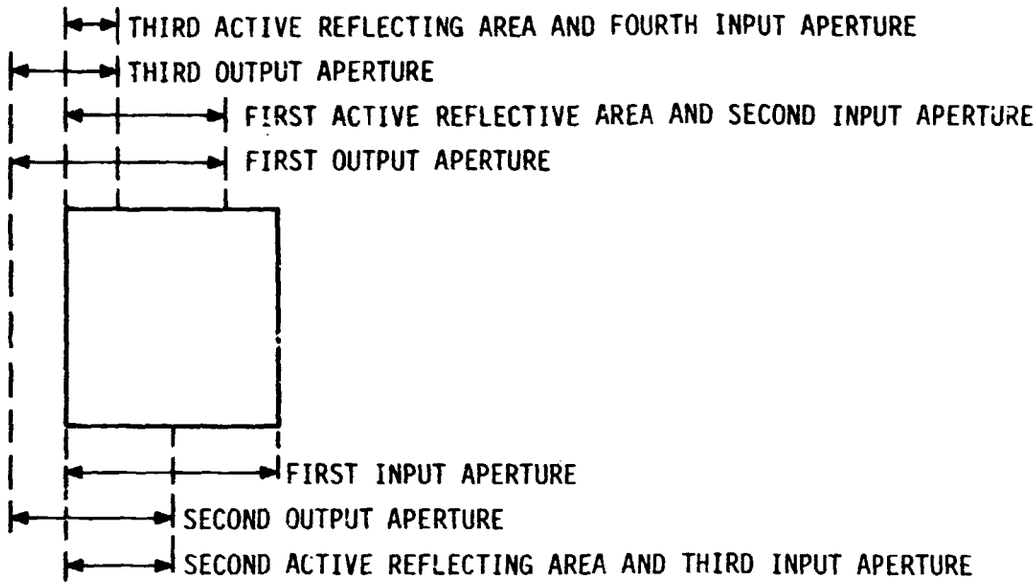

Figure 17. Widths of successive apertures for multiple retroreflection.

Let T be the transmission coefficient given by 1 - R and let Wo be the intensity of the incident beam $\vec{A}$. Table 1 gives the width of each beam for a square retroreflector with sides of unit length and incidence angle such that $2L \cos \phi = 0.25$. The intensities of each beam are calculated for R = 0.035 and T = 0.965.

Table 1. Intensity and width of successive reflections within a cube corner.

Beam	Width	Intensity	
		Analytical	Numerical
$\vec{A}$	Indefinite	Wo	Wo
$\vec{B}$	1	RWo	0.035Wo
$\vec{C}$	1	TWo	0.965Wo
$\vec{D}$	0.75	T^2Wo	0.931Wo
$\vec{E}$	0.75	RTWo	0.0338Wo
$\vec{F}$	0.50	RT^2Wo	0.0326Wo
$\vec{G}$	0.50	R^2TWo	0.00118Wo
$\vec{H}$	0.25	R^2T^2Wo	0.00114Wo
$\vec{I}$	0.25	R^3TWo	0.00004Wo
$\vec{J}$	0.00	R^3T^2Wo	0.00004Wo

In the above case, only beams $\vec{D}$ and $\vec{H}$ are in the retroreflection direction, and the intensity of each successive retroreflected beam is decreased by $R^2 = 0.001225$. The separation of the input and output apertures increases by $4L \tan \phi'$ between each successive retroreflection. The cutoff angle occurs when the width of the front face is less than $2L \tan \phi'$ for the first retroreflection and when it is less than $6L \tan \phi'$ for the second.

2.11 Dihedral-Angle Offsets

In a perfect retroreflector, the angle between any pair of reflecting faces is exactly 90° and the reflected beam is exactly antiparallel to the incident beam. If the dihedral angles differ from 90° by a small amount, the reflected beam will be split into two, four, or six beams, depending on whether one, two, or three dihedral angles are changed. Each spot corresponds to a particular order of reflection. There are $3! = 6$ possible orders of reflection. The orientation of each face is given by the unit normals $\hat{n}_1$, $\hat{n}_2$, and $\hat{n}_3$ to each face. The reflection from each face reverses that component of the light's velocity vector that is normal to the face. Let $\vec{V}$ and $\vec{V}'$ be the directions of a ray before and after reflection, respectively, with the vector $\vec{V}'$ given by

$$\vec{V}' = \vec{V} - 2(\vec{V} \cdot \hat{n})\hat{n} \quad ,$$

where $\hat{n}$ is the normal to the face. Application of the above formula three times yields the direction of the reflected beam for a particular order of reflection. Formulas for the direction of the reflected rays after the three reflections are given in Yoder (1958), Chandler (1960), and Rityn (1967). Chandler's formula is

$$\vec{t} = \vec{q} + 2\vec{q} \times (\alpha\vec{a} - \beta\vec{b} + \gamma\vec{c}) \quad , \tag{2-5}$$

where $\vec{t}$ is the final direction; $\vec{q}$ is the original direction; α, β, and γ are the small angles by which the angles between the three mirrors exceed right angles; and $\vec{a}$, $\vec{b}$, and $\vec{c}$ are the normals to the three mirrors taken in order in a right-hand sense. Equation (2-5) is valid to first order when the mirrors are nearly mutually perpendicular. The angle α is the angle between the faces whose normals are $\vec{b}$ and $\vec{c}$, etc.

The normals may be strictly perpendicular; that is, they do not need to include the small deviations caused by the dihedral-angle offsets.

In the transfer functions given in Weiffenbach (1973) and Arnold (1972, 1974, 1975a, b), the directions of the reflected rays were computed by applying the law of reflection three times. The small deviations in the normals must be included to use this technique.

The unit normals to the faces can be computed as follows (see Figure 18). Let the normals to the faces without dihedral-angle offsets be the unit vectors $\hat{i}$, $\hat{j}$, and $\hat{k}$ along the three coordinate axes x, y, and z, respectively. If the angle between the xz plane and the yz plane is $(\pi/2) + \delta$, this can be expressed by

$$\hat{n}_1 = \hat{i} + \frac{\delta}{2}\hat{j} \quad ,$$

$$\hat{n}_2 = \hat{j} + \frac{\delta}{2}\hat{i} \quad ,$$

$$\hat{n}_3 = \hat{k} \quad .$$

For small angles δ, the above expressions are quite adequate. Offsets in the other two dihedral angles can be similarly represented. The normals should be divided by their absolute magnitudes to ensure that they are strictly unit vectors.

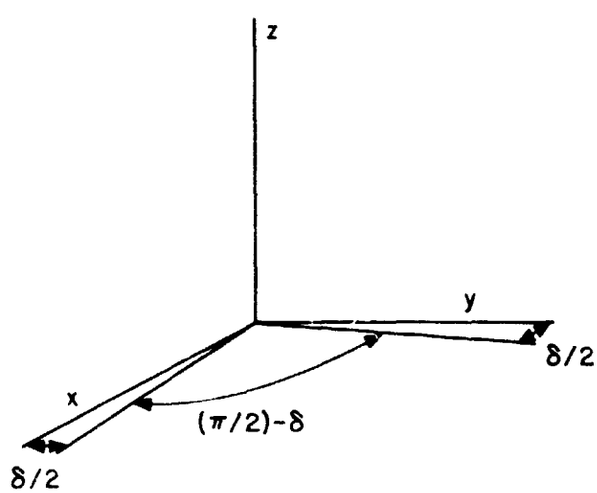

Figure 18. Normals to the reflecting faces with dihedral-angle offsets.

It is desirable to have the unit normals given in the coordinate system of the symmetry axis of the corner cube since the incidence angle of the laser beam is given with respect to this axis. The symmetry axis is in the direction of the vector $x = y = z = 1$, as shown in Figure 19, and is given by the angles θ_A and λ_A. From

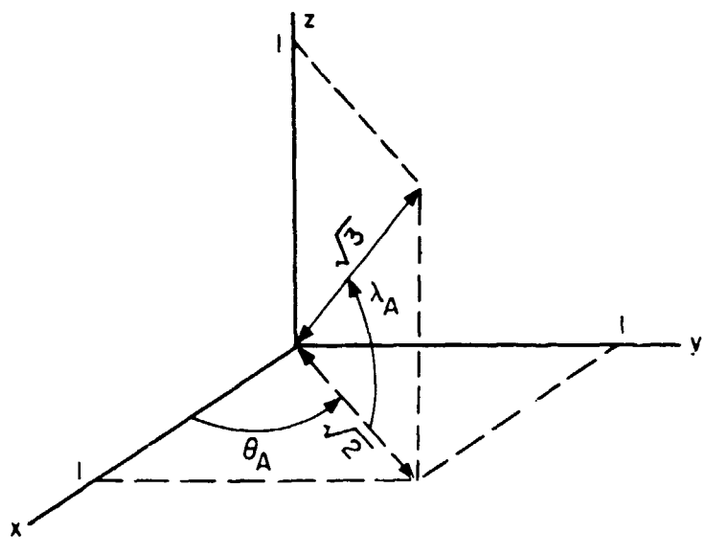

Figure 19. Direction of symmetry axis.

Figure 19, we see that

$$\cos \theta_A = 1/\sqrt{2} \quad ,$$

$$\sin \theta_A = 1/\sqrt{2} \quad ,$$

$$\cos \lambda_A = \sqrt{2}/\sqrt{3} \quad ,$$

$$\sin \lambda_A = 1/\sqrt{3} \quad .$$

The normals in the xyz coordinate system can be given in the coordinate system of the symmetry axis by rotating the original coordinate system about the z axis by θ_A and about the y axis by $-\lambda_A$. This brings the x axis along the axis of the cube. In matrix form, the total rotation is given by

$$\begin{pmatrix} x' \\ y' \\ z' \end{pmatrix} = \begin{pmatrix} \cos\lambda_A & 0 & \sin\lambda_A \\ 0 & 1 & 0 \\ -\sin\lambda_A & 0 & \cos\lambda_A \end{pmatrix} \begin{pmatrix} \cos\theta_A & \sin\theta_A & 0 \\ -\sin\theta_A & \cos\theta_A & 0 \\ 0 & 0 & 1 \end{pmatrix} \begin{pmatrix} x \\ y \\ z \end{pmatrix} \quad .$$

Substituting the values of the sines and cosines and multiplying the matrices, we get

$$x' = \frac{1}{\sqrt{3}} (x + y + z) \quad ,$$

$$y' = \frac{1}{\sqrt{2}} (y - x) \quad ,$$

$$z' = \frac{1}{\sqrt{6}} (2z - x - y) \quad .$$

In Figure 20, the unprimed axes represent the original coordinate system, and the primed axes are the rotated coordinates.

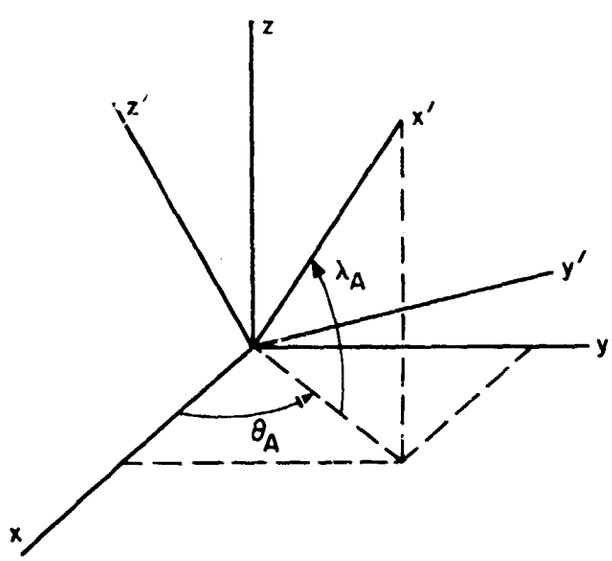

Figure 20. Relationship of x, y, z and x', y', z' coordinate axes.

The incident laser beam after refraction at the front face is in a direction given by the angles θ' and ϕ' in the primed coordinate system (see Figure 21).

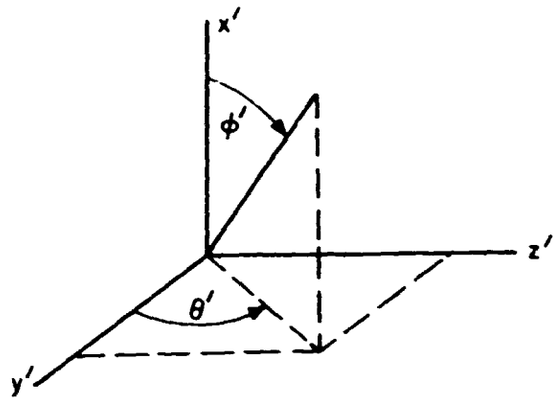

Figure 21. Direction of incident beam after refraction.

A second rotation of the coordinate system must be performed to get the normals to the faces in the coordinate system of the laser beam. By rotating the coordinate system about the x′ axis by θ′ and then about the new z′ axis by ϕ′, we get

$$\begin{pmatrix} x'' \\ y'' \\ z'' \end{pmatrix} = \begin{pmatrix} \cos\phi' & \sin\phi' & 0 \\ -\sin\phi' & \cos\phi' & 0 \\ 0 & 0 & 1 \end{pmatrix} \begin{pmatrix} 1 & 0 & 0 \\ 0 & \cos\theta' & \sin\theta' \\ 0 & -\sin\theta' & \cos\theta' \end{pmatrix} \begin{pmatrix} x' \\ y' \\ z' \end{pmatrix} .$$

The relationship of the primed and double-primed coordinate axes is given in Figure 22. The x′ axis is the symmetry axis of the reflector, the y′z′ plane is parallel to the front face, and the x″ axis is parallel to the beam after it enters the cube corner.

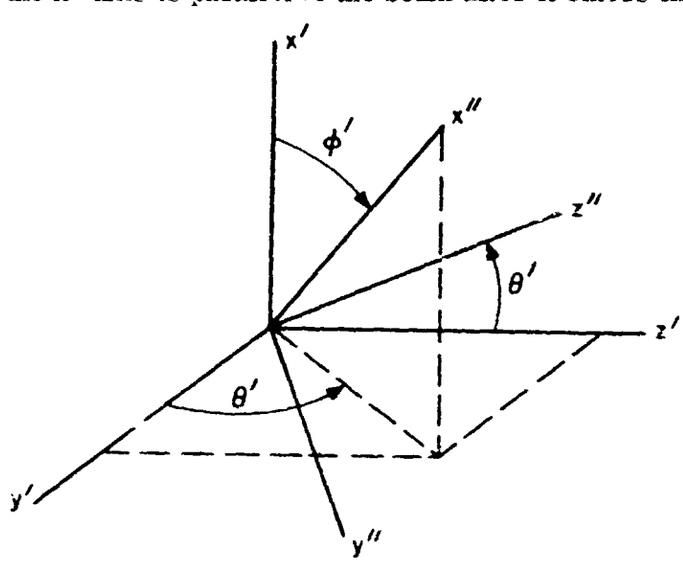

Figure 22. Relationship of x′, y′, z′ and x″, y″, z″ axes.

If the corner cube is hollow, the reflections can be done for all six possible sequences of reflections by taking the incident beam, given by the vector $x'' = -1$, $y'' = z'' = 0$, and reflecting it from each of the normals to the faces in the double-primed coordinate system. The y'' and z'' coordinates of the reflected beam give the deviations from the incident direction. The effect on these deviations due to refraction when the rays exit from a solid cube corner is discussed below.

2.11.1 Effect of refraction on beam divergence

Let the incident beam on the cube corner be in the direction (θ, ϕ) and let the direction of the beam after refraction be (θ', ϕ'), where

$$\theta' = \theta \quad ,$$

$$\sin \phi = n \sin \phi' \quad .$$

Owing to dihedral-angle offsets, the direction of the retroreflected beam before being refracted out of the cube corner is $(\theta' + d\theta', \phi' + d\phi')$ for a particular order of reflection. After refraction, the direction becomes $(\theta + d\theta, \phi + d\phi)$, where

$$\theta + d\theta = \theta' + d\theta' \quad ,$$

$$d\theta = d\theta' \quad ,$$

$$\sin (\phi + d\phi) = n \sin (\phi' + d\phi') \quad .$$

Since the arc distance between (θ', ϕ') and $(\theta' + d\theta', \phi')$ is $s' = \sin \phi' \, d\theta'$ and that between (θ, ϕ) and $(\theta + d\theta, \phi)$ is $s = d\theta \sin \phi$, the deviation of the ray perpendicular to the plane of incidence has been increased by the ratio s/s':

$$\frac{s}{s'} = \frac{d\theta \sin \phi}{d\theta' \sin \phi'} = \frac{\sin \phi}{\sin \phi'} = n \quad .$$

To obtain the change in the component of the deviation in the plane of incidence, we expand $\sin (\phi + d\phi)$ and $\sin (\phi' + d\phi')$, which yields

$$\sin(\phi + d\phi) = n \sin(\phi' + d\phi') \quad ,$$

$$\sin\phi \cos d\phi + \cos\phi \sin d\phi = n(\sin\phi' \cos d\phi' + \cos\phi' \sin d\phi') \quad .$$

Since $d\phi$ and $d\phi'$ are very small, we have approximately

$$\sin\phi + d\phi \cos\phi = n \sin\phi' + n\, d\phi' \cos\phi' \quad .$$

By using $\sin\phi = n \sin\phi'$, this reduces to

$$d\phi \cos\phi = n\, d\phi' \cos\phi' \quad .$$

Therefore, the component of the deviation parallel to the plane of incidence is increased by the ratio

$$\frac{d\phi}{d\phi'} = n \frac{\cos\phi'}{\cos\phi} \quad .$$

2.11.2 Beam spread at normal incidence

The beam spread at normal incidence when all dihedral angles are offset by an equal amount is given by the formula (Rityn, 1967)

$$\gamma = \frac{4}{3} \sqrt{6}\, n\delta \quad ,$$

where, following Rityn's notation, δ is the angle by which the dihedral angles exceed $90°$ and γ is the angle between the incident and the reflected rays. This formula is good to first order when the dihedral angles are nearly $90°$. If the deviation γ is large compared to the beam spread due to diffraction, the positions of the reflected spots in the far field can be accurately predicted. If γ is on the order of the spreading due to diffraction, the formula represents the deviation of the exiting phase fronts exactly, but the positions of the maxima in the far-field pattern are altered as a result of interference among the six reflected beams. In this case, a diffraction

calculation for the whole cube corner is necessary in order to predict the intensity distribution in the far field to a sufficient accuracy.

2.11.3 Phase gradients due to dihedral-angle offsets

Let the direction of the reflected beam from a cube corner for a particular sequence of reflections be given by the unit vector

$$\hat{v} = \begin{pmatrix} v_x \\ v_y \\ v_z \end{pmatrix} ,$$

where $-\hat{x}$ points toward the illuminating source. Since the dihedral-angle offsets are assumed to be small, we have

$$v_x \approx 1 ,$$
$$v_y \ll 1 ,$$
$$v_z \ll 1 .$$

The rates of change of phase across each sector in the y and z directions are

$$a = kv_y ,$$
$$b = kv_z ,$$

where

$$k = 2\pi/\lambda ,$$

λ being the wavelength.

Figure 23 shows a ray going to the vertex of a hollow cube corner. The two reflected rays correspond to different orders of reflection from the back surfaces,

which results from the incident ray being infinitesimally displaced from the vertex in different directions. Two factors are evident from the diagram, but they can be neglected because v_y and v_z are so small. First, the space between each ray and the incident ray is a dead spot containing no reflected radiation. Second, the phase fronts drawn perpendicular to the unit vectors, giving the directions of the reflected rays, do not intersect the incident ray at exactly the same point. In diffraction calculations, the phase difference due to dihedral-angle offsets will be taken as zero at the point where the phase fronts intersect the incident ray going to the vertex. These effects are insignificant in terms of their effect on the far-field pattern. A larger effect, which has also been neglected, is the reflecting area lost owing to the rounding of the back edges to prevent chipping in solid cube corners.

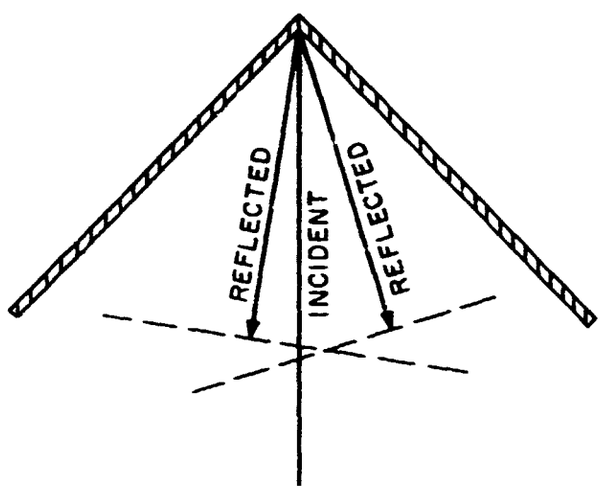

Figure 23. Relationship of phase fronts for different sectors.

2.12 Six Sectors

A ray retroreflected from a cube corner undergoes three successive reflections at the back faces. The order in which the reflections occur is determined by where the incident ray strikes the cube corner. Since the direction and polarization of the reflected ray may depend on the order of reflection, we must determine the regions corresponding to the six orders of reflection.

In Section 2.11, the normals to the reflecting surfaces were computed in the x", y", z" coordinate system. The x" axis is antiparallel to the incident beam after refraction into the cube corner, and the y" axis is in the plane of incidence. In Figure 24, the projections of the normals onto the y"z" plane are shown as two-dimensional vectors labeled 1 to 3. The dotted-line vectors 1′ to 3′ are antiparallel, respectively, to the first three. These six vectors form the angular boundaries of the six sectors of the cube corner as viewed from the direction of the incident beam inside the reflector. Let the reflecting faces be identified by their unit normals. The three-digit number in each sector gives the order of reflection for light emerging from that sector. The order of reflection is determined from the principle that the incident and reflected rays are symmetrical with respect to the vertex. For example, all rays leaving the sector between the 1 axis and the 3′ axis must have originated in the 1′–3 sector. The normal to the 1′–3 sector is the 1 axis, and that to the 1–3′ sector is the 3 axis. By a process of elimination, since the first reflection is from the 1 plane and the last from the 3 plane, the second is from the 2 plane. The order of reflection is therefore 123, as shown in the 1–3′ sector.

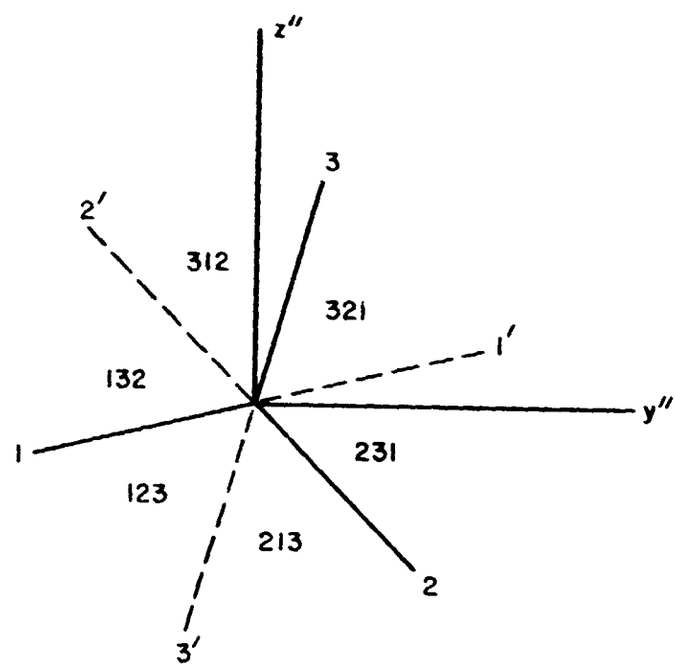

Figure 24. Order of reflection for each sector.

The angular boundaries of the six sectors will be modified by refraction of the rays at the front face. Let an x, y, z coordinate system be set up outside the reflector. The x axis is antiparallel to the incident beam outside the cube corner and collinear with the ray to the vertex. The z and z″ axes are parallel, and the y axis is in the plane of incidence. The boundary lines of the Ith sector outside the cube corner are given by the Ith vector in the yz plane, whose components are

$$y_I = y''_I \frac{\cos\phi}{\cos\phi'} \quad ,$$

$$z_I = z''_I \quad ,$$

where

$$\frac{\sin\phi}{\sin\phi'} = n \quad .$$

The slopes of the boundary lines when y_I is not zero are given by

$$S_I = \frac{z_I}{y_I} \quad ,$$

and the angles of the lines are

$$a_I = \tan^{-1}\frac{z_I}{y_I} \quad .$$

3. ACTIVE REFLECTING AREA

In this section, analytical expressions are derived for the active reflecting area of a retroreflector whose face is in the shape of a circle, triangle, or hexagon. For all cases, the separation of the input and output apertures in the plane of the front face is given by

$$D = 2L \tan \phi' \quad ,$$

where L is the length of the cube corner and ϕ' is the angle of refraction:

$$\phi' = \sin^{-1}\left(\frac{\sin \phi}{n}\right) \quad ,$$

in which n is the index of refraction and ϕ is the angle of incidence.

3.1 Circular Retroreflector

The active reflecting area of a coated circular retroreflector is independent of the azimuth angle of the incident beam and is a function only of the angle between the beam and the normal to the front face. The input and output apertures are circles in the plane of the front face.

Let the radius of the front face be r. The maximum possible value for r for a given L occurs when the circular face is tangent to each of the reflecting faces (and perpendicular to the symmetry axis of the cube corner). In Section 2.11, it was shown that the angle between the symmetry axis and each face is the angle whose tangent is $1/\sqrt{2}$. From Figure 25, we see that

$$\frac{r_{max}}{L} = \frac{1}{\sqrt{2}} \quad ,$$

or

$$r_{max} = \frac{L}{\sqrt{2}} \quad .$$

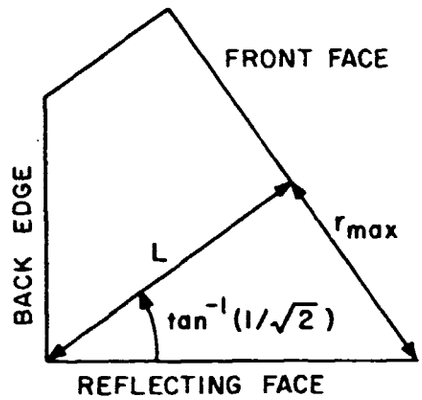

Figure 25. Ratio of cube-corner length to the radius of the front face.

The active reflecting area is cos ϕ times the intersection of two circles of radius r separated by the distance D. The intersection of the two circles is four times the shaded area shown in Figure 26. The angle θ is given by

$$\theta = \cos^{-1}\left(\frac{D/2}{r}\right) .$$

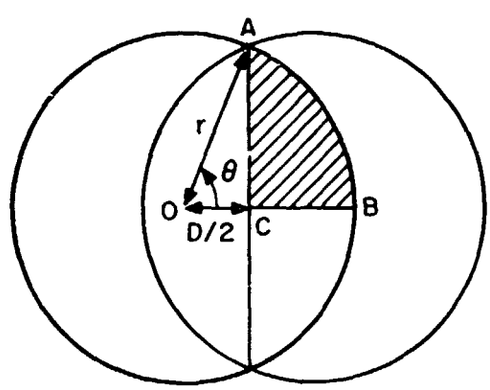

Figure 26. Active reflecting area for a circular retroreflector.

The area of the sector OAB is

$$(\pi r^2)\frac{\theta}{2\pi} = r^2\,\frac{\theta}{2} ,$$

and the area of the triangle OAC is

$$\frac{1}{2}\left(\frac{D}{2}\right)(r \sin \theta) = \frac{Dr \sin \theta}{4} \quad .$$

The active reflecting area is

$$4 \cos \phi \left(r^2 \frac{6}{2} - \frac{Dr \sin \theta}{4}\right) = (2r^2\theta - Dr \sin \theta) \cos \phi \quad ,$$

which is zero when

$$\frac{D}{2} \geq r \quad .$$

The cutoff angle ϕ_c is defined by

$$\frac{D_c}{2} = r \quad .$$

Substituting $D_c = 2L \tan \phi_c'$ into the above equation, we get

$$\frac{2L \tan \phi_c'}{2} = r \quad ,$$

$$\phi_c' = \tan^{-1} \frac{r}{L} \quad .$$

From Snell's law,

$$\phi_c = \sin^{-1} (n \sin \phi_c') \quad .$$

In summary, if $D/2 < r$, the active reflecting area of a circular retroreflector is

$$\text{area} = (2r^2\theta - Dr \sin \theta) \cos \phi = (2r^2\theta - 2r^2 \cos \theta \sin \theta) \cos \phi$$
$$= 2r^2(\theta - \cos \theta \sin \theta) \cos \phi$$

where

$$\theta = \cos^{-1} \frac{D}{2r} \quad .$$

If $D/2 \geq r$, the area is zero.

3.2 Triangular Retroreflector

The active reflecting area of a triangular retroreflector is independent of the azimuth as long as the intersection of the input and output apertures has six sides. A somewhat lengthy calculation is required to derive this simple result. When the overlap has four sides, there is an azimuth dependence, which is repeated every 120°. Only cases with θ between 0° and 60° need be considered, since the result for θ between 60° and 120° is the same as for 120° - θ. Let the radius of the inscribed circle in the front face be r. The maximum value of r is $L/\sqrt{2}$, which occurs when the circle is tangent to the reflecting faces. Let W be the width of the hexagonal active reflecting area at normal incidence (see Figure 27). The relationship of W and r is

$$W = 2r.$$

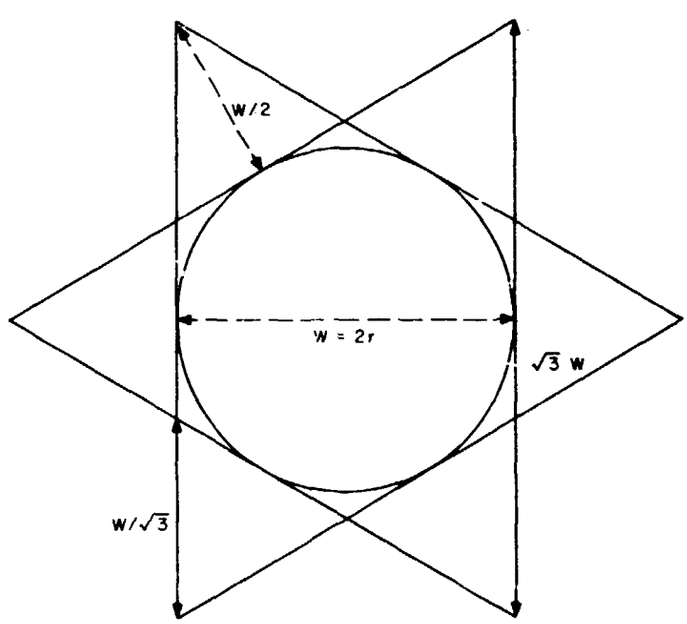

Figure 27. Triangular retroreflector at normal incidence.

The analysis is divided into two cases. In Case 1, which occurs at small values of D, the active reflecting area has six sides. Case 2 runs from the transition point to the cutoff of the cube corner, and the active area has four sides.

The following areas must be calculated in order to get the overlap of the input and output apertures in Case 1, as shown in Figure 28.

$$\text{area}_{I} = \frac{1}{2}\,\overline{hi}\;\overline{ai}$$

$$= \frac{1}{2}\,\frac{1}{2\sqrt{3}}\,(W - D\cos\theta + \sqrt{3}D\sin\theta)\,\frac{1}{2}\,(W - D\cos\theta + \sqrt{3}D\sin\theta)$$

$$= \frac{1}{8\sqrt{3}}\,(W - D\cos\theta + \sqrt{3}D\sin\theta)^2 \quad ,$$

$$\text{area}_{II} = \frac{1}{2}\,\overline{bj}\;\overline{bk}$$

$$= \frac{1}{2}\,(\sqrt{3}D\sin\theta)\;(D\sin\theta)$$

$$= \frac{\sqrt{3}}{2}\,D^2\sin^2\theta \quad ,$$

$$\text{area}_{III} = \overline{ab}\;(\overline{ae} - \overline{\ell e})$$

$$= (W - D\cos\theta)\left[\frac{1}{\sqrt{3}}\,(W + 2D\cos\theta) - D\sin\theta\right]$$

$$= \frac{1}{\sqrt{3}}\,(W - D\cos\theta)\;(W + 2D\cos\theta - \sqrt{3}D\sin\theta) \quad .$$

The overlap of the two aperatures is

$$\text{overlap} = 4\,\text{area}_{I} - 2\,\text{area}_{II} + \text{area}_{III}$$

$$= \frac{1}{2\sqrt{3}}\,(W - D\cos\theta + \sqrt{3}D\sin\theta)^2 - \sqrt{3}D^2\sin^2\theta$$

$$+ \frac{1}{\sqrt{3}}\,(W - D\cos\theta)\;(W + 2D\cos\theta - \sqrt{3}D\sin\theta) \quad . \qquad (3\text{-}1)$$

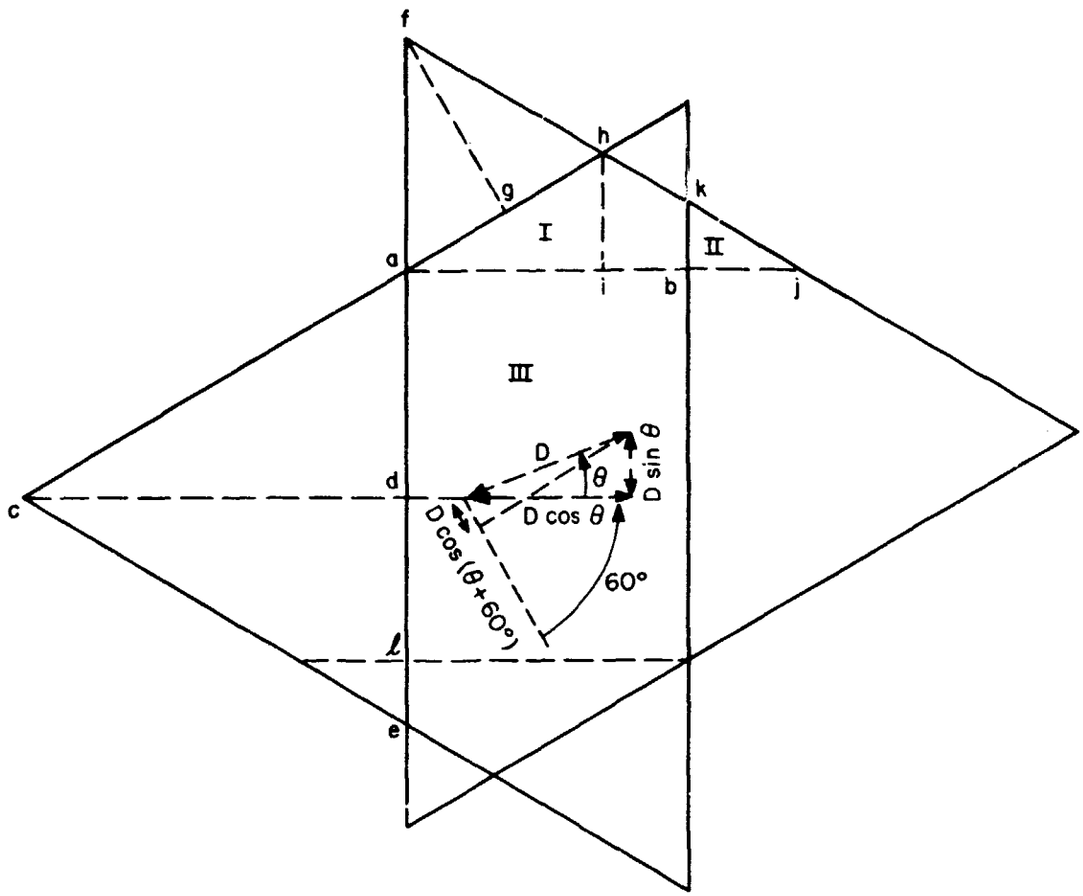

Figure 28. Triangular retroreflector, Case 1.

CALCULATION OF DISTANCES IN FIGURE 28

$\overline{ab}$ = the width of the hexagon minus the displacement of the apertures in the $\theta = 0°$ direction

$= W - D \cos \theta$

$\overline{cd}$ = the height of a star point plus the displacement of the apertures in the $\theta = 0°$ direction

$= \frac{W}{2} + D \cos \theta$

Figure 28 (Cont.)

$$\overline{ae} = \frac{2}{\sqrt{3}}\,\overline{cd} = \frac{2}{\sqrt{3}}\left(\frac{W}{2} + D\cos\theta\right)$$

$$= \frac{1}{\sqrt{3}}\,(W + 2D\cos\theta)$$

$\overline{fg}$ = the height of a star point minus the displacement of the apertures in the $\theta = -60°$ direction

$$= \frac{W}{2} - D\cos(60° + \theta)$$

$$= \frac{W}{2} - D(\cos 60°\cos\theta - \sin 60°\sin\theta)$$

$$= \frac{W}{2} - D\left(\frac{1}{2}\cos\theta - \frac{\sqrt{3}}{2}\sin\theta\right)$$

$$= \frac{1}{2}\,(W - D\cos\theta + \sqrt{3}D\sin\theta)$$

$$\overline{ah} = \frac{2}{\sqrt{3}}\,\overline{fg}$$

$$= \frac{1}{\sqrt{3}}\,(W - D\cos\theta + \sqrt{3}D\sin\theta)$$

$$\overline{hi} = \frac{1}{2}\,\overline{ah}$$

$$= \frac{1}{2\sqrt{3}}\,(W - D\cos\theta + \sqrt{3}D\sin\theta)$$

$$\overline{ai} = \frac{\sqrt{3}}{2}\,\overline{ah} = \overline{fg}$$

$$= \frac{1}{2}\,(W - D\cos\theta + \sqrt{3}D\sin\theta)$$

$$\overline{bj} = 2\overline{ai} - \overline{ab} = (W - D\cos\theta + \sqrt{3}D\sin\theta) - (W - D\cos\theta) = \sqrt{3}D\sin\theta$$

$$\overline{bk} = \frac{1}{\sqrt{3}}\,\overline{bj} = D\sin\theta$$

$$\overline{\ell e} = \overline{bk} = D\sin\theta$$

After evaluating equation (3-1) by use of an algebra computer program, we get the following result:

$$\text{overlap} = \frac{\sqrt{3}}{2}\,(W^2 - D^2) \quad .$$

The evaluation, though lengthy, is straightforward and involves nothing more complicated than recognizing the identity $-D^2 \cos^2\theta - D^2 \sin^2\theta = -D^2$.

The active reflecting area for Case 1, then, is

$$\frac{\sqrt{3}}{2}\,(W^2 - D^2)\cos\phi \quad . \tag{3-2}$$

The transition from six sides (Case 1) to four sides (Case 2) occurs when

$$\overline{bj} = \overline{ai} \quad ,$$

$$\sqrt{3}D \sin\theta = \frac{1}{2}\,(W - D\cos\theta + \sqrt{3}D\sin\theta) \quad ,$$

$$2\sqrt{3}D \sin\theta = W - D\cos\theta + \sqrt{3}D\sin\theta \quad ,$$

$$\sqrt{3}D \sin\theta = W - D\cos\theta \quad . \tag{3-3}$$

The two cases are thus defined by

Case 1: $\sqrt{3}D \sin\theta < W - D\cos\theta$,

Case 2: $\sqrt{3}D \sin\theta > W - D\cos\theta$.

The geometry of the active reflecting area for Case 2 is shown in Figure 29. The intersection of the apertures for Case 2 is

$$\overline{be} \times \overline{ab} = \frac{1}{\sqrt{3}}\,(W - D\cos\theta)\,(2W + D\cos\theta - \sqrt{3}D\sin\theta) \quad .$$

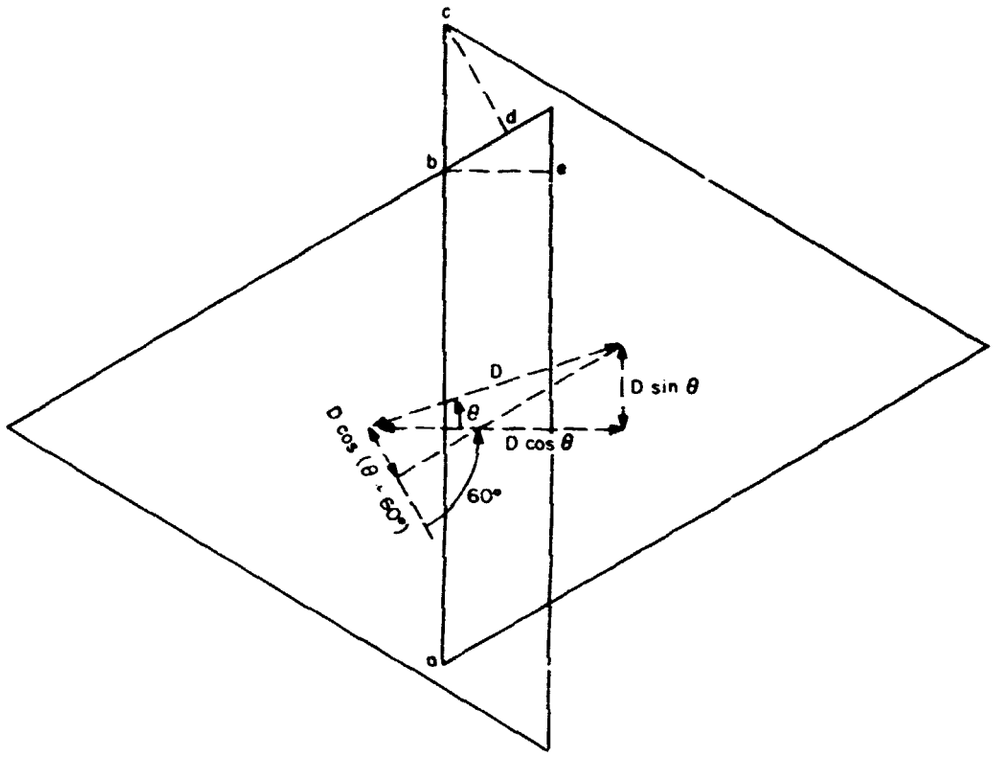

Figure 29. Triangular retroreflector, Case 2.

CALCULATION OF DISTANCES IN FIGURE 29

$$\overline{be} = W - D \cos \theta$$

$$\overline{cd} = \frac{W}{2} - D \cos (60° + \theta) = \overline{fg} \text{ (from Case 1)}$$

$$= \frac{1}{2} (W - D \cos \theta + \sqrt{3} D \sin \theta)$$

$$\overline{cb} = \frac{2}{\sqrt{3}} \overline{cd}$$

$$= \frac{1}{\sqrt{3}} (W - D \cos \theta + \sqrt{3} D \sin \theta)$$

$$\overline{ab} = \overline{ac} - \overline{cb}$$

$$= \sqrt{3} W - \frac{1}{\sqrt{3}} (W - D \cos \theta + \sqrt{3} D \sin \theta)$$

$$= \frac{2}{\sqrt{3}} W - \frac{1}{\sqrt{3}} (-D \cos \theta + \sqrt{3} D \sin \theta)$$

$$= \frac{1}{\sqrt{3}} (2W + D \cos \theta - \sqrt{3} D \sin \theta)$$

The active reflecting area is

$$\frac{\cos\phi}{\sqrt{3}}\,(W - D\cos\theta)\,(2W + D\cos\theta - \sqrt{3}D\sin\theta) \quad . \tag{3-4}$$

Cutoff occurs when

$$\overline{be} = W - D\cos\theta = 0 \quad , \tag{3-5}$$

and thus the active reflecting area is zero when

$$D\cos\theta > W \quad .$$

Since equation (3-2) for Case 1 is independent of θ, there are no special formulas for different azimuths. When $\theta = 0°$, the cutoff and transition points coincide, so the reflecting area is given for all ϕ by Case 1. The cutoff angle for $\theta = 0°$ is obtained by setting $\cos\theta = 1$ in equation (3-5), which gives

$$W - D = 0 \quad ,$$

$$W = D \quad .$$

Substituting $D = 2L\tan\phi_c'$, we have

$$2L\tan\phi_c' = W \quad ,$$

$$\phi_c'\,(\theta = 0°) = \tan^{-1}\left(\frac{W}{2L}\right) \quad .$$

The active reflecting area for Case 2 with $\theta = 60°$ is obtained by putting $\cos\theta = 1/2$ and $\sin\theta = \sqrt{3}/2$ in equation (3-4), giving

$$\frac{\cos\phi}{\sqrt{3}}\,(W - D\cos\theta)\,(2W + D\cos\theta - \sqrt{3}D\sin\theta)\Big|_{\theta=60^\circ}$$

$$= \frac{\cos\phi}{\sqrt{3}}\left(W - \frac{D}{2}\right)\left(2W + \frac{D}{2} - \frac{3}{2}D\right) = \frac{\cos\phi}{2\sqrt{3}}\,(2W - D)\,(2W - D)$$

$$= \frac{\cos\phi}{2\sqrt{3}}\,(2W - D)^2 \quad .$$

The transition for $\theta = 60°$ using equation (3-3) is

$$\sqrt{3}D\sin\theta\Big|_{\theta=60^\circ} = W - D\cos\theta\Big|_{\theta=60^\circ} \quad ,$$

$$\sqrt{3}D\,\frac{\sqrt{3}}{2} = W - \frac{D}{2} \quad ,$$

$$\frac{3}{2}D + \frac{D}{2} = W \quad ,$$

$$D = W/2 \quad ,$$

while cutoff for $\theta = 60°$ using equation (3-5) is defined by

$$W - D\cos\theta\Big|_{\theta=60^\circ} = 0 \quad ,$$

$$W - \frac{D}{2} = 0 \quad ,$$

$$D = 2W \quad .$$

Substituting $D = 2L\tan\phi_c'$, we get

$$2L\tan\phi_c' = 2W \quad ,$$

$$\phi_c'\,(\theta = 60^\circ) = \tan^{-1}\left(\frac{W}{L}\right) \quad .$$

This is the largest possible cutoff angle for any retroreflector design. If application of the formula

$$\phi_c = \sin^{-1} (n \sin \phi_c')$$

leads to imaginary values of ϕ_c, then $\phi_c = 90°$.

In summary, the active reflecting area of a triangular cube corner is given by the following formulas for the range $0° < \theta < 60°$. For $\sqrt{3}D \sin \theta < W - D \cos \theta$,

$$\text{area} = \frac{\sqrt{3}}{2} (W^2 - D^2) \cos \phi \quad ;$$

for $\sqrt{3}D \sin \theta > W - D \cos \theta > 0$,

$$\text{area} = \frac{\cos \phi}{\sqrt{3}} (W - D \cos \theta) (2W + D \cos \theta - \sqrt{3}D \sin \theta) \quad ;$$

and for $W - D \cos \theta < 0$,

$$\text{area} = 0 \quad .$$

The active area for other values of θ is obtained by using the following symmetry properties:

$$\text{area } (\theta) = \text{area } (\theta + N \times 120°) \quad ,$$

$$\text{area } (\theta) = \text{area } (-\theta) \quad ,$$

$$\text{area } (\theta) = \text{area } (120° - \theta) \quad ,$$

where N is an integer.

3.3 Hexagonal Retroreflector

The active reflecting area of a hexagonal retroreflector varies with the azimuth angle θ except at normal incidence. This variation repeats every 60°. Also, since all cases between 30° and 60° give the same answer as for $60° - \theta$, we need consider

only the cases where θ is between 0° and 30°. The active reflecting area may be bounded by either six sides (Case 1) or four sides (Case 2), as shown in Figure 30, depending on the values of θ and ϕ.

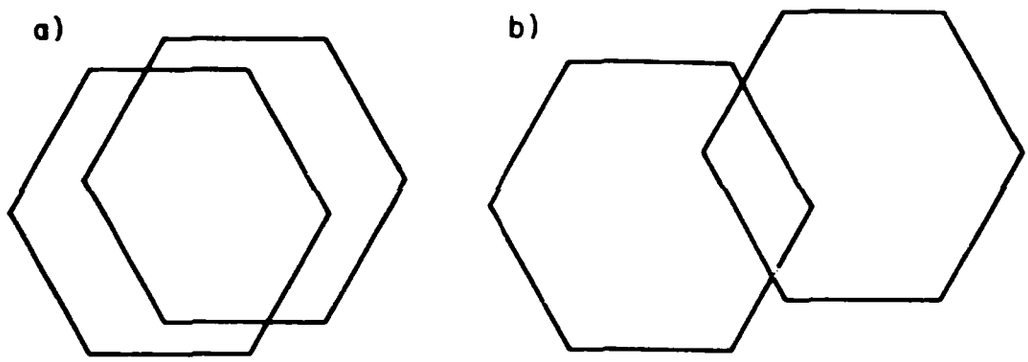

Figure 30. Hexagonal retroreflector: a) Case 1, b) Case 2.

The width W of the hexagon is 2r, where r is the radius of the inscribed circle (see Figure 31). The maximum value of r for a given L is

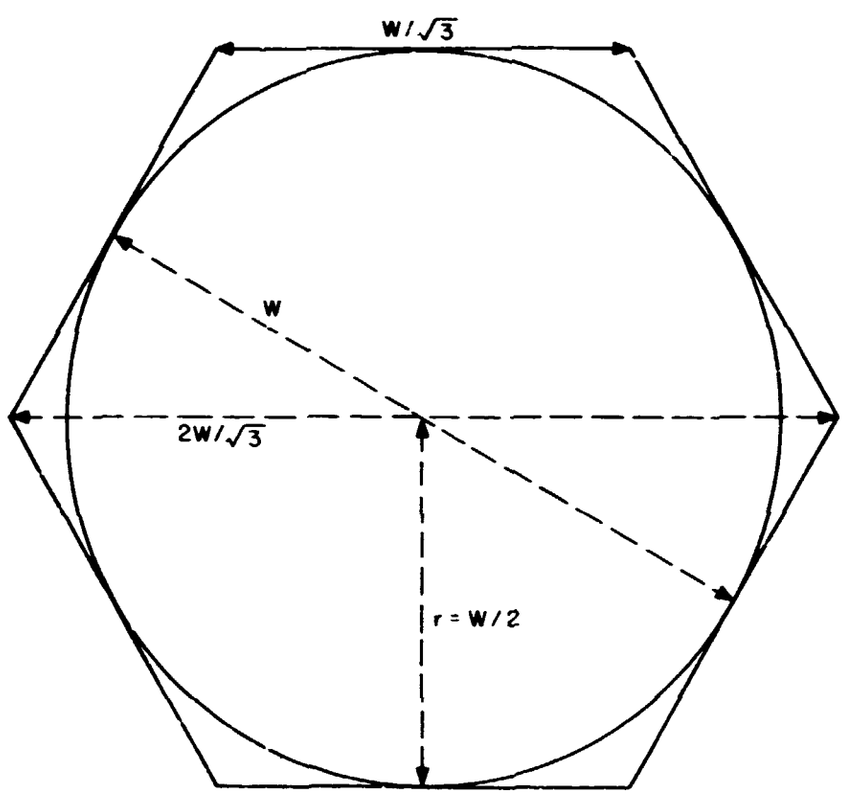

Figure 31. Hexagonal retroreflector at normal incidence.

$$r_{max} = \frac{L}{\sqrt{2}} \quad ,$$

as in the case of the circular reflector; this value occurs when the inscribed circle is tangent to the reflecting surfaces. In the diagram for Case 1 (Figure 32), the following areas must be calculated:

$$\begin{aligned}
\text{area}_{I} &= \frac{1}{2}\left(\overline{bk} + \overline{hi}\right)\overline{bj} \\
&= \frac{1}{2}\left[\frac{1}{\sqrt{3}}\left(2W - \sqrt{3}D\cos\theta - D\sin\theta\right) + \frac{1}{\sqrt{3}}\left(W - \sqrt{3}D\cos\theta + D\sin\theta\right)\right] \\
&\quad \times \frac{1}{2}\left(W - 2D\sin\theta\right) \\
&= \frac{1}{4\sqrt{3}}\left(3W - 2\sqrt{3}D\cos\theta\right)\left(W - 2D\sin\theta\right) \quad ,
\end{aligned}$$

$$\begin{aligned}
\text{area}_{II} &= \overline{bc}\,\overline{de} \\
&= D\sin\theta\left[\frac{1}{\sqrt{3}}\left(2W - \sqrt{3}D\cos\theta - D\sin\theta\right)\right] \quad ,
\end{aligned}$$

$$\text{area}_{III} = \text{area}_{I} \quad .$$

The intersection of the apertures is

$$\begin{aligned}
\text{area} &= 2\,\text{area}_{I} + \text{area}_{II} \\
&= \frac{1}{2}\left(\sqrt{3}W - 2D\cos\theta\right)\left(W - 2D\sin\theta\right) + D\sin\theta\left[\frac{1}{\sqrt{3}}\left(2W - \sqrt{3}D\cos\theta - D\sin\theta\right)\right] \quad .
\end{aligned}$$

Evaluating the above expression gives

$$\text{area} = \frac{1}{\sqrt{3}}\left[\frac{3}{2}W^2 - DW\left(\sqrt{3}\cos\theta + \sin\theta\right) + D^2\sin\theta\left(\sqrt{3}\cos\theta - \sin\theta\right)\right] \quad .$$

The active reflecting area for Case 1, therefore, is

$$\frac{\cos\phi}{\sqrt{3}}\left[\frac{3}{2}W^2 - DW(\sqrt{3}\cos\theta + \sin\theta) + D^2\sin\theta\,(\sqrt{3}\cos\theta - \sin\theta)\right] \quad . \tag{3-6}$$

The transition from Case 1 to Case 2 occurs when

$$\overline{hi} = \frac{1}{\sqrt{3}}(W - \sqrt{3}D\cos\theta + D\sin\theta) = 0 \quad . \tag{3-7}$$

The two cases are defined by

Case 1: $W > D(\sqrt{3}\cos\theta - \sin\theta)$,

Case 2: $W < D(\sqrt{3}\cos\theta - \sin\theta)$.

In the diagram for Case 2 (Figure 33), the area of intersection consists of area II plus two times area I. Defining

$$\begin{aligned} T = \overline{bk} &= \frac{1}{\sqrt{3}}(2W - \sqrt{3}D\cos\theta - D\sin\theta) \\ &= \frac{1}{\sqrt{3}}[2W - D(\sqrt{3}\cos\theta + \sin\theta)] \end{aligned} \tag{3-8}$$

and

$$\overline{jm} = \frac{\sqrt{3}}{2}\overline{bk} \equiv \frac{\sqrt{3}}{2}T \quad ,$$

we have

$$\begin{aligned} \text{area}_I &= \frac{1}{2}\overline{bk}\,\overline{jm} = \frac{1}{2}T\left(\frac{\sqrt{3}}{2}T\right) \\ &= \frac{\sqrt{3}}{4}T^2 \quad , \end{aligned}$$

$$\text{area}_{II} = \overline{bc}\,\overline{bk} = (D\sin\theta)T \quad ,$$

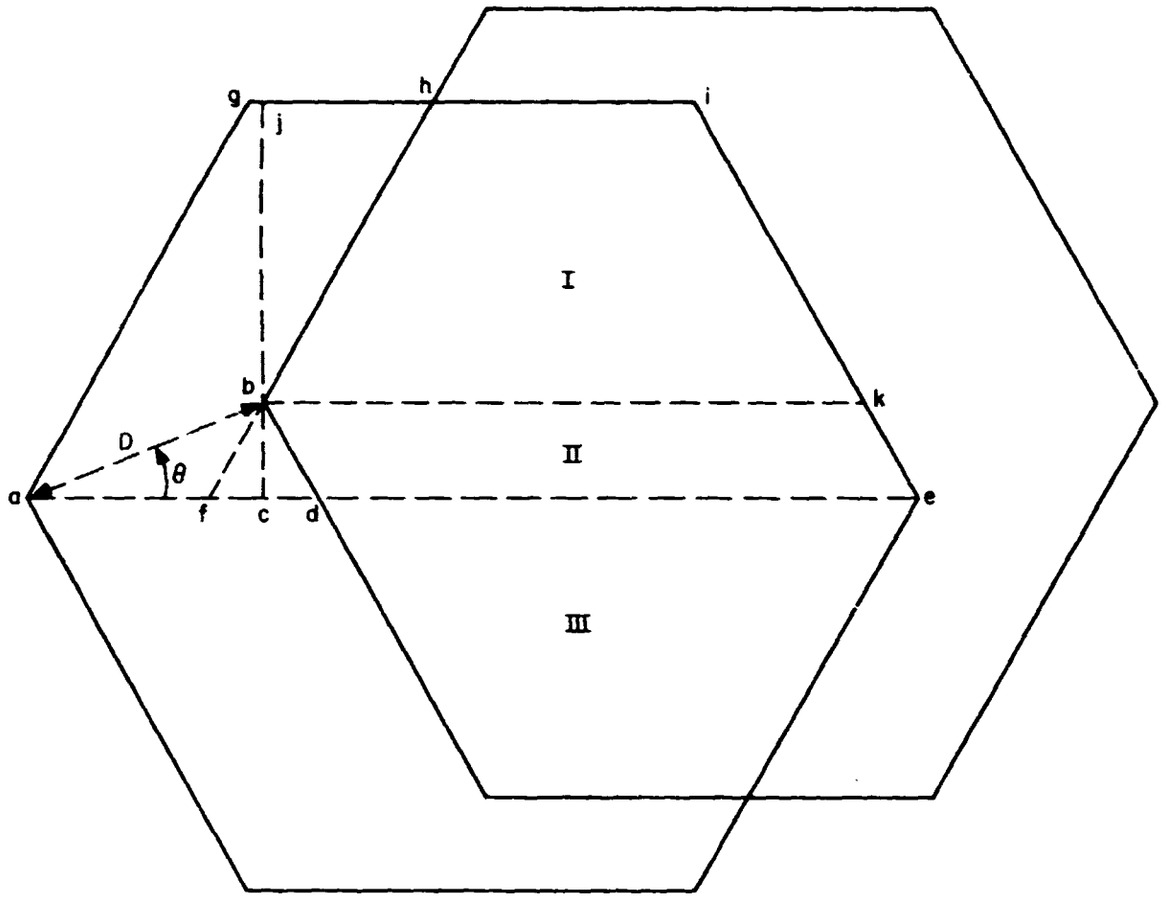

Figure 32. Hexagonal retroreflector, Case 1.

CALCULATION OF DISTANCES IN FIGURE 32

$$\overline{bc} = D \sin \theta$$

$$\overline{ac} = D \cos \theta$$

$$\overline{fc} = \frac{1}{\sqrt{3}} \overline{bc}$$

$$= \frac{1}{\sqrt{3}} D \sin \theta$$

Figure 32 (Cont.)

$$\overline{cd} = \overline{fc}$$

$$= \frac{1}{\sqrt{3}} D \sin\theta$$

$$\overline{af} = \overline{ac} - \overline{fc} = D\cos\theta - \frac{1}{\sqrt{3}} D \sin\theta$$

$$\overline{gh} = \overline{af}$$

$$= D\cos\theta - \frac{1}{\sqrt{3}} D \sin\theta$$

$$\overline{hi} = \overline{gi} - \overline{gh} = \frac{W}{\sqrt{3}} - D\cos\theta + \frac{1}{\sqrt{3}} D \sin\theta$$

$$= \frac{1}{\sqrt{3}} (W - \sqrt{3}D\cos\theta + D\sin\theta)$$

$$\overline{bj} = \overline{cj} - \overline{bc} = \frac{W}{2} - D\sin\theta$$

$$= \frac{1}{2} (W - 2D\sin\theta)$$

$$\overline{de} = \overline{ae} - \overline{ac} - \overline{cd}$$

$$= \frac{2W}{\sqrt{3}} - D\cos\theta - \frac{1}{\sqrt{3}} D \sin\theta$$

$$= \frac{1}{\sqrt{3}} (2W - \sqrt{3}D\cos\theta - D\sin\theta)$$

$$\overline{bk} = \overline{de}$$

$$= \frac{1}{\sqrt{3}} (2W - \sqrt{3}D\cos\theta - D\sin\theta)$$

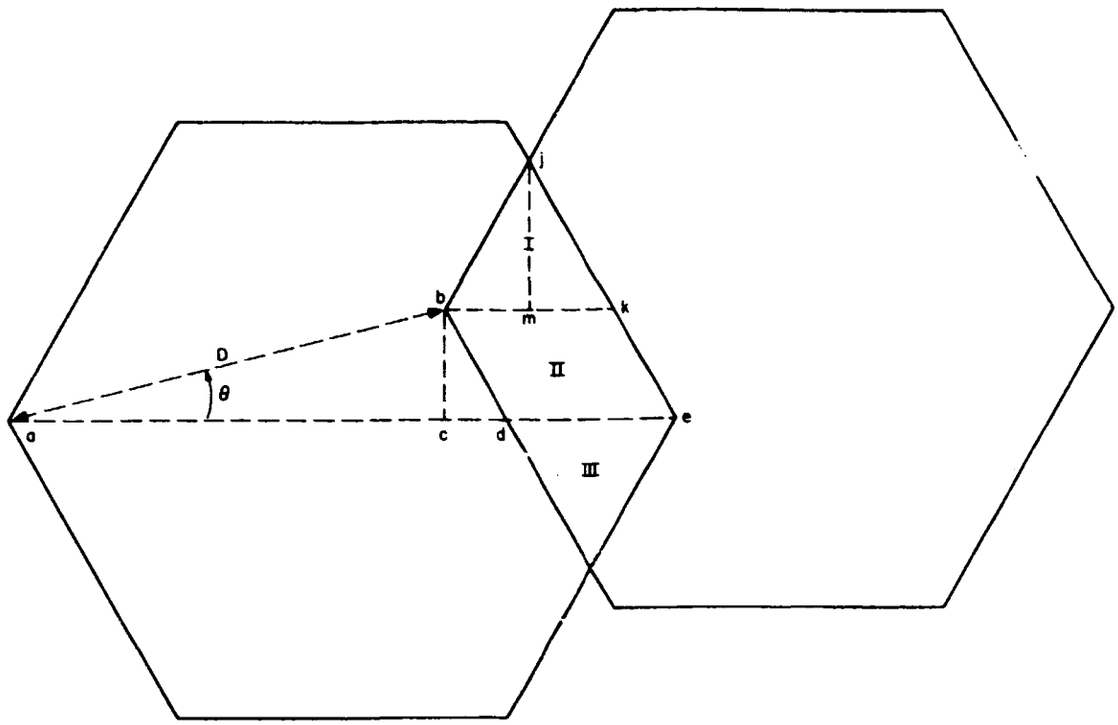

Figure 33. Hexagonal retroreflector, Case 2.

CALCULATION OF DISTANCES IN FIGURE 33

$$\overline{ac} = D \cos \theta$$

$$\overline{bc} = D \sin \theta$$

$$\overline{cd} = \frac{1}{\sqrt{3}} \overline{bc}$$
$$= \frac{1}{\sqrt{3}} D \sin \theta$$

$$\overline{de} = \overline{ae} - \overline{ac} - \overline{cd}$$

$$= \frac{2W}{\sqrt{3}} - D \cos \theta - \frac{1}{\sqrt{3}} D \sin \theta$$
$$= \frac{1}{\sqrt{3}} (2W - \sqrt{3}D \cos \theta - D \sin \theta)$$

$$\overline{bk} = \overline{de}$$

$$= \frac{1}{\sqrt{3}} (2W - \sqrt{3}D \cos \theta - D \sin \theta)$$

$$\overline{jm} = \frac{\sqrt{3}}{2} \overline{bk}$$

$$= \frac{1}{2} (2W - \sqrt{3}D \cos \theta - D \sin \theta)$$

and the intersection of the apertures is

$$\text{area} = 2\ \text{area}_{I} + \text{area}_{II}$$

$$= \frac{\sqrt{3}}{2} T^2 + D \sin \theta T \quad .$$

The active reflecting area for Case 2 is

$$\cos \phi \left(D \sin \theta\ T + \frac{\sqrt{3}}{2} T^2\right) = T \left(D \sin \theta + \frac{\sqrt{3}}{2} T\right) \cos \phi \quad . \tag{3-9}$$

This expression has been evaluated by using an algebra computer program, with the following result:

$$\frac{2 \cos \phi}{\sqrt{3}} \left[W(W - \sqrt{3}D \cos \theta) + D^2\left(\cos^2 \theta - \frac{1}{4}\right)\right] \quad . \tag{3-10}$$

Cutoff occurs when

$$T = \frac{1}{\sqrt{3}} \left[2W - D(\sqrt{3} \cos \theta + \sin \theta)\right] = 0 \quad , \tag{3-11}$$

and the active reflecting area is zero when

$$D(\sqrt{3} \cos \theta + \sin \theta) > 2W \quad .$$

The cutoff angle ϕ_c' as a function of θ can be computed by substituting $D = 2L \tan \phi_c'$ into the above the expression, which yields

$$2L \tan \phi_c' \ (\sqrt{3} \cos \theta + \sin \theta) = 2W \quad ,$$

$$\phi_c' = \tan^{-1}\left[\frac{W}{L(\sqrt{3} \cos \theta + \sin \theta)}\right] \quad . \tag{3-12}$$

The unrefracted cutoff angle ϕ_c is

$$\phi_c = \sin^{-1} (n \sin \phi_c') \quad .$$

The cutoff angle is largest when $\theta = 0°$ and smallest when $\theta = 30°$. At 30°, the transition and cutoff points coincide, so a single formula expresses the active reflecting area for all values of ϕ. The active reflecting area for this special case is obtained by substituting

$$\theta = 30° \quad ,$$

$$\cos\theta = \frac{\sqrt{3}}{2} \quad ,$$

$$\sin\theta = \frac{1}{2}$$

into equation (3-6) for Case 1:

$$\frac{\cos\phi}{\sqrt{3}}\left[\frac{3}{2}W^2 - DW(\sqrt{3}\cos\theta + \sin\theta) + D^2 \sin\theta\,(\sqrt{3}\cos\theta - \sin\theta)\right]\Bigg|_{\theta=30°}$$

$$= \frac{\cos\phi}{\sqrt{3}}\left[\frac{3}{2}W^2 - DW\left(\frac{3}{2}+\frac{1}{2}\right) + \frac{D^2}{2}\left(\frac{3}{2}-\frac{1}{2}\right)\right]$$

$$= \frac{\cos\phi}{2\sqrt{3}}\,[3W^2 - 4DW + D^2]$$

$$= \frac{\cos\phi}{2\sqrt{3}}\,(3W - D)\,(W - D) \quad .$$

The cutoff angle for $\theta = 30°$ using equation (3-12) is

$$\phi_c'\,(\theta = 30°) = \tan^{-1}\left\{\frac{W}{L\,[\sqrt{3}\,(\sqrt{3}/2) + (1/2)]}\right\}$$

$$= \tan^{-1}\left(\frac{W}{2L}\right) \quad .$$

The other special case, $\theta = 0°$, is obtained by setting

$$\theta = 0° \quad ,$$

$$\cos\theta = 1 \quad ,$$

$$\sin\theta = 0$$

in Case 1. The formula before transition using equation (3-6) becomes

$$\frac{\cos\phi}{\sqrt{3}}\left[\frac{3}{2}W^2 - DW(\sqrt{3}\cos\theta + \sin\theta) + D^2 \sin\theta\,(\sqrt{3}\cos\theta - \sin\theta)\right]\Bigg|_{\theta=0°}$$

$$= \frac{\cos\phi}{\sqrt{3}}\left(\frac{3}{2}W^2 - \sqrt{3}DW\right)$$

$$= W\left(\frac{\sqrt{3}}{2}W - D\right)\cos\phi \quad ,$$

and after transition, by using equation (3-8) with $\theta = 0°$

$$T(\theta = 0°) = \frac{1}{\sqrt{3}}\,[2W - D(\sqrt{3}\cos\theta + \sin\theta)]\Big|_{\theta=0°} = \frac{2}{\sqrt{3}}W - D \quad ,$$

in equation (3-9) it becomes

$$T\left(D\sin\theta + \frac{\sqrt{3}}{2}T\right)\cos\phi\Bigg|_{\theta=0°} = \frac{\sqrt{3}}{2}T^2\cos\phi = \frac{\sqrt{3}}{2}\left(\frac{2}{\sqrt{3}}W - D\right)^2\cos\phi \quad .$$

Transition from Case 1 to Case 2 at $\theta = 0°$ occurs using equation (3-7) when

$$\frac{1}{\sqrt{3}}\,[W - D(\sqrt{3}\cos\theta + \sin\theta)]\Big|_{\theta=0°} = 0 \quad ,$$

$$W - \sqrt{3}D = 0 \quad ,$$

while cutoff takes place using equation (3-11) when

$$\frac{1}{\sqrt{3}}\,[2W - D(\sqrt{3}\cos\theta + \sin\theta)]\Big|_{\theta=0°} = 0 = 2W - \sqrt{3}D \quad .$$

Substituting $D = 2L\tan\phi'_c$, we get

$$2W = \sqrt{3}D = 2\sqrt{3}\,L\tan\phi'_c \quad ,$$

or

$$\phi'_c\,(\theta = 0°) = \tan^{-1}\left(\frac{W}{\sqrt{3}L}\right) \quad .$$

In summary, the active reflecting area of a hexagonal cube corner is given by the following formulas for the range $0° < \theta < 30°$. For $D(\sqrt{3}\cos\theta - \sin\theta) < W$,

$$\text{area} = \frac{\cos\phi}{\sqrt{3}}\left[\frac{3}{2}W^2 - DW(\sqrt{3}\cos\theta + \sin\theta) + D^2\sin\theta\,(\sqrt{3}\cos\theta - \sin\theta)\right] \quad ;$$

for $D(\sqrt{3}\cos\theta - \sin\theta) > W$ and $D(\sqrt{3}\cos\theta + \sin\theta) < 2W$,

$$\text{area} = \frac{2\cos\phi}{\sqrt{3}}\left[W(W - \sqrt{3}D\cos\theta) + D^2\left(\cos^2\theta - \frac{1}{4}\right)\right] \quad ;$$

and for $D(\sqrt{3}\cos\theta + \sin\theta) > 2W$,

$$\text{area} = 0 \quad .$$

The active area for other values of θ is obtained by using the following symmetry properties:

$$\text{area}(\theta) = \text{area}(\theta + N \times 60°) \quad ,$$

$$\text{area}(\theta) = \text{area}(-\theta) \quad ,$$

$$\text{area}(\theta) = \text{area}(60° - \theta) \quad ,$$

where N is an integer.

3.4 Cutoff Angles for Total Internal Reflection

The cutoff angle for total internal reflection is defined by the equation

$$n \sin r_c = 1 \quad , \tag{3-13}$$

where r_c is the angle of incidence of the ray. There will be total internal reflection whenever the incidence angle r satisfies the relation

$$r > r_c = \sin^{-1} \frac{1}{n} \quad .$$

The incidence angles that do not give total internal reflection are contained in a cone of half-angle r_c about the normal to the dielectric boundary (see Figure 34).

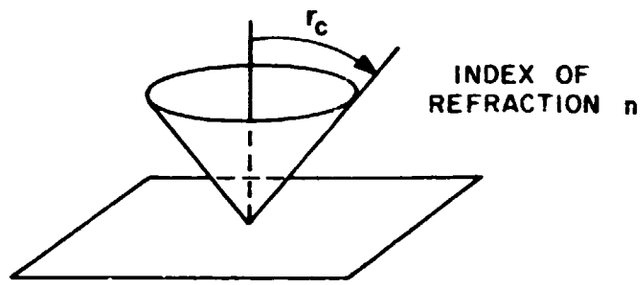

Figure 34. Total-internal-reflection cone.

As shown in Section 2.2, the angle of incidence of the light with a particular reflecting face in a cube corner is the same as the angle that the incident beam makes with that face after refraction at the front surface. This property makes it possible to visualize the directions of the incident beams that do not undergo total internal reflection at all the back faces. In Figure 35, a quarter-cone of half-angle r_c has been drawn about the normal to each reflecting face of a cube corner. If a vector drawn

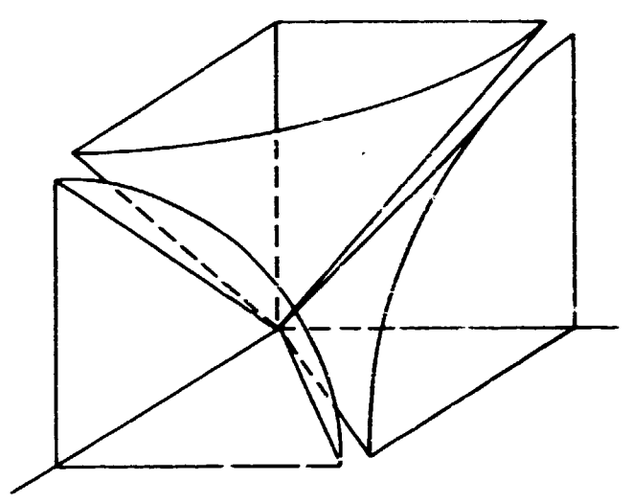

Figure 35. Total-internal-reflection cones about each axis.

from the origin antiparallel to the incident beam (after refraction) lies within any of the three quarter-cones, the beam will not undergo total internal reflection when it is incident on the face whose normal is the axis of the cone. As depicted in Figure 35, the cones do not overlap, and total internal reflection is lost at only one face in this case. If r_c is greater than 45°, the cones intersect and the incidence angles in the intersection lose total reflection at two faces. Viewed from the front face of the reflector (Figure 36), a Y-shaped region is formed by the intersection of the cones

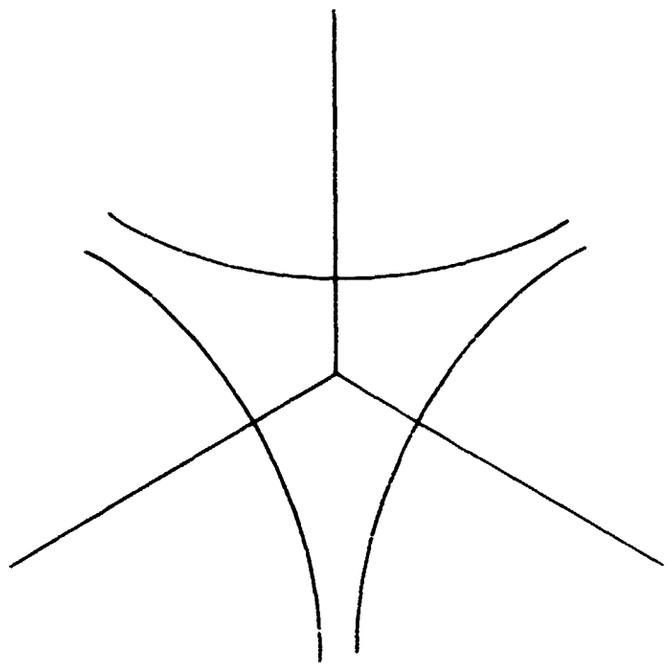

Figure 36. Region of total internal reflection.

with the front face. The ray that goes to the vertex must be incident on the front face within this Y-shaped area to give total internal reflection. Let ϕ be the angle of incidence of the beam on the front face (measured from normal incidence) and ϕ' be the angle after refraction. The smallest value of ϕ that does not give total reflection is ϕ'_c, which is given by

$$\phi'_c = \alpha - r_c \quad ,$$

where α, the angle between the symmetry axis of the prism and a back edge (see Figure 37), is given by

$$\alpha = \tan^{-1} \sqrt{2} \quad .$$

Substituting values for α and r_c, we get

$$\phi'_c = \tan^{-1} \sqrt{2} - \sin^{-1} \frac{1}{n} \quad .$$

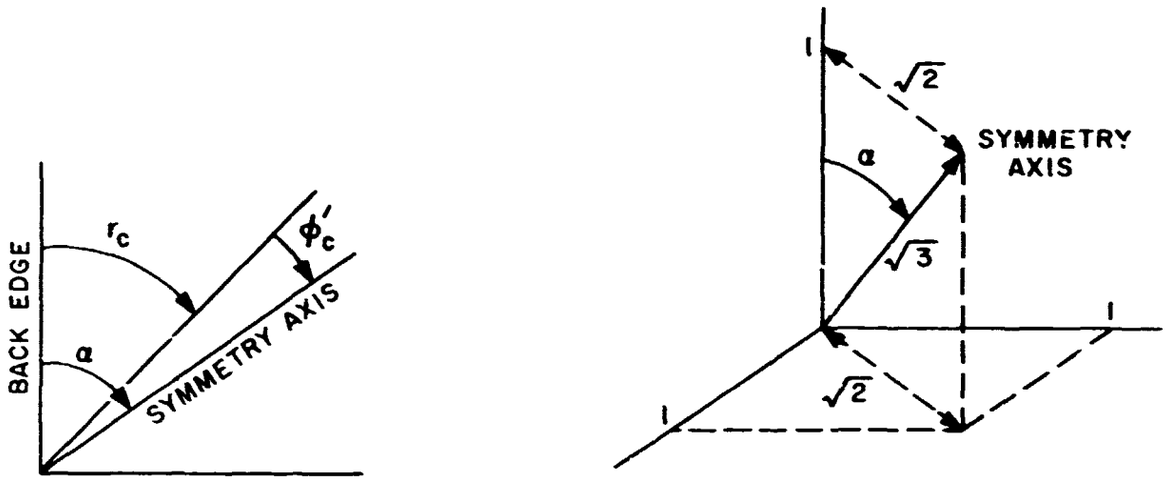

Figure 37. Minimum cutoff angle for total internal reflection.

For a given ϕ', we can compute the azimuth limit θ_c for total reflection. Let θ_c be measured from the projection of a back edge onto the front face, as shown in Figure 38. The circle is the intersection with the front face of a cone of half-angle ϕ' about the symmetry axis of the cube corner. The Y-shaped area is the intersection of the three cones of half-angle r_c with the front face. To compute θ_c, let the symmetry axis of the prism be the z axis, and let the back edge $\hat{A}$ defining the origin of θ_c be in the xz plane (see Figure 39). The angle α between the symmetry axis (z axis) and the back edge ($\hat{A}$) has been shown to be $\tan^{-1} \sqrt{2}$. The unit vector $\hat{A}$ is given by

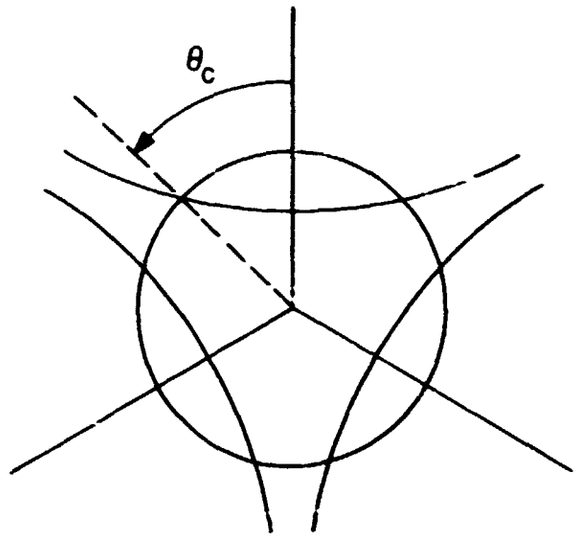

Figure 38. Azimuth angle for loss of total internal reflection.

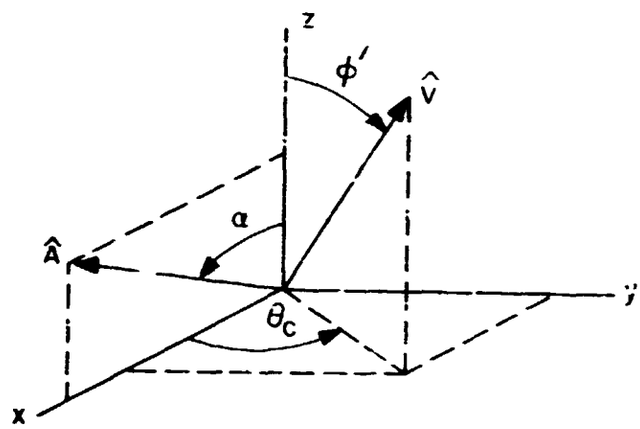

Figure 39. Diagram for computing total-internal-reflection cutoff angles.

$$\hat{A} = (\sin\alpha,\ 0,\ \cos\alpha)$$

$$= \left(\frac{\sqrt{2}}{\sqrt{3}},\ 0,\ \frac{1}{\sqrt{3}}\right) \quad .$$

The unit vector $\hat{V}$ antiparallel to the incident beam after refraction is

$$\hat{V} = (\sin\phi' \cos\theta_c,\ \sin\phi' \sin\theta_c,\ \cos\phi') \quad .$$

In order for the angle between $\hat{V}$ and $\hat{A}$ to be the cutoff angle r_c, we must have

$$\cos r_c = \hat{A} \cdot \hat{V}$$

$$= \frac{\sqrt{2}}{\sqrt{3}} \sin\phi' \cos\theta_c + \frac{1}{\sqrt{3}} \cos\phi' \quad .$$

Solving for θ_c, we get

$$\sqrt{3} \cos r_c - \cos\phi' = \sqrt{2} \sin\phi' \cos\theta_c \ ,$$

$$\theta_c = \cos^{-1}\left(\frac{\sqrt{3} \cos r_c - \cos\phi'}{\sqrt{2} \sin\phi'}\right) \quad . \tag{3-14}$$

Equation (3-13) can be used to rewrite $\cos r_c$ as

$$\cos r_c = \sqrt{1 - \sin^2 r_c} = \sqrt{1 - \frac{1}{n^2}} = \frac{1}{n}\sqrt{n^2 - 1} \quad .$$

Also, $\cos\phi'$ can be written as

$$\cos\phi' = \sqrt{1 - \sin^2\phi'} = \sqrt{1 - \frac{\sin^2\phi}{n^2}} = \frac{1}{n}\sqrt{n^2 - \sin^2\phi} \quad .$$

Substituting these expressions into equation (3-14) gives

$$\theta_c = \cos^{-1}\left[\frac{\sqrt{3}\,(1/n)\sqrt{n^2 - 1} - (1/n)\sqrt{n^2 - \sin^2\phi}}{\sqrt{2}\,\sin\phi/n}\right]$$

$$= \cos^{-1}\left(\frac{\sqrt{3}\sqrt{n^2 - 1} - \sqrt{n^2 - \sin^2\phi}}{\sqrt{2}\,\sin\phi}\right) \quad .$$

For a thorough discussion of the loss of total internal reflection in uncoated cube corners, see Chang (1970). In his paper, Chang gives $\sin\phi$ as a function of θ_c. If we convert his notation to ours, his result becomes

$$\sin\phi = \frac{\sqrt{6}\sqrt{n^2 - 1}\cos\theta_c - \sqrt{3 - 2n^2\sin^2\theta_c}}{2\cos^2\theta_c + 1} .$$

4. POLARIZATION

A beam of light retroreflected from a solid cube corner undergoes two refractions and three reflections. Each encounter with a boundary introduces a change in either the amplitude or the phase or both. Since the changes are different for the components of the ray parallel and perpendicular to the plane of incidence, the polarization state of the ray is also changed. Changes in amplitude affect the total energy retroreflected and thereby reduce the apparent active reflecting area of a cube corner. The diffraction pattern of the prism is affected by both phase and amplitude changes. The following three cases will be considered:

A. Transmission across a dielectric boundary.

B. Reflection from a dielectric boundary, including
   1) Ordinary reflection.
   2) Total internal reflection.

C. Reflection from a metal surface, including
   1) Perfect metal.
   2) Real metal.

At each encounter with a boundary, the ray must be resolved into components parallel and perpendicular to the plane of incidence. The coordinate system with unit vectors defining the directions of the components is shown in Figure 40. The angle of incidence is θ_0, and the angle of refraction is θ_1. The complex vectors for the incident, refracted, and reflected electric vectors are $\vec{E}$, $\vec{E}'$, and $\vec{E}''$, respectively, given by

$$\vec{E} = E_\perp \hat{E}_\perp + E_\parallel \hat{E}_\parallel \quad ,$$

$$\vec{E}' = E'_\perp \hat{E}'_\perp + E'_\parallel \hat{E}'_\parallel \quad ,$$

$$\vec{E}'' = E''_\perp \hat{E}''_\perp + E''_\parallel \hat{E}''_\parallel \quad .$$

The unit vectors are real, and the coefficients are, in general, complex. The transmission and reflection coefficients used in this report are taken from Stratton (1941, pp. 494-506).

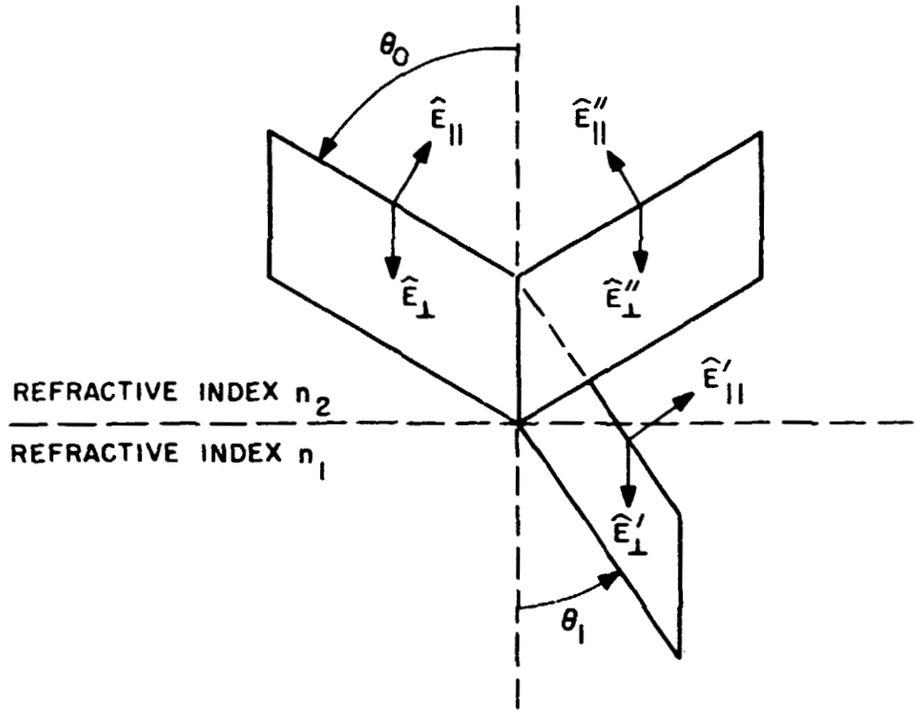

Figure 40. Polarization coordinate system.

4.1 Transmission across a Dielectric Boundary

After refraction across a dielectric boundary, the components of $\vec{E}'$ are given by the Fresnel relations

$$E'_{\perp} = \frac{2 \cos \theta_0 \sin \theta_1}{\sin (\theta_0 + \theta_1)} E_{\perp} \quad ,$$

$$E'_{\parallel} = \frac{2 \cos \theta_0 \sin \theta_1}{\sin (\theta_0 + \theta_1) \cos (\theta_0 - \theta_1)} E_{\parallel} \quad .$$

At normal incidence, both formulas reduce to the same relationship:

$$E'_{\perp} = \frac{2}{n_{12} + 1} E_{\perp} \quad ,$$

$$E'_{\parallel} = \frac{2}{n_{12} + 1} E_{\parallel} \quad ,$$

with

$$n_{12} \equiv \frac{n_1}{n_2} \quad ,$$

where n_1 is the index of refraction of the transmitting medium and n_2 is the index of refraction of the incident medium. The angles θ_0 and θ_1 are related by Snell's law

$$n_2 \sin \theta_0 = n_1 \sin \theta_1 \quad .$$

The transmitted ray is always in phase with the incident ray. In the case of a light beam crossing the front face of a cube corner at an incidence angle ϕ and a refracted angle ϕ', we have

$$\theta_0 = \phi \quad ,$$
$$\theta_1 = \phi' \quad ,$$
$$n_{12} = n$$

as the beam enters the cube corner and

$$\theta_0 = \phi' \quad ,$$
$$\theta_1 = \phi \quad ,$$
$$n_{12} = \frac{1}{n}$$

as it leaves the retroreflector.

4.2 Reflection from a Dielectric Boundary

4.2.1 Ordinary reflection

In uncoated cube corners, the reflection at a particular back face is partial when the incidence angle satisfies the relation

$$n \sin \theta_0 < 1$$

and total when

$$n \sin \theta_0 \geq 1 \quad .$$

The reflected electric field components $E''_{\perp}$ and $E''_{\parallel}$ in the case of partial reflection are

$$E''_{\perp} = - \frac{\sin (\theta_0 - \theta_1)}{\sin (\theta_0 + \theta_1)} E_{\perp} \quad ,$$

$$E''_{\parallel} = \frac{\tan (\theta_0 - \theta_1)}{\tan (\theta_0 + \theta_1)} E_{\parallel} \quad ,$$

which, at normal incidence, reduce to

$$E''_{\perp} = - \frac{n_{12} - 1}{n_{12} + 1} E_{\perp} \quad , \tag{4-1a}$$

$$E''_{\parallel} = \frac{n_{12} - 1}{n_{12} + 1} E_{\parallel} \quad . \tag{4-1b}$$

In the case of a ray incident on the back face from inside the solid cube corner,

$$n_{12} = \frac{1}{n} \quad .$$

Therefore, equations (4-1) become

$$E''_{\perp} = -\frac{(1/n) - 1}{(1/n) + 1} E_{\perp} = -\frac{1 - n}{n + 1} E_{\perp} = \frac{n - 1}{n + 1} E_{\perp} \quad ,$$

$$E''_{\parallel} = -\frac{n - 1}{n + 1} E_{\parallel} \quad .$$

The difference in sign is due to the fact that at normal incidence,

$$\hat{E}''_{\perp} = \hat{E}_{\perp} \quad ,$$

$$\hat{E}''_{\parallel} = -\hat{E}_{\parallel} \quad .$$

4.2.2 Total internal reflection

For total internal reflection ($n \sin \theta_0 \geq 1$), the components of the reflected field are

$$E''_{\perp} = Z_{\perp} E_{\perp} \quad ,$$

$$E''_{\parallel} = Z_{\parallel} E_{\parallel} \quad ,$$

where

$$Z_{\perp} = \frac{n \cos \theta_0 - i\sqrt{n^2 \sin^2 \theta_0 - 1}}{n \cos \theta_0 + i\sqrt{n^2 \sin^2 \theta_0 - 1}} \quad ,$$

$$Z_{\parallel} = \frac{\cos \theta_0 - in\sqrt{n^2 \sin^2 \theta_0 - 1}}{\cos \theta_0 + in\sqrt{n^2 \sin^2 \theta_0 - 1}} \quad .$$

4.3 Reflection from a Metal Surface

4.3.1 Perfect metal

The case of reflection from a perfect-metal surface (infinite conductivity) gives the simple relations

$$E''_{\perp} = -E_{\perp} \quad ,$$

$$E''_{\parallel} = E_{\parallel} \quad .$$

4.3.2 Real metal

Reflection from a real-metal surface produces changes in both phase and amplitude. The reflecting properties of the metal are specified by the complex index of refraction $\alpha + i\beta$. For a perfect metal, $\beta = \infty$. If the conductivity is zero, $\beta = 0$ and the material is a perfect dielectric with index of refraction α. The components of the reflected electric field are

$$E''_{\perp} = Z_{\perp} E_{\perp} \quad ,$$

$$E''_{\parallel} = Z_{\parallel} E_{\parallel} \quad ,$$

where

$$Z_{\perp} = \frac{(n \cos \theta_0 - q) - ip}{(n \cos \theta_0 + q) + ip} \quad ,$$

$$Z_{\parallel} = \frac{[\cos \theta_0 (\alpha^2 - \beta^2) - nq] + i (2\alpha\beta \cos \theta_0 - np)}{[\cos \theta_0 (\alpha^2 - \beta^2) + nq] + i (2\alpha\beta \cos \theta_0 - np)} \quad ,$$

$$q = \sqrt{(C + D)/2} \quad ,$$

$$p = \sqrt{(C - D)/2} \quad ,$$

$$C = \sqrt{4\alpha^2\beta^2 + (\alpha^2 - \beta^2 - n^2 \sin^2 \theta_0)^2} \quad ,$$

$$D = \alpha^2 - \beta^2 - n^2 \sin^2 \theta_0 \quad .$$

Values of α and β for certain metals are given in Schulz (1954).

4.4 Polarization State of Each Sector

The direction of incidence of a beam on a cube corner is specified by the angles θ and ϕ, where ϕ is measured from the normal to the front face (see Figure 41). The polarization state of the incident beam is given as a complex vector

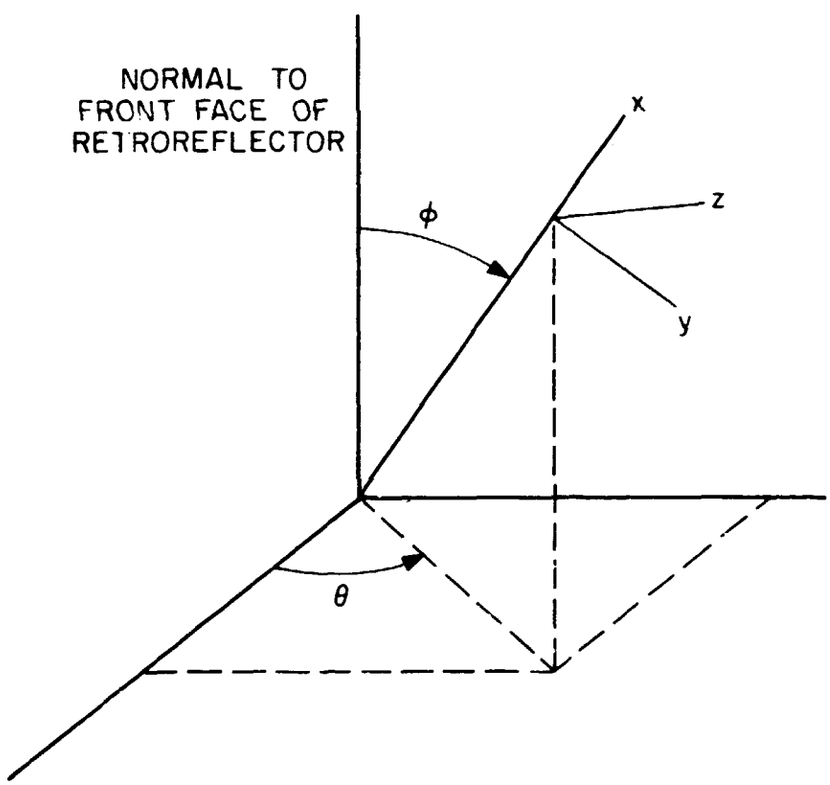

Figure 41. Coordinate system for an incident beam.

$$\vec{E} = E_x\hat{x} + E_y\hat{y} + E_z\hat{z} \quad ,$$

where E_x, E_y, and E_z are complex numbers and $\hat{x}$, $\hat{y}$, and $\hat{z}$ are real unit vectors. The unit vector $\hat{x}$ points toward the source, $\hat{y}$ is in the plane of incidence pointing in the direction of increasing ϕ, and $\hat{z}$ is perpendicular to the plane of incidence pointing in the direction of increasing θ. The polarization state of the beam incident on an array is given as a complex vector $\vec{E}'$ in a coordinate system related to the coordinate system of $\vec{E}$ by a rotation about the x' axis through an angle γ. The components of $\vec{E}$ are

$$E_x = E'_x \quad ,$$

$$E_y = E'_y \cos\gamma + E'_z \sin\gamma \quad ,$$

$$E_z = -E'_y \sin\gamma + E'_z \cos\gamma \quad .$$

Both E_x and E'_x are zero because electromagnetic radiation is a transverse wave. If there are dihedral-angle offsets in the cube corner, the polarization state $\vec{E}_I$ of the radiation emerging from the Ith sector will have a small component in the x direction because the direction of the emerging beam has been changed slightly. This component will not be considered in the polarization calculations. The effect of dihedral-angle offsets will be included only through the phase changes that they produce across each sector.

The polarization states $\vec{E}_I$ of the six sectors are obtained by computing the changes in polarization due to refraction on entering the cube corner, to reflection at each of the back faces in the appropriate order for each sector, and to refraction on leaving the cube corner. The changes in the components of the polarization vector parallel and perpendicular to the plane of incidence were given in Sections 4.1, 4.2, and 4.3, and the order of the reflections for each sector was given in Section 2.12.

The formulas for the change in polarization during refraction can be applied directly to the incident polarization state $\vec{E}$ since E_y is parallel and E_z is perpendicular to the plane of incidence. After refraction, the direction of the beam is (θ', ϕ'), where

$$\theta' = \theta \quad ,$$

$$\phi' = \sin^{-1}\left(\frac{\sin\phi}{n}\right) \quad .$$

Section 2.11 showed how to compute the normals $\hat{n}_1$, $\hat{n}_2$, and $\hat{n}_3$ in the x'', y'', z'' coordinate system. This system has the x'' axis in the direction (θ', ϕ'), the y'' axis in the plane of incidence in the direction of increasing ϕ', and the z'' axis perpendicular to the plane of incidence in the direction of increasing θ'. The polarization state $\vec{E}_0$ after refraction into the cube has the components

$$E_{x''} = 0 \quad ,$$

$$E_{y''} = R_{\parallel} E_y \quad ,$$

$$E_{z''} = R_{\perp} E_z \quad ,$$

where $R_{\parallel}$ and $R_{\perp}$ are coefficients giving the change in the parallel and perpendicular components of the polarization vector due to refraction. The direction of propagation after refraction in the x'', y'', z'' coordinate system is $\hat{v}_0$, given by

$$\hat{v}_0 = -\hat{x}'' \quad .$$

In order to apply the changes in polarization at each reflection, the polarization vector must be resolved into components parallel and perpendicular to the plane of incidence (see Figure 42). Let $\hat{v}_{IJ}$ be the unit vector giving the direction of motion of the ray for the Ith sector before the Jth reflection takes place, and let $\vec{E}_{IJ}$ be the polarization state for the ray with direction $\hat{v}_{IJ}$. For all sectors,

$$\hat{v}_{I0} = \hat{v}_0 \quad ,$$

$$\vec{E}_{I0} = \vec{E}_0 \quad .$$

Let $\hat{n}_{IJ}$ be the normal to the plane from which a ray of the Ith sector is reflected on its Jth reflection. The direction of motion after the Jth reflection is

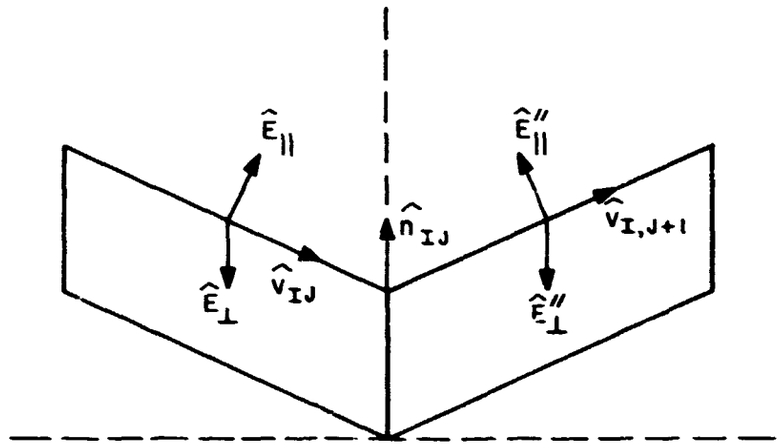

Figure 42. Unit vectors for parallel and perpendicular components of the electric field.

$$\hat{v}_{I,J+1} = \hat{v}_{IJ} - 2(\hat{v}_{IJ} \cdot \hat{n}_{IJ})\hat{n}_{IJ} \quad .$$

The unit vectors parallel and perpendicular to the plane of incidence, then, are

$$\hat{E}_{\perp} = \frac{\hat{v}_{IJ} \times \hat{n}_{IJ}}{|\hat{v}_{IJ} \times \hat{n}_{IJ}|} \quad ,$$

$$\hat{E}_{\parallel} = \hat{E}_{\perp} \times \hat{v}_{IJ} \quad ,$$

$$\hat{E}''_{\perp} = \hat{E}_{\perp} \quad ,$$

$$\hat{E}''_{\parallel} = \hat{E}''_{\perp} \times \hat{v}_{I,J+1} \quad .$$

The parallel and perpendicular components of the polarization vector $\vec{E}_{IJ}$ are $\vec{E}_{IJ} \cdot \hat{E}_{\parallel}$ and $\vec{E}_{IJ} \cdot \hat{E}_{\perp}$, respectively. The components of $\vec{E}_{IJ}$ are complex, and those of $\hat{E}_{\parallel}$ and $\hat{E}_{\perp}$ are real. To compute the dot product, we multiply the corresponding components of the vectors without taking the complex conjugate of any of the numbers. The polarization vector after reflection is

$$\vec{E}_{I,J+1} = R_{\parallel}(\vec{E}_{IJ} \cdot \hat{E}_{\parallel})\hat{E}''_{\parallel} + R_{\perp}(\vec{E}_{IJ} \cdot \hat{E}_{\perp})\hat{E}''_{\perp} \quad ,$$

where $R_{\parallel}$ and $R_{\perp}$ are the complex coefficients giving the change in the parallel and perpendicular components of the polarization vector due to reflection. After three reflections, the direction of motion is nearly $\hat{x}''$ if we neglect the effects of dihedral-angle offsets. Since the y'' and z'' components of the polarization vector are parallel and perpendicular, respectively, to the plane of incidence, the complex coefficients $R_{\parallel}$ and $R_{\perp}$ (giving the change in polarization on leaving the front face) can be applied directly to obtain the polarization vector $\vec{E}_I$ for each sector. The components of $\vec{E}_I$ are therefore

$$E_{x_I} = 0 \quad ,$$

$$E_{y_I} = R_{\parallel} E_{y''_{I3}} \quad ,$$

$$E_{z_I} = R_{\perp} E_{z''_{I3}} \quad .$$

Peck (1972) gives a study of the polarization states produced by either single cube corners or cavities consisting of two cube corners facing each other.

5. DIFFRACTION

5.1 Diffraction Integral

According to Huygen's principle, the field u_p at a point p due to radiation emitted from a surface s is

$$u_p = a \int_s u \frac{e^{ikR}}{R} df_n \quad , \tag{5-1}$$

where a is a constant to be determined, u is the field on the surface s, $k = 2\pi/\lambda$, λ is the wavelength, df_n is the projection of the surface element in the direction of point p, and R is the distance from df_n to p. The constant a can be evaluated by considering the case of radiation from an infinite plane with u equal to a constant. The value of u_p must then be the same as u. The result of performing the integral for this case (Landau and Lifschitz, 1962, pp. 167-168) shows that

$$a = \frac{k}{2\pi i} = \frac{1}{\lambda i} \quad .$$

Substituting this into equation (5-1) gives

$$u_p = \frac{1}{\lambda i} \int_s u \frac{e^{ikR}}{R} df_n \quad . \tag{5-2}$$

The intensity I_p at point p is

$$I_p = u_p u_p^* \quad .$$

Let a coordinate system be set up with the x axis antiparallel to the beam illuminating a cube corner and with the origin just outside the cube corner. The y and z axes are parallel and perpendicular, respectively, to the plane of incidence. Let an x', y', z' coordinate system be established in the far field parallel to the x, y, z system with the x and x' axes collinear (see Figure 43). The reflected field from the cube corner in the yz plane is u, and the field at point p in the $y'z'$ plane is u_p. Finally, let the distance between the coordinate systems be D.

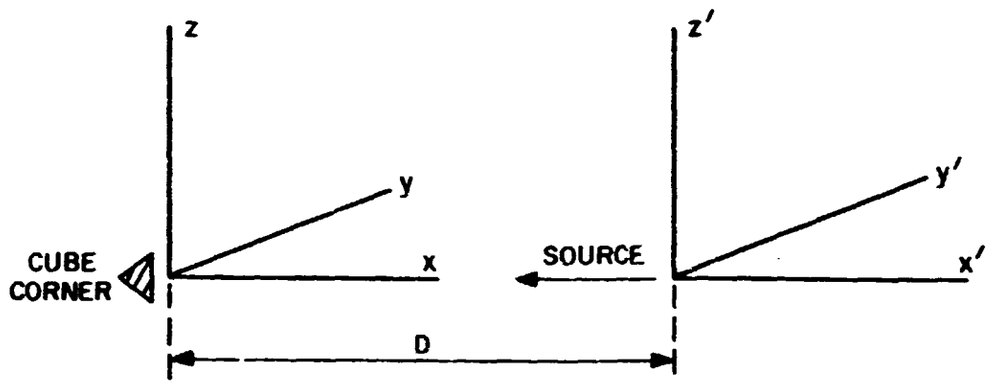

Figure 43. Coordinate system for the far-field diffraction pattern.

5.1.1 Fraunhofer diffraction

When the distance D is very large and when the problem is restricted to cases where the angular spread of the beam due to diffraction is small, equation (5-2) reduces to the simpler formula of Fraunhofer diffraction. The distance R is given by

$$R = \sqrt{D^2 + (y'-y)^2 + (z'-z)^2}$$

$$= D\sqrt{1 + \frac{1}{D^2}\left[(y'-y)^2 + (z'-z)^2\right]}$$

$$\approx D\left\{1 + \frac{1}{2D^2}\left[(y'-y)^2 + (z'-z)^2\right]\right\}$$

$$\approx D + \frac{1}{2D}\left(y'^2 - 2yy' + y^2 + z'^2 - 2zz' + z^2\right) \quad .$$

It is assumed that D is so much larger than the size of the area s that the quantities $y^2/2D$ and $z^2/2D$ are always much less than a wavelength and can be neglected. Therefore,

$$R \approx D + \frac{y'^2 + z'^2}{2D} - \left(y\frac{y'}{D} + z\frac{z'}{D}\right) \quad .$$

Since it is desirable to have the diffraction pattern given in terms of angles rather than as a function of y' and z' at a distance D, we can define the angular coordinates of the observer (θ_1, θ_2) as

$$\theta_1 \equiv \frac{y'}{D} \quad , \qquad\qquad \theta_2 \equiv \frac{z'}{D} \quad ,$$

so that R becomes

$$R = \left(D + \frac{y'^2 + z'^2}{2D}\right) - (y\theta_1 + z\theta_2) \quad .$$

Substituting this for the factor R in equation (5-2) and setting R = D in the denominator, we get

$$u_p = \frac{1}{\lambda i}\int_s u\,\frac{e^{ikR}}{R}\,df_n$$

$$= \frac{1}{\lambda i D}\int_s u \exp\left\{ik\left[\left(D + \frac{y'^2 + z'^2}{2D}\right) - (y\theta_1 + z\theta_2)\right]\right\} dy\,dz$$

$$= \frac{1}{\lambda i D}\exp\left[ik\left(D + \frac{y'^2 + z'^2}{2D}\right)\right]\int_s u \exp\left[-ik(y\theta_1 + z\theta_2)\right] dy\,dz \quad .$$

The exponential outside the integral is a constant phase factor, which will disappear when u_p is multiplied by u_p^* to obtain I_p. It can therefore be neglected, resulting in

$$u_p \sim \frac{1}{\lambda i D} \int_S u\, e^{-ik(y\theta_1 + z\theta_2)}\, dy\, dz \quad . \tag{5-3}$$

5.1.2 Modified Fraunhofer formulas

In equation (5-3), the intensity $I_p = u_p u_p^*$ is in units of energy per unit area per unit time, and the formula contains the range in the denominator. But it is desirable to compute diffraction patterns in a way that is independent of the range and the incident field strength. These quantities can be provided when calculating particular cases by using the range equation [eq. (7-12)] from Section 7.11. Omitting the range causes u_p to be in units of area – i.e., the results have to be given in a particular system of units. The equation can be written in a dimensionless form, however, as follows:

$$E'(\theta_1, \theta_2) \equiv \frac{1}{S} \int_S u'\, e^{-ik(y\theta_1 + z\theta_2)}\, dy\, dz \quad , \tag{5-4}$$

where S is the active reflecting area at normal incidence and

$$u' = u/u_0 \quad ,$$

in which u_0 is the incident field. Let a function $F'(\theta_1, \theta_2)$ be defined as

$$F'(\theta_1, \theta_2) = E'(\theta_1, \theta_2)\, E'^*(\theta_1, \theta_2) \quad .$$

In the above form, the intensity $F'(\theta_1, \theta_2)$ is unity at the center of the diffraction pattern of a perfect retroreflector at normal incidence. The relationship of the modified Fraunhofer formulas to the original forms is

$$u_p = u_0 \frac{S}{\lambda i D} E'(\theta_1, \theta_2) \quad ,$$

$$I_p = \frac{S^2}{\lambda^2 D^2} F'(\theta_1, \theta_2) I_0 \quad ,$$

where $I_0 = u_0 u_0^*$ is the incident intensity.

In doing the integration over various sections of a cube corner, the formula

$$E(\theta_1, \theta_2) = \int u' \, e^{-ik(y\theta_1 + z\theta_2)} \, dy \, dz \tag{5-5}$$

will be used to calculate the pieces of the integral in equation (5-4).

5.2 Calculation of Diffraction Patterns from an Array of Phases

To calculate diffraction patterns from an array of phases, let the field u' in the modified Fraunhofer formula [eq. (5-4)] be given as an array u_{IJ} of field values at the points (y_I, z_J) where

$$y_I = I \Delta y \quad ,$$
$$z_J = J \Delta z \quad .$$

The complex number u' is related to the amplitude A and phase δ of the field by

$$u' = Ae^{i\delta} = A \cos \delta + iB \sin \delta \quad .$$

Let the field $E'(\theta_1, \theta_2)$ be given as an array E'_{LM} at the points $(\theta_{1L}, \theta_{2M})$ where

$$\theta_{1L} = L \, \Delta\theta_1 \quad ,$$
$$\theta_{2M} = M \, \Delta\theta_2 \quad .$$

Since the aperture may not be rectangular, all values of u_{IJ} that are outside the aperture can be set equal to zero. The area element $\Delta y \, \Delta z$ is S/N, where N is the number of nonzero items in the u_{IJ} array.

The modified Fraunhofer formula in the discrete case becomes

$$E'_{LM} = \frac{1}{N} \sum_{IJ} u_{IJ} \, e^{-ik[(I \, \Delta y)(L \, \Delta\theta_1) + (J \, \Delta z)(M \, \Delta\theta_2)]} \quad , \tag{5-6a}$$

$$E'_{LM} = \frac{1}{N} \sum_{LJ} u_{LJ}\, e^{-i(k\,\Delta y\,\Delta\theta_1)IL}\, e^{-i(k\,\Delta z\,\Delta\theta_2)JM} \quad . \tag{5-6b}$$

Defining

$$C_1 = k\,\Delta y\,\Delta\theta_1 \quad ,$$

$$C_2 = k\,\Delta z\,\Delta\theta_2 \quad ,$$

the expression for E'_{LM} becomes

$$E'_{LM} = \frac{1}{N} \sum_{LJ} u_{LJ}\, e^{-iC_1 IL}\, e^{-iC_2 JM}$$

$$= \frac{1}{N} \sum_{I} \left[\sum_{J} u_{LJ} \left(e^{-iC_2}\right)^{JM} \right] \left(e^{-iC_1}\right)^{IL}$$

$$= \frac{1}{N} \sum_{I} S_{IM} \left(e^{-iC_1}\right)^{IL} \quad , \tag{5-7}$$

where

$$S_{IM} \equiv \sum_{J} u_{LJ} \left(e^{-iC_2}\right)^{JM} \quad .$$

All the complex exponentials in equation (5-7) are integral powers of e^{-iC_2} and e^{-iC_1}. This very useful property results from the equal spacing between points across the aperture and between points in the far field. If $\Delta y = \Delta z$ and $\Delta\theta_1 = \Delta\theta_2$, then $C_1 = C_2$ and all terms are powers of a single exponential. Since complex multiplication involves only four multiplications and complex exponentiation involves the computation of two transcendental functions (a sine and a cosine) by means of series expansions, it is much faster to compute the powers by repeated multiplication and

to save all the powers in an array. If each of the indices has a range of n values, there are n^2 complex numbers to be stored (or $2n^2$ if $C_1 \neq C_2$). A second property that can be exploited to reduce computation time is the fact that S_{IM} does not contain the index L. For each value of M, the n quantities S_{IM} can be computed and saved while the quantities E'_{LM} can be computed for the n values of the index L. The physical reason that S_{IM} does not contain L is that the phase differences between the rows across the aperture are constant for each row in the far field, and thus the summation over each column of the aperture needs to be done only once for each row in the far field.

A straightforward computation based on equation (5-6a) requires n^2 complex exponentiations per point, resulting in a total of n^4 exponentiations for the whole matrix. Equation (5-7) requires n^2 complex multiplications to compute the powers of the exponential. For each value of S_{IM}, n complex multiplications are needed, for a total of n^3 for all S_{IM}. Each point E'_{LM} requires n complex multiplications, for a total of n^3 for all E'_{LM}. The complete computation therefore requires $2n^3 + n^2 \approx 2n^3$ complex multiplications, a considerable savings compared to n^4 exponentiations.

5.3 Diffraction Integral for a Trapezoid

To calculate the diffraction integral for a trapezoid, let the field u′ be given by

$$u' = e^{i(ay + bz)} \tag{5-8}$$

over a plane surface with linear boundaries, where a is the rate of change of phase in the y direction due to dihedral-angle offsets and b is the rate of change of phase in the z direction. The Fraunhofer equation is integrable in closed form under these conditions. Let the area be divided into vertical strips bounded by straight lines on the top and bottom, as shown in Figure 44.

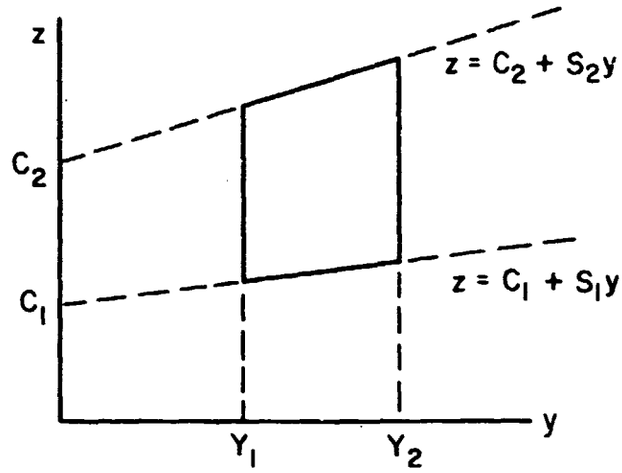

Figure 44. Trapezoid aperture.

By employing the modified Fraunhofer formula [eq. (5-5)], the integral over the area shown in the figure is

$$E(\theta_1, \theta_2) = \int_{y=Y_1}^{Y_2} \int_{z=C_1+S_1y}^{C_2+S_2y} e^{i(ay + bz)} e^{-ik(y\theta_1 + z\theta_2)} \, dy \, dz$$

$$= \int_{y=Y_1}^{Y_2} \int_{z=C_1+S_1y}^{C_2+S_2y} e^{i[(a - k\theta_1)y + (b - k\theta_2)z]} \, dy \, dz \quad .$$

Defining

$$\alpha \equiv a - k\theta_1 \quad , \qquad \beta \equiv b - k\theta_2 \quad , \tag{5-9}$$

we have

$$E(\alpha, \beta) = \int_{y=Y_1}^{Y_2} \int_{z=C_1+S_1y}^{C_2+S_2y} e^{i(\alpha y + \beta z)} \, dy \, dz \quad . \tag{5-10}$$

If $\beta \neq 0$, the integration over z gives

$$E(\alpha,\beta) = \int_{y=Y_1}^{Y_2} \frac{1}{i\beta} \left\{ e^{i[\alpha y + \beta(C_2 + S_2 y)]} - e^{i[\alpha y + \beta(C_1 + S_1 y)]} \right\} dy$$

$$= \int_{y=Y_1}^{Y_2} \frac{1}{i\beta} \left\{ e^{i[\beta C_2 + (\alpha + \beta S_2)y]} - e^{-i[\beta C_1 + (\alpha + \beta S_1)y]} \right\} dy \quad .$$

If we further define

$$Q_I \equiv \alpha + \beta S_I \quad , \qquad I = 1,2 \quad , \tag{5-11}$$

then

$$E(\alpha,\beta) = \int_{y=Y_1}^{Y_2} \frac{1}{i\beta} \left[e^{i(\beta C_2 + Q_2 y)} - e^{i(\beta C_1 + Q_1 y)} \right] dy \quad . \tag{5-12}$$

If $Q_1 \neq 0$, the second term in equation (5-12) is

$$\int_{y=Y_1}^{Y_2} -\frac{1}{i\beta} e^{i(\beta C_1 + Q_1 y)} dy = -\frac{1}{i\beta} \frac{1}{iQ_1} \left[e^{i(\beta C_1 + Q_1 Y_2)} - e^{i(\beta C_1 + Q_1 Y_1)} \right] \quad .$$

Using

$$P_{IJ} \equiv \beta C_I + Q_I Y_J \quad , \qquad \begin{matrix} I = 1,2 \quad , \\ J = 1,2 \quad , \end{matrix} \tag{5-13}$$

in the above expression, we get

$$\int_{y=Y_1}^{Y_2} -\frac{1}{i\beta} e^{i(\beta C_1 + Q_1 y)} dy = \frac{1}{\beta Q_1} \left(e^{iP_{12}} - e^{iP_{11}} \right) \quad .$$

If $Q_1 = 0$,

$$\int_{y=Y_1}^{Y_2} -\frac{1}{i\beta} e^{i(\beta C_1 + Q_1 y)} dy = \int_{y=Y_1}^{Y_2} \frac{i}{\beta} e^{i\beta C_1} dy$$

$$= \frac{i}{\beta} e^{i\beta C_1} (Y_2 - Y_1) \quad .$$

If $Q_2 \neq 0$, the first term in equation (5-12) becomes

$$\int_{y=Y_1}^{Y_2} \frac{1}{i\beta} e^{i(\beta C_2 + Q_2 y)} dy = \frac{1}{i\beta} \frac{1}{iQ_2} \left[e^{i(\beta C_2 + Q_2 Y_2)} - e^{i(\beta C_2 + Q_2 Y_1)} \right]$$

$$= -\frac{1}{\beta Q_2} \left[e^{iP_{22}} - e^{iP_{21}} \right] \quad ;$$

and if $Q_2 = 0$,

$$\int_{y=Y_1}^{Y_2} \frac{1}{i\beta} e^{i(\beta C_2 + Q_2 y)} dy = \int_{y=Y_1}^{Y_2} -\frac{i}{\beta} e^{i\beta C_2} dy$$

$$= -\frac{i}{\beta} e^{i\beta C_2} (Y_2 - Y_1) \quad .$$

If $\beta = 0$, equation (5-10) becomes

$$E(\alpha, 0) = \int_{y=Y_1}^{Y_2} \int_{z=C_1+S_1 y}^{C_2+S_2 y} e^{i\alpha y} dy\, dz$$

$$= \int_{y=Y_1}^{Y_2} e^{i\alpha y} \left[(C_2 + S_2 y) - (C_1 + S_1 y) \right] dy$$

[eq. cont. on next page]

$$= \int_{y=Y_1}^{Y_2} e^{i\alpha y} \left[(C_2 - C_1) + (S_2 - S_1)y\right] dy \quad .$$

If $\alpha \neq 0$,

$$E(\alpha, 0) = -\frac{i}{\alpha}(C_2 - C_1)\left(e^{i\alpha Y_2} - e^{i\alpha Y_1}\right)$$

$$+ (S_2 - S_1)\left[-\frac{i}{\alpha}\left(Y_2 e^{i\alpha Y_2} - Y_1 e^{i\alpha Y_1}\right) + \frac{1}{\alpha^2}\left(e^{i\alpha Y_2} - e^{i\alpha Y_1}\right)\right] \quad ,$$

while if $\alpha = 0$, we have

$$E(0, 0) = \int_{y=Y_1}^{Y_2} \left[(C_2 - C_1) + (S_2 - S_1)y\right] dy$$

$$= (C_2 - C_1)(Y_2 - Y_1) + \frac{1}{2}(S_2 - S_1)\left(Y_2^2 - Y_1^2\right)$$

$$= (Y_2 - Y_1)\left[(C_2 - C_1) + \frac{1}{2}(S_2 - S_1)(Y_2 + Y_1)\right] \quad .$$

In summary, if $\beta \neq 0$, $Q_1 \neq 0$, and $Q_2 \neq 0$,

$$E(\alpha, \beta) = \frac{1}{\beta}\left[\frac{1}{Q_1}\left(e^{iP_{12}} - e^{iP_{11}}\right) - \frac{1}{Q_2}\left(e^{iP_{22}} - e^{iP_{21}}\right)\right] \quad . \tag{5-14a}$$

If $\beta \neq 0$, $Q_1 = 0$, and $Q_2 \neq 0$,

$$E(\alpha, \beta) = \frac{1}{\beta}\left[ie^{i\beta C_1}(Y_2 - Y_1) - \frac{1}{Q_2}\left(e^{iP_{22}} - e^{iP_{21}}\right)\right] \quad . \tag{5-14b}$$

If $\beta \neq 0$, $Q_1 \neq 0$, and $Q_2 = 0$,

$$E(\alpha, \beta) = \frac{1}{\beta}\left[\frac{1}{Q_1}\left(e^{iP_{12}} - e^{iP_{11}}\right) - ie^{i\beta C_2}(Y_2 - Y_1)\right] \quad . \tag{5-14c}$$

If $\beta \neq 0$, $Q_1 = 0$, and $Q_2 = 0$,

$$E(\alpha, \beta) = \frac{i}{\beta} (Y_2 - Y_1) \left(e^{i\beta C_1} - e^{i\beta C_2}\right) \quad . \tag{5-14d}$$

If $\beta = 0$, $\alpha \neq 0$,

$$E(\alpha, 0) = -\frac{i}{\alpha} (C_2 - C_1) \left(e^{i\alpha Y_2} - e^{i\alpha Y_1}\right)$$

$$+ (S_2 - S_1) \left[-\frac{i}{\alpha}\left(Y_2 e^{i\alpha Y_2} - Y_1 e^{i\alpha Y_1}\right) + \frac{1}{\alpha^2}\left(e^{i\alpha Y_2} - e^{i\alpha Y_1}\right)\right] \quad . \tag{5-14e}$$

Finally, if $\beta = \alpha = 0$,

$$E(0, 0) = (Y_2 - Y_1) \left[(C_2 - C_1) + \frac{1}{2} (S_2 - S_1) (Y_2 + Y_1)\right] \quad . \tag{5-14f}$$

5.3.1 Factorization of the diffraction integral

As shown in Section 7.4, the angles θ_1 and θ_2 are

$$\theta_1 = \theta'_1 \cos \gamma + \theta'_2 \sin \gamma \quad ,$$
$$\theta_2 = -\theta'_1 \sin \gamma + \theta'_2 \cos \gamma \quad ,$$

where θ'_1 and θ'_2 are the angles to the observer in the coordinate system for the array diffraction pattern.

The diffraction pattern of the array is given at a matrix of points (θ'_1, θ'_2) at intervals $\Delta\theta$ in both directions. Let

$$\theta'_{1L} = L\, \Delta\theta \quad ,$$
$$\theta'_{2M} = M\, \Delta\theta \quad ,$$

where L and M are indices labeling points in the array diffraction pattern. Substituting the expressions for θ_1' and θ_2' into those for θ_1 and θ_2, we have

$$\theta_{1L} = L\,\Delta\theta \cos\gamma + M\,\Delta\theta \sin\gamma \quad ,$$

$$\theta_{2M} = -\,L\,\Delta\theta \sin\gamma + M\,\Delta\theta \cos\gamma \quad .$$

Putting these expressions into equations (5-9) gives

$$\alpha = a - k\,\Delta\theta\,(L \cos\gamma + M \sin\gamma) \quad , \tag{5-15a}$$

$$\beta = b - k\,\Delta\theta\,(-\,L \sin\gamma + M \cos\gamma) \quad . \tag{5-15b}$$

The expression for Q_I from equation (5-11) can be substituted into equation (5-13) for P_{IJ}:

$$\begin{aligned} P_{IJ} &= \beta C_I + (\alpha + \beta S_I)\,Y_J \\ &= \alpha Y_J + \beta(C_I + S_I Y_J) \\ &= \alpha Y_J + \beta Z_{IJ} \quad , \end{aligned} \tag{5-16}$$

where

$$Z_{IJ} = C_I + S_I Y_J \quad ,$$

in which C_I is the slope of the boundary line, S_I is the intercept of the boundary line, and Y_J represents the integration limits in Y. Incorporating α and β into P_{IJ}, we get

$$P_{IJ} = \left[a - k\,\Delta\theta\,(L\cos\gamma + M\sin\gamma)\right] Y_J + \left[b - k\,\Delta\theta\,(-L\sin\gamma + M\cos\gamma)\right] Z_{IJ}$$

$$= aY_J + bZ_{IJ} + Lk\,\Delta\theta\,(-Y_J\cos\gamma + Z_{IJ}\sin\gamma)$$

$$+ Mk\,\Delta\theta\,(-Y_J\sin\gamma - Z_{IJ}\cos\gamma) \quad .$$

We can simplify this by defining

$$U_{IJ} \equiv aY_J + bZ_{IJ} \quad ,$$

$$V_{IJ} \equiv k\,\Delta\theta\,(-Y_J\cos\gamma + Z_{IJ}\sin\gamma) \quad ,$$

$$W_{IJ} \equiv k\,\Delta\theta\,(-Y_J\sin\gamma - Z_{IJ}\cos\gamma) \quad ,$$

which gives us

$$P_{IJ} = U_{IJ} + LV_{IJ} + MW_{IJ} \quad . \tag{5-17}$$

The terms $e^{iP_{IJ}}$ for a trapezoid in equations (5-14a, b, c) can then be written

$$e^{iP_{IJ}} = e^{i(U_{IJ} + LV_{IJ} + MW_{IJ})}$$

$$= e^{iU_{IJ}} \left(e^{iV_{IJ}}\right)^L \left(e^{iW_{IJ}}\right)^M \quad .$$

The above expression is the product of two factors, the first containing only the index L and the second containing only the index M. When computing the diffraction pattern for all values of L and M, the computation time can be reduced by precomputing and saving the factors $e^{iU_{IJ}}\left(e^{iV_{IJ}}\right)^L$ and $\left(e^{iW_{IJ}}\right)^M$. The powers of the exponentials can be computed by repeated complex multiplication. Since I and J have two values each, and since the range of L and M is n, each matrix has 4n terms. It is not necessary to store all the powers of $e^{iW_{IJ}}$ simultaneously; the values of $E(\theta'_{1L}, \theta'_{2M})$ can be computed for all L for the first value of M and then $\left(e^{iW_{IJ}}\right)^M$ can be raised to the M+1 power to find $E(\theta'_{1L}, \theta'_{2,M+1})$ for all values of L.

Substitution of α and β into $e^{i\beta C_I}$ and $e^{i\alpha Y_J}$ gives

$$e^{i\beta C_I} = e^{i(b + k\,\Delta\theta\, L \sin\gamma) C_I}\, e^{i(-k\,\Delta\theta\, M \cos\gamma) C_I} ,$$

$$e^{i\alpha Y_J} = e^{i(a - k\,\Delta\theta\, L \cos\gamma) Y_J}\, e^{i(-k\,\Delta\theta\, M \sin\gamma) Y_J} .$$

These expressions can also be factored into terms involving only the index L or M, and thus the diffraction pattern can be computed by complex multiplication.

5.3.2 Reverse order of integration

When it is necessary to reverse the order of integration over the variables, the problem is reformulated, as shown in Figure 45. The solution proceeds as before, except that the roles of y and z and those of α and β are interchanged. The formulas summarized in the previous section and the results derived therein can be converted to the present case by making those substitutions plus, when α and β do not appear explicitly, the following:

$L \rightarrow M$,

$M \rightarrow L$,

$\gamma \rightarrow -\gamma$.

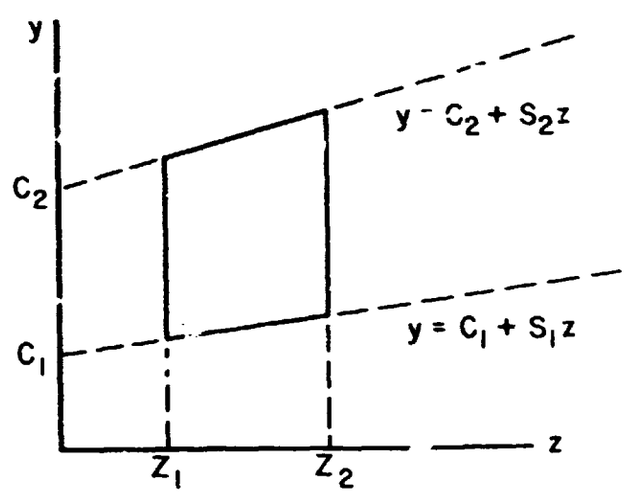

Figure 45. Trapezoid aperture, reverse order of integration.

5.4 Diffraction Integral for an Arbitrary Shape

For an arbitrary shape, we can calculate the diffraction integral by letting the field u′ be given by equation (5-8) over a plane surface bounded by a curve $z_1(y)$ on the bottom and $z_2(y)$ on the top (see Figure 46). The Fraunhofer equation is integrable along any line in the plane, as the phase of u′ is linear over the region. Since the integration limits are not linear, integration over the second variable cannot, in general, be done, although numerical integration can be used.

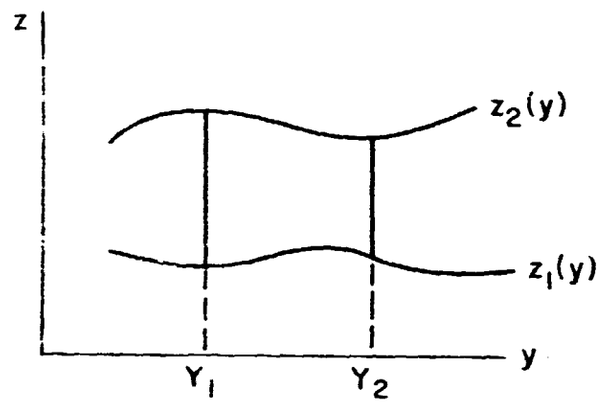

Figure 46. Aperture of arbitrary shape.

We get the following integral over the area by use of the modified Fraunhofer equation:

$$E(\theta_1, \theta_2) = \int_{y=Y_1}^{Y_2} \int_{z=z_1(y)}^{z_2(y)} e^{i(ay + bz)} e^{-ik(y\theta_1 + z\theta_2)} \, dy \, dz$$

$$= \int_{y=Y_1}^{Y_2} \int_{z=z_1(y)}^{z_2(y)} e^{i[(a - k\theta_1)y + (b - k\theta_2)z]} \, dy \, dz \quad .$$

Using α and β as defined previously [eq. (5-9)], we get

$$E(\alpha,\beta) = \int_{y=Y_1}^{Y_2} \int_{z=z_1(y)}^{z_2(y)} e^{i(\alpha y + \beta z)}\, dy\, dz \quad .$$

If $\beta \neq 0$,

$$E(\alpha,\beta) = \int_{y=Y_1}^{Y_2} \frac{1}{i\beta} \left\{ e^{i[\alpha y + \beta z_2(y)]} - e^{i[\alpha y + \beta z_1(y)]} \right\} dy \quad . \tag{5-18}$$

The integral consists of two terms, both of the form

$$\int_{y=Y_1}^{Y_2} \frac{1}{i\beta}\, e^{i[\alpha y + \beta z_I(y)]}\, dy \quad ,$$

where I is either 1 or 2. The integral can thus be represented approximately by

$$\int_{y=Y_1}^{Y_2} \frac{1}{i\beta}\, e^{i[\alpha y + \beta z_I(y)]}\, dy \approx \sum_J \frac{1}{i\beta}\, e^{i(\alpha Y_J + \beta Z_{IJ})}\, \Delta y \quad . \tag{5-19}$$

The diffraction pattern will be computed at equal intervals $\Delta\theta$ of the angles θ_1' and θ_2'. The quantity $\alpha Y_J + \beta Z_{IJ}$ is the same as P_{IJ} as given in equation (5-16). Substituting equation (5-17) for $\alpha Y_J + \beta Z_{IJ}$ into equation (5-19), we get

$$\sum_J \frac{1}{i\beta} e^{i(\alpha Y_J + \beta Z_{IJ})} = \sum_J \frac{1}{i\beta}\, e^{i(U_{IJ} + LV_{IJ} + MW_{IJ})}$$

$$= \sum_J \left[\frac{1}{i\beta}\, e^{iU_{IJ}} \left(e^{iV_{IJ}}\right)^L \right] \left(e^{iW_{IJ}}\right)^M \quad ,$$

which, in turn, can be substituted into equation (5-18) to give

$$E_{LM} = \frac{1}{i} \sum_J \left\{ \left[\frac{1}{\beta} e^{iU_{2J}} \left(e^{iV_{2J}} \right)^L \right] \left(e^{iW_{2J}} \right)^M - \left[\frac{1}{\beta} e^{iU_{1J}} \left(e^{iV_{1J}} \right)^L \right] \left(e^{iW_{1J}} \right)^M \right\} \Delta y \quad . \tag{5-20}$$

Equation (5-20) can be factored into terms containing only L or only M. The computation time can be reduced by precomputing and saving the factors, so that each value of E_{LM} can be determined by complex multiplication.

The quantities $e^{iU_{LJ}} \left(e^{iV_{LJ}} \right)^L$ and $\left(e^{iW_{LJ}} \right)^M$ each consist of 2mn terms, where 2 is the range of I, m is the range of J, and n is the range of L and M. The powers of $e^{iW_{LJ}}$ do not need to be stored simultaneously. The values of E_{LM} for the first value of M can be computed for all L and then the quantities $\left(e^{iW_{LJ}} \right)^M$ can be raised to the M+1 power to find $E_{L,M+1}$ for all L.

If $\beta = 0$,

$$E(\alpha, 0) = \int_{y=Y_1}^{Y_2} \int_{z=z_1(y)}^{z_2(y)} e^{i(\alpha y)} \, dy \, dz$$

$$= \int_{y=Y_1}^{Y_2} e^{i\alpha y} \left[z_2(y) - z_1(y) \right] dy$$

$$\approx \sum_J e^{i\alpha Y_J} \left(Z_{2J} - Z_{1J} \right) \Delta y \quad .$$

After incorporating equation (5-15a), we get

$$E_{LM} = \sum_J e^{i[\alpha - k \Delta\theta (L \cos \gamma + M \sin \gamma)] Y_J} \left(Z_{2J} - Z_{1J} \right) \Delta y$$

$$= \sum_J e^{iU_J} \left(e^{iV_J} \right)^L \left(e^{iW_J} \right)^M \left(Z_{2J} - Z_{1J} \right) \Delta y \quad ,$$

where

$$U_J \equiv aY_J \quad ,$$

$$V_J \equiv -k\,\Delta\theta\, Y_J \cos\gamma \quad ,$$

$$W_J \equiv -k\,\Delta\theta\, Y_J \sin\gamma \quad .$$

The quantities $e^{iU_J}\left(e^{iV_J}\right)^L$, e^{iW_J}, and Z_{IJ} should be precomputed and saved. Those for $\left(e^{iW_J}\right)^M$ are computed by multiplying each successive power by e^{iW_J} to obtain the next higher power.

If $\alpha = \beta = 0$,

$$E(\alpha,\beta) = \int_{y=Y_1}^{Y_2} \int_{z=z_1(y)}^{z_2(y)} dx\, dy \approx \sum_J (Z_{2J} - Z_{1J})\,\Delta y \quad .$$

5.5 Diffraction Pattern of a Cube Corner

From the modified Fraunhofer integral [eq. (5-4)], the complex polarization state $\vec{E}'(\theta_1,\theta_2)$ in the far field of a cube corner is

$$\vec{E}'(\theta_1,\theta_2) = \frac{1}{S}\sum_I \vec{E}_I \iint_{s_I} e^{i(a_I y + b_I z)}\, e^{-ik(y\theta_1 + z\theta_2)}\, dy\, dz \quad , \tag{5-21}$$

where $\vec{E}_I$ is the polarization vector for the Ith sector, s_I is the area of the Ith sector, and a_I and b_I are the phase gradients in the y and z directions, respectively, due to dihedral-angle offsets for the Ith sector. The intensity of each component of polarization is

$$F'_y(\theta_1,\theta_2) = E'_y(\theta_1,\theta_2)\, E'^{*}_y(\theta_1,\theta_2) \quad ,$$

$$F'_z(\theta_1,\theta_2) = E'_z(\theta_1,\theta_2)\, E'^{*}_z(\theta_1,\theta_2) \quad ,$$

and the total intensity is

$$F'(\theta_1, \theta_2) = F'_y(\theta_1, \theta_2) + F'_z(\theta_1, \theta_2) \quad .$$

The amplitude A_p of the reflected field in a polarization state given by the complex unit vector $\vec{P}$ is obtained by taking the dot product of $\vec{P}$ and $\vec{E}'$:

$$A_p = \vec{P} \cdot \vec{E}' = P_y^* E'_y + P_z^* E'_z \quad .$$

The field $\vec{E}'_p$ having the polarization $\vec{P}$ is

$$\vec{E}'_p = A_p \vec{P} \quad ,$$

and its intensity I_p is

$$I_p = \vec{E}'_p \cdot \vec{E}'_p = A_p^* A_p \quad .$$

The method of computing the six polarization vectors E_I was given in Section 4.4, and the phase gradients a_I and b_I were computed in Section 2.11.3. The angular boundaries of the six sectors and the order of reflection corresponding to each were given in Section 2.12. The active reflecting area S at normal incidence and the integration limits for each section s_I will depend on the shape of the front face. The integration for the polygon can be done analytically since the integration limits are linear. The circular reflector requires numerical integration over one variable.

5.5.1 Diffraction pattern of triangular and hexagonal retroreflectors

The previous section gave the diffraction integral for a cube corner. Now we need to determine the integration limits for each section s_I and for the total active reflecting area S at normal incidence. For both triangular and hexagonal cube corners, the active area at normal incidence is a hexagon of area $\sqrt{3}W^2/2$, where W

is the width across flats. The following subsections describe how to set up the integration limits and perform the integration over each of the six sectors. Since each section is a polygon, the region of integration is defined by giving the vertices of the polygon. The coordinates of the vertices of the total active reflecting area are given in Sections 5.5.1.1 and 5.5.1.2.

If the phase and amplitude of the reflected beam are constant over the face of the cube corner, the retroreflector acts like a simple aperture. The methods described in Smith and Marsh (1974) are applicable in this case.

Julian, Hieser, and Magill (1970) compared measured and computed diffraction patterns of hexagonal cube corners. The analysis includes the effects of dihedral-angle offsets and polarization changes at the reflecting faces. The technique is completely analytical and can be applied to any cube corner whose face is cut in the shape of a regular polygon. A circular face can be adequately approximated by a regular polygon with a large number of sides.

5.5.1.1 Vertices of the active reflecting area for a triangular retroreflector

In Section 3.2, the active reflecting area was computed for a triangular retroreflector. Here, we compute the coordinates of the vertices of the active reflecting area for use in calculating the diffraction pattern of the cube corner. Much of the information needed to locate the vertices was provided in Section 3.2.

Referring to Figure 28 for Case 1 in Section 3.2, let y, z coordinate axes be set up as shown in Figure 47. Three of the vertices are numbered counterclockwise; the positions of the other three can be computed by symmetry from the positions of the first three (see Section 2.3). By using the distances calculated for Case 1, the coordinates of the three vertices numbered in the diagram are

$$y_1 = W + \frac{W}{2} = \frac{3W}{2} \quad ,$$

$$z_1 = -\frac{\overline{ae}}{2} + \overline{\ell e}$$

$$= -\frac{1}{\sqrt{3}}\left(\frac{W}{2} + D\cos\theta\right) + D\sin\theta \quad ,$$

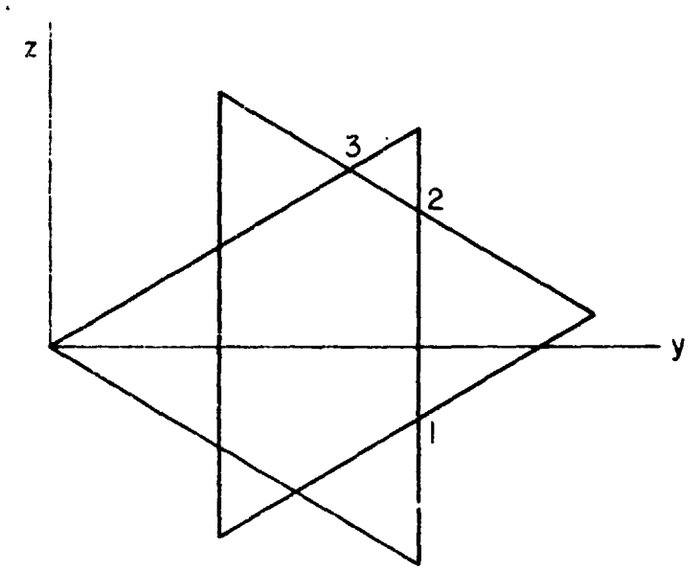

Figure 47. Triangular retroreflector ($\theta > 0°$), Case 1.

$$y_2 = y_1 = \frac{3W}{2} \quad ,$$

$$z_2 = \overline{ad} + \overline{bk} = \frac{\overline{ae}}{2} + \overline{bk}$$

$$= \frac{1}{\sqrt{3}}\left(\frac{W}{2} + D\cos\theta\right) + D\sin\theta \quad ,$$

$$y_3 = \overline{cd} + \overline{ai}$$

$$= \frac{W}{2} + D\cos\theta + \frac{1}{2}\left(W - D\cos\theta + \sqrt{3}D\sin\theta\right)$$

$$= W + \frac{D}{2}\cos\theta + \sqrt{3}\,\frac{D}{2}\sin\theta$$

$$= W + \frac{1}{2}\left(D\cos\theta + \sqrt{3}D\sin\theta\right) \quad ,$$

$$z_3 = \frac{\overline{ae}}{2} + \overline{hi}$$

$$= \frac{1}{2\sqrt{3}}\left(W + 2D\cos\theta\right) + \frac{1}{2\sqrt{3}}\left(W - D\cos\theta + \sqrt{3}D\sin\theta\right)$$

$$= \frac{1}{2\sqrt{3}}\left(2W + D\cos\theta + \sqrt{3}D\sin\theta\right) \quad .$$

The above formulas apply to the range $0° < \theta < 60°$. Since the physical situation repeats every 120°, all cases can be covered by adding formulas for the range $-60° < \theta < 0°$. In Figure 48, three of the vertices are numbered for the case $\theta < 0°$. This figure is the same as Figure 47, reversed from top to bottom; thus, we can obtain the coordinates of the vertices for the case $-60° < \theta < 0°$ by computing the coordinates for θ and then reversing both the order of the points and the sign of the z coordinates. Since only $\sin\theta$ is affected by a change of sign in θ, the expressions for the case $-60° < \theta < 0°$ can be written

$$y_1 = W + \frac{1}{2}\left(D\cos\theta + \sqrt{3}D\,|\sin\theta|\right) \quad ,$$

$$z_1 = -\frac{1}{2\sqrt{3}}\left(2W + D\cos\theta + \sqrt{3}D\,|\sin\theta|\right) \quad ,$$

$$y_2 = \frac{3W}{2} \quad ,$$

$$z_2 = -\frac{1}{\sqrt{3}}\left(\frac{W}{2} + D\cos\theta\right) - D\,|\sin\theta| \quad ,$$

$$y_3 = \frac{3W}{2} \quad ,$$

$$z_3 = \frac{1}{\sqrt{3}}\left(\frac{W}{2} + D\cos\theta\right) - D\,|\sin\theta| \quad .$$

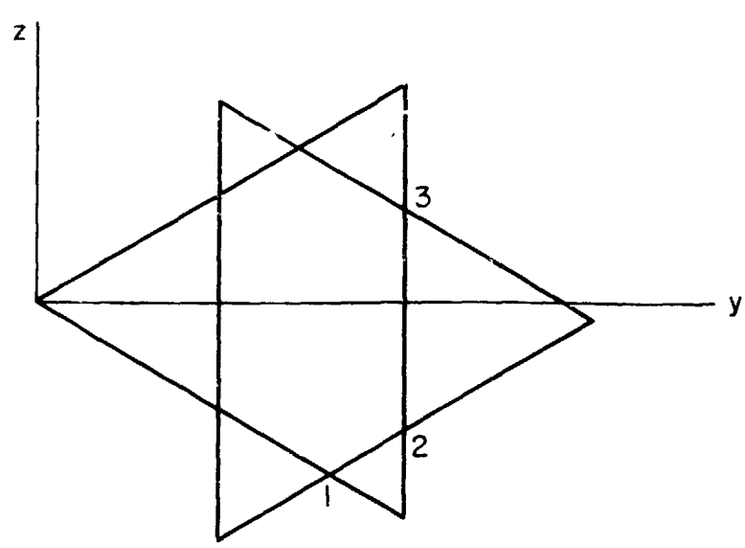

Figure 48. Triangular retroreflector ($\theta < 0°$), Case 1.

Case 2 is given in Figure 49 with coordinate axes drawn and two of the vertices numbered. The distances needed were given in Figures 27 and 28 for normal incidence and Case 1 in Section 3.2. The coordinates of the points are

$$y_1 = \frac{W}{2} + W = \frac{3W}{2} \quad ,$$

$$z_1 = \frac{\sqrt{3}W}{2} \quad ,$$

$$y_2 = \overline{cd} = \frac{W}{2} + D \cos \theta \quad ,$$

$$z_2 = \frac{1}{\sqrt{3}} \overline{cd} = \frac{1}{\sqrt{3}} \left(\frac{W}{2} + D \cos \theta\right) \quad .$$

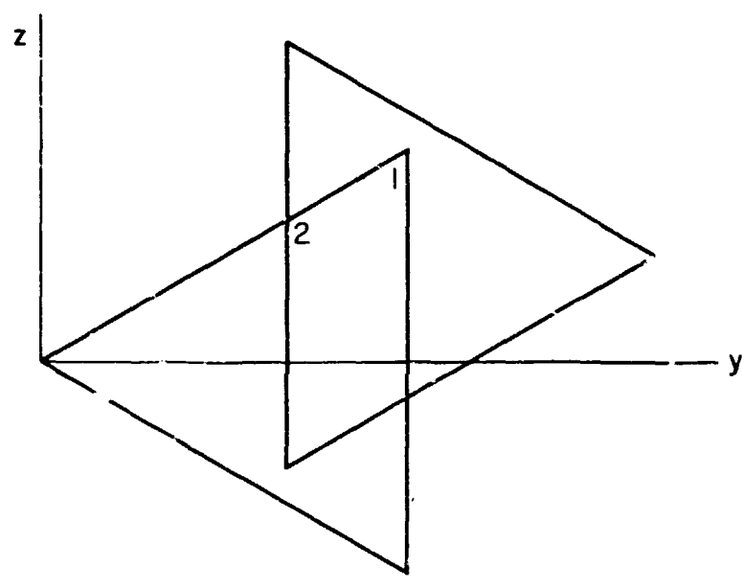

Figure 49. Triangular retroreflector ($\theta > 0°$), Case 2.

The above formulas apply to the range $0° < \theta < 60°$, while Figure 50 shows the case $-60° < \theta < 0°$. The coordinates of these vertices are

$$y_1 = \frac{W}{2} + D \cos \theta \quad ,$$

$$z_1 = -\frac{1}{\sqrt{3}} \left(\frac{W}{2} + D \cos \theta \right) \quad ,$$

$$y_2 = \frac{3W}{2} \quad ,$$

$$z_2 = -\frac{\sqrt{3}W}{2} \quad .$$

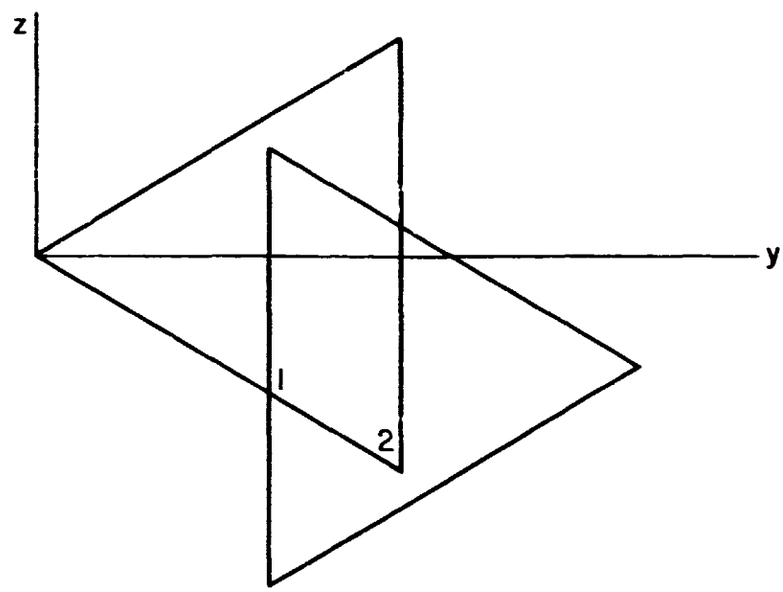

Figure 50. Triangular retroreflector ($\theta < 0°$), Case 2.

From Figure 27, we see that the coordinates of the center of the active reflecting area at normal incidence are $y = W$, $z = 0$, while for other incidence angles (see Figure 28), the right-hand triangle is displaced by $\Delta y = D \cos \theta$, $\Delta z = D \sin \theta$ and the center of the active reflecting area is displaced by $\Delta y/2$, $\Delta z/2$. Therefore, the coordinates of the center of the active reflecting area are

$$y_c = W + \frac{1}{2} D \cos \theta \quad ,$$

$$z_c = \frac{1}{2} D \sin \theta \quad ,$$

and those of the vertices with respect to this center are

$$y_i' = y_i - y_c \quad , \tag{5-22a}$$

$$z_i' = z_i - z_c \quad . \tag{5-22b}$$

Figure 51 shows the y'', z'' axes, where the z'' axis is perpendicular to the plane of incidence. The coordinates of these vertices are

$$y_i'' = y_i' \cos\theta + z_i' \sin\theta \quad , \tag{5-23a}$$

$$z_i'' = -y_i' \sin\theta + z_i' \cos\theta \quad . \tag{5-23b}$$

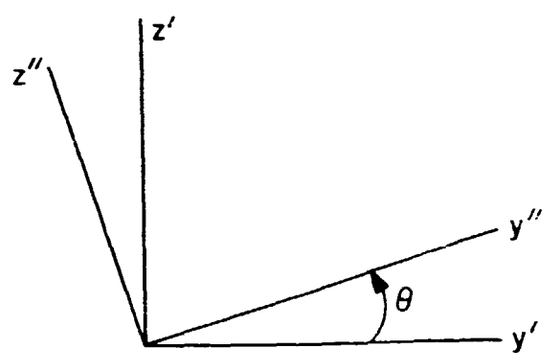

Figure 51. Relationship between y', z' and y'', z'' axes.

Equations (5-22) and (5-23) are in a form that can easily be used in a computer program. The algebra, though, is somewhat tedious: First we have to substitute the expressions for y_i, z_i to obtain y_i', z_i' and then substitute y_i', z_i' to obtain y_i'', z_i''. We have employed an algebra program to perform the substitutions, and the results are given below.

Case 1

$$y_1 = \frac{W}{2}\left(\cos\theta - \frac{|\sin\theta|}{\sqrt{3}}\right) + D\left(\sin^2\theta - \frac{1}{2} - \frac{\cos\theta\,|\sin\theta|}{\sqrt{3}}\right)$$

$$z_1 = -\frac{W}{2}\left(|\sin\theta| + \frac{\cos\theta}{\sqrt{3}}\right) + D\left(\cos\theta\,|\sin\theta| - \frac{\cos^2\theta}{\sqrt{3}}\right) ,$$

$$y_2 = \frac{W}{2}\left(\frac{|\sin\theta|}{\sqrt{3}} + \cos\theta\right) + D\left(\sin^2\theta - \frac{1}{2} + \frac{\cos\theta\,|\sin\theta|}{\sqrt{3}}\right) \quad ,$$

$$z_2 = \frac{W}{2}\left(\frac{\cos\theta}{\sqrt{3}} - |\sin\theta|\right) + D\left(\cos\theta\,|\sin\theta| + \frac{\cos^2\theta}{\sqrt{3}}\right) \quad ,$$

$$y_3 = W\frac{|\sin\theta|}{\sqrt{3}} + \frac{2D}{\sqrt{3}}\cos\theta\,|\sin\theta| \quad ,$$

$$z_3 = W\frac{\cos\theta}{\sqrt{3}} + \frac{2D}{\sqrt{3}}\left(\frac{1}{4} - \sin^2\theta\right) \quad .$$

<u>Case 2</u>

$$y_1 = \frac{W}{2}(\sqrt{3}\,|\sin\theta| + \cos\theta) - \frac{D}{2} \quad ,$$

$$z_1 = \frac{W}{2}(\sqrt{3}\cos\theta - |\sin\theta|) \quad ,$$

$$y_2 = \frac{W}{2}\left(\frac{|\sin\theta|}{\sqrt{3}} - \cos\theta\right) + D\left(\frac{1}{2} - \sin^2\theta + \frac{\cos\theta\,|\sin\theta|}{\sqrt{3}}\right) \quad ,$$

$$z_2 = \frac{W}{2}\left(|\sin\theta| + \frac{\cos\theta}{\sqrt{3}}\right) + D\left(\frac{\cos^2\theta}{\sqrt{3}} - \cos\theta\,|\sin\theta|\right) \quad .$$

These equations are for the range $0° < \theta < 60°$. The absolute-value signs on $\sin\theta$ make it possible to use the same expressions for the range $-60° < \theta < 0°$ by reversing the order of the points as well as the sign of z_i. All y coordinates must be multiplied by $\cos\phi$ to get the coordinate of each vertex parallel to the plane of incidence on a plane perpendicular to the line of sight.

5.5.1.2 Vertices of the active reflecting area for a hexagonal retroreflector

In this section, the coordinates of the vertices of the active reflecting area are computed for use in calculating the diffraction pattern of a hexagonal cube corner. Distances calculated in Section 3.3 are used in the derivation.

Referring to Figure 32 for Case 1 in Section 3.3, let the y, z coordinate axes be set up as shown in Figure 52. Only three of the vertices are numbered; the positions of the other three can be computed by symmetry (see Section 2.3). By using the distances calculated for Case 1, the coordinates of the numbered vertices are

$$y_1 = \frac{1}{2}\overline{ag} + \overline{gi} + \overline{fc}$$

$$= \frac{1}{2}\frac{W}{\sqrt{3}} + \frac{W}{\sqrt{3}} + \frac{D}{\sqrt{3}}\sin\theta$$

$$= \frac{\sqrt{3}W}{2} + \frac{D}{\sqrt{3}}\sin\theta \quad .$$

$$z_1 = -\frac{W}{2} + \overline{bc}$$

$$= -\frac{W}{2} + D\sin\theta \quad ,$$

$$y_2 = \frac{2W}{\sqrt{3}} \quad ,$$

$$z_2 = 0 \quad ,$$

$$y_3 = \frac{1}{2}\overline{ag} + \overline{gi}$$

$$= \frac{1}{2}\frac{W}{\sqrt{3}} + \frac{W}{\sqrt{3}}$$

$$= \frac{\sqrt{3}W}{2} \quad ,$$

$$z_3 = \frac{W}{2} \quad .$$

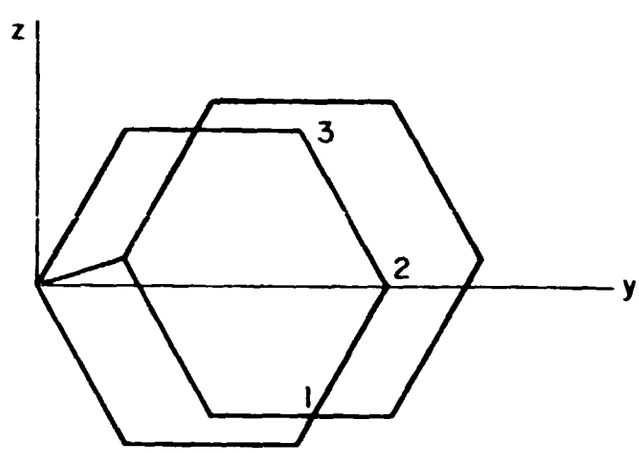

Figure 52. Hexagonal retroreflector ($\theta > 0°$), Case 1.

These formulas apply to the range $0° < \theta < 30°$. Since the geometry repeats every 60°, all cases can be covered by adding formulas for the range $-30° < \theta < 0°$. In Figure 53, three of the vertices are numbered for the case $\theta < 0°$. Figure 53 is the same as the one for $\theta > 0°$, reversed from top to bottom. The coordinates of the vertices are obtained by computing the coordinates with $|\theta|$ in the formulas for $\theta > 0°$ and then reversing the order of the points and the sign of the z coordinates. Since only $\sin\theta$ is affected by the sign of θ, the coordinates of the vertices for the range $-30° < \theta < 0°$ can be written

$$y_1 = \frac{\sqrt{3}W}{2} \quad ,$$

$$z_1 = -\frac{W}{2} \quad ,$$

$$y_2 = \frac{2W}{\sqrt{3}} \quad ,$$

$$z_2 = 0 \quad ,$$

$$y_3 = \frac{\sqrt{3}W}{2} + \frac{D}{\sqrt{3}} |\sin\theta| \quad ,$$

$$z_3 = \frac{W}{2} - D |\sin\theta| \quad .$$

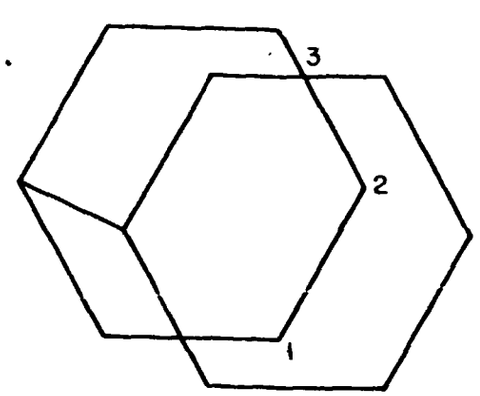

Figure 53. Hexagonal retroreflector ($\theta < 0°$), Case 1.

Figure 54 shows Case 2 with coordinate axes drawn and two of the vertices numbered. Using the distances from Figures 31 and 33 in Section 3.3, we get the following coordinates of the points:

$$y_1 = \frac{2W}{\sqrt{3}} \quad ,$$

$$z_1 = 0 \quad ,$$

$$y_2 = \overline{ac} + \frac{1}{2}\,\overline{bk}$$

$$= D\cos\theta + \frac{1}{2}\frac{1}{\sqrt{3}}\,(2W - \sqrt{3}D\cos\theta - D\sin\theta) \quad ,$$

$$z_2 = \overline{bc} + \overline{jm}$$

$$= D\sin\theta + \frac{1}{2}\,(2W - \sqrt{3}D\cos\theta - D\sin\theta) \quad .$$

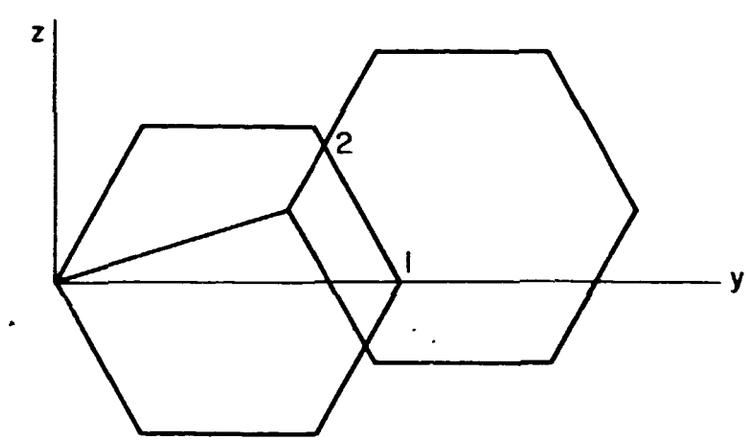

Figure 54. Hexagonal retroreflector ($\theta > 0°$), Case 2.

These formulas apply to the range $0° < \theta < 30°$. For the range $-30° < \theta < 0°$, the coordinates of the vertices (see Figure 55) are

$$y_1 = D \cos\theta + \frac{1}{2}\frac{1}{\sqrt{3}}(2W - \sqrt{3}D \cos\theta - D|\sin\theta|) \quad ,$$

$$z_1 = -D|\sin\theta| - \frac{1}{2}(2W - \sqrt{3}D \cos\theta - D|\sin\theta|) \quad ,$$

$$y_2 = \frac{2W}{\sqrt{3}} \quad ,$$

$$z_2 = 0 \quad .$$

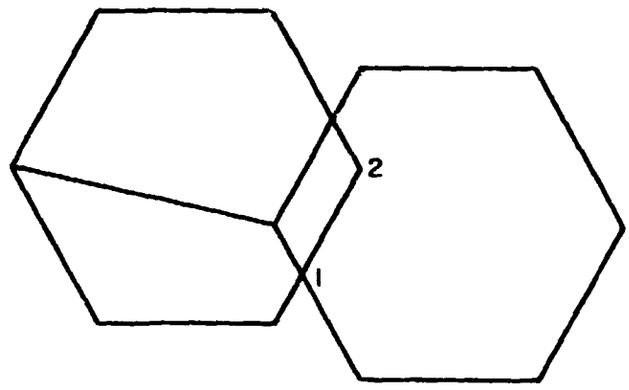

Figure 55. Hexagonal retroreflector ($\theta < 0°$), Case 2.

Figure 31 in Section 3.3 gave $y = W/\sqrt{3}$, $z = 0$ as the coordinates of the center of the active reflecting area at normal incidence. At other incidence angles, the right-hand hexagon is displaced by $\Delta y = D \cos\theta$, $\Delta z = D \sin\theta$, and the center of the active reflecting area, by $\Delta y/2$, $\Delta z/2$. Therefore, the coordinates of the active reflecting area are

$$y_c = \frac{W}{\sqrt{3}} + \frac{1}{2} D \cos\theta \quad ,$$

$$z_c = \frac{1}{2} D \sin\theta \quad ,$$

and the coordinates of the vertices with respect to the center of the active reflecting area are given by equations (5-22). The transformation to y″, z″ coordinates with the z″ axis perpendicular to the plane of incidence is shown in equations (5-23).

Using an algebra program for the substitutions, we get the following expressions for y_i'' and z_i'':

Case 1

$$y_1 = \frac{W}{2}\left(\frac{\cos\theta}{\sqrt{3}} - |\sin\theta|\right) + D\left(\sin^2\theta - \frac{1}{2} + \frac{\cos\theta\,|\sin\theta|}{\sqrt{3}}\right) ,$$

$$z_1 = -\frac{W}{2}\left(\frac{|\sin\theta|}{\sqrt{3}} + \cos\theta\right) + D\left(\cos\theta\,|\sin\theta| - \frac{\sin^2\theta}{\sqrt{3}}\right) ,$$

$$y_2 = W\frac{\cos\theta}{\sqrt{3}} - \frac{D}{2} ,$$

$$z_2 = -W\frac{|\sin\theta|}{\sqrt{3}} ,$$

$$y_3 = \frac{W}{2}\left(|\sin\theta| + \frac{\cos\theta}{\sqrt{3}}\right) - \frac{D}{2} ,$$

$$z_3 = \frac{W}{2}\left(\cos\theta - \frac{|\sin\theta|}{\sqrt{3}}\right) .$$

Case 2

$$y_1 = W\frac{\cos\theta}{\sqrt{3}} - \frac{D}{2} ,$$

$$z_1 = -W\frac{|\sin\theta|}{\sqrt{3}} ,$$

$$y_2 = W|\sin\theta| - 2D\frac{\cos\theta\,|\sin\theta|}{\sqrt{3}} ,$$

$$z_2 = W\cos\theta + 2D\left(\frac{\sin^2\theta}{\sqrt{3}} - \frac{\sqrt{3}}{4}\right) .$$

These equations are for the range $0° < \theta < 30°$. Because of the absolute-value signs on $\sin\theta$, we can use the same expressions for the range $-30° < \theta < 0°$ by reversing the order of the points and the sign of z_i. All y coordinates must be multiplied by $\cos\phi$ to obtain the coordinate of each vertex parallel to the plane of incidence on a plane perpendicular to the line of sight.

5.5.1.3 Vertices of a sector

The vectors $\vec{A}_I$ dividing the active reflecting area of a cube corner into six sectors were computed in Section 2.12. Let V_{yJ} and V_{zJ} be the coordinates of the vertices of the active reflecting area on a plane perpendicular to the line of sight. The angles v_J to each vertex are

$$v_J = \tan^{-1} \frac{V_{zJ}}{V_{yJ}} ,$$

and the angles of the boundary lines are

$$a_I = \tan^{-1} \frac{A_{zI}}{A_{yI}} .$$

The vertices within a sector whose boundary lines have the angles a_I and a_{I+1} are those for which

$$a_I \leq v_J \leq a_{I+1} .$$

In addition, the vertices of a sector include the origin and the intersections of the two boundary lines with the sides of the active reflecting area. The intersections are computed by means of the method described in Section 5.5.1.4. Figure 56 gives an example of a sector with the vertices numbered.

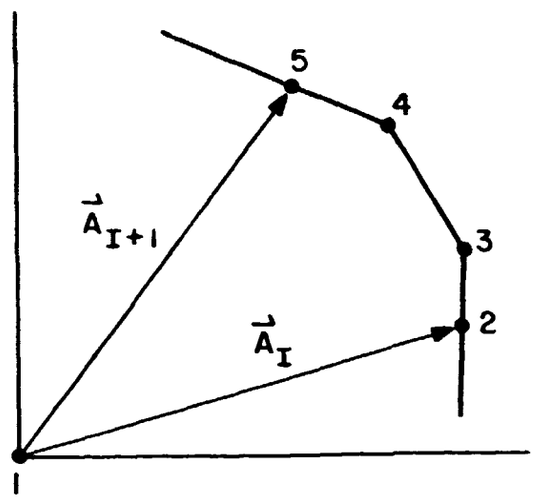

Figure 56. Vertices of a sector.

5.5.1.4 Intersection of two line segments

We give herein a systematic method of testing for singularities in computing the intersection of a sector boundary and a side of the active reflecting area. The sector boundary is a line starting at the origin ($y = z = 0$) and extending to one of the sides. Let the other end of the sector boundary be given by the coordinates y_A, z_A. Let y_1, z_1 and y_2, z_2 be the ends of the side that is intersected by the boundary (Figure 57).

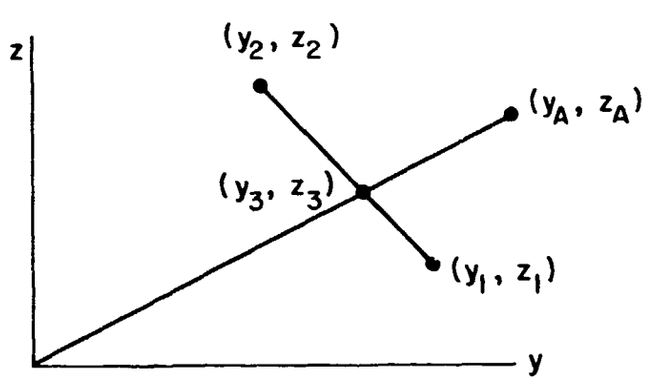

Figure 57. Intersection of two line segments.

Let

$$\Delta y = y_2 - y_1 \quad , \tag{5-24a}$$

$$\Delta z = z_2 - z_1 \quad . \tag{5-24b}$$

The slopes of the lines are

$$S_A = \frac{y_A}{z_A} \quad ,$$

$$S_B = \frac{\Delta y}{\Delta z} \quad .$$

The equation of the sector boundary is

$$z = S_A y \quad , \tag{5-25}$$

and that of the intersecting side is

$$z = C + S_B y \quad , \tag{5-26}$$

where

$$C = z_1 - S_B y_1 \quad .$$

If there are no singularities, the intersection y_3, z_3 is obtained by solving equations (5-25) and (5-26) simultaneously. Substituting the former into the latter, we get

$$S_A y = C + S_B y \quad .$$

The y_3 coordinate of the intersection is

$$y_3 = \frac{C}{S_A - S_B} \quad .$$

By substituting y_3 into equation (5-25), the other coordinate of the intersection is

$$z_3 = S_A y_3 \quad .$$

After equations (5-24) have been computed, we can apply the following outline as a sequence for performing the computations and testing for singularities and error conditions:

A. If $y_A \neq 0$, compute $S_A = z_A/y_A$.

1. If $y_1 \neq y_2$, compute

$$S_B = \Delta z/\Delta y \quad ,$$
$$C = z_1 - Sy_1 \quad .$$

a. If $S_B \neq S_A$, compute

$$y_3 = C/(S_A - S_B) \quad ,$$
$$z_3 = S_A y_3 \quad .$$

b. If $S_B = S_A$, the lines do not intersect.

2. If $y_1 = y_2$, then

$$y_3 = y_1 = y_2 \quad ,$$
$$z_3 = S_A y_3 \quad .$$

B. If $y_A = 0$, then $y_3 = 0$.

1. If $y_1 \neq y_2$, compute

$$S_B = \Delta z/\Delta y \quad ,$$

$$z_3 = z_1 - S_B y_1 \quad .$$

2. If $y_1 = y_2$, the lines do not intersect.

5.5.1.5 Integration limits for a sector

Let Y_J and Z_J be the coordinates of the vertices defining one of the sectors of a retroreflector. The diffraction integral must be performed over the surface enclosed by connecting successive vertices by straight lines. Let the first and last vertices be the origin of coordinates and let the other points be given counterclockwise around the sector. The diffraction integral is done for each successive pair of points using equations (5-14) from Section 5.3. The integration limits for each pair of points indexed J and J+1 are

$$\int_{y=Y_{J+1}}^{Y_J} \int_{z=0}^{C+Sy} \quad ,$$

where

$$S = \frac{Z_{J+1} - Z_J}{Y_{J+1} - Y_J} \quad ,$$

$$C = Z_J - SY_J \quad .$$

If $Y_J = Y_{J+1}$, the integral is omitted for that pair of points.

5.5.2 Diffraction pattern of a circular reflector

Section 5.5 discussed the diffraction integral for a cube corner, except for how to determine the integration limits for each sector s_I and the total active reflecting area S at normal incidence. For a circular face with radius r, we have $S = \pi r^2$.

The integration is partly analytical, based on formulas (5-14), and partly numerical, based on Section 5.4. The numerical integration is done with a second-order technique (Section 5.5.2.7), with Section 5.5.2.6 showing which parts of the integration are numerical. To obtain the best results, it is sometimes necessary to reverse the order of integration over the variables (Section 5.5.2.5). Formulas for the z values at each numerical-integration point are given in Section 5.5.2.2, and the end points of the section of the ellipse bounding a sector are computed in Section 5.5.2.3. The Airy formula, which is useful for checking the more general methods in the special case of the Airy pattern, is given in Section 5.5.2.1.

Chang, Currie, and Alley (1971) present an analytical solution for the far-field diffraction pattern of a circular cube corner at normal incidence. Polarization effects are included, based on results from Peck (1972). The diffraction integral for each sextant is evaluated according to the methods of Mahan, Bitterli, and Cannon (1964).

5.5.2.1 Airy pattern

If the field u is constant across a circular aperture, the diffraction pattern is a function only of the angle θ from the center of the pattern. The intensity I is given by

$$I = I_0 G^2 \quad ,$$

where I_0 is the intensity at the center of the pattern and

$$G = \frac{2J_1(\pi d\theta/\lambda)}{\pi d\theta/\lambda} \quad ,$$

in which J_1 is the Bessel function of the first order and d is the diameter of the aperture. This formula is useful both for testing the numerical-integration techniques to make sure that they give the correct answer for this special case and for determining the accuracy of the numerical integration for various integration intervals.

5.5.2.2 Ellipse geometry

The active reflecting area of a circular retroreflector consists of the intersection of two circles as viewed in the plane of the front face (Figure 58) and two ellipses as viewed from the direction of the incident beam. The separation of the two circles is 2c, given by

$$2c = 2L \tan \phi' \quad ,$$

$$c = L \tan \phi' \quad ,$$

where L is the length of the cube corner and

$$\phi = \sin^{-1}\left(\frac{\sin \phi}{n}\right) \quad .$$

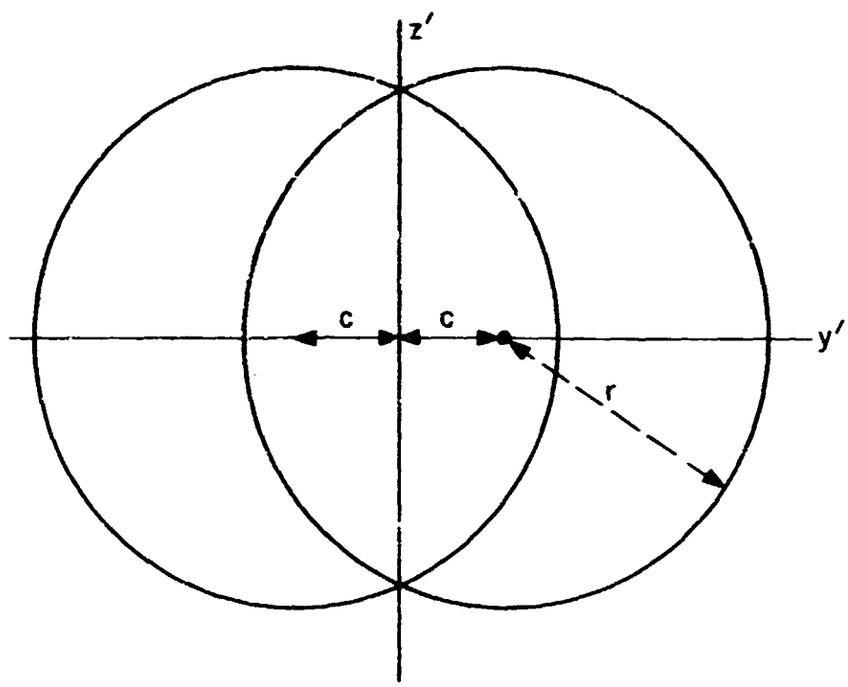

Figure 58. Intersection of input and output apertures for a circular reflector.

When viewed from the direction of the incident beam, distances in the y' direction are contracted by a factor a, where

$$a = \cos\phi \quad .$$

The equation of the circle in Figure 59a is

$$(y' - c)^2 + z'^2 = r^2 \quad .$$

The equation of the ellipse in Figure 59b is obtained by substituting $y' = y/a$ and $z' = z$, resulting in

$$\left(\frac{y}{a} - c\right)^2 + z^2 = r^2 \quad .$$

To integrate the diffraction pattern numerically, we must have values of z at equal intervals in y. Solving for z, we get

$$z = \pm\sqrt{r^2 - \left(\frac{y}{a} - c\right)^2} \quad , \tag{5-27}$$

where the plus sign gives the values at the top of the ellipse and the minus sign gives those at the bottom. Equation (5-27) is used for the left half of the aperture ($y \leq 0$). For the right half, the ellipse is centered at $y = -ac$, and the formula is

$$\left(\frac{y}{a} + c\right)^2 + z^2 = r^2 \quad ,$$

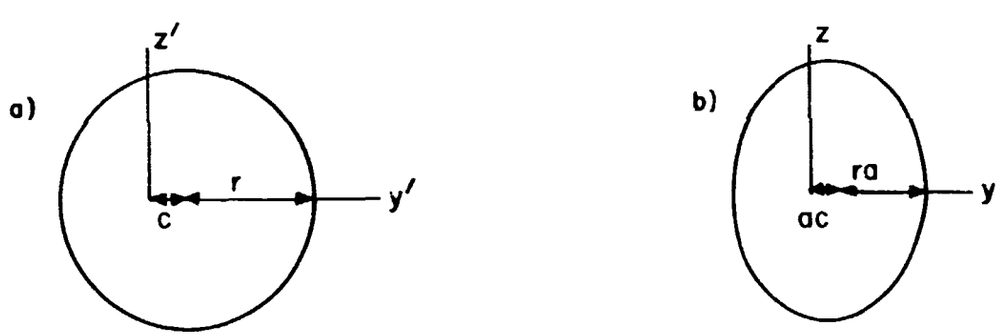

Figure 59. Ellipse geometry.

which can be solved for z to give

$$z = \pm \sqrt{r^2 - \left(\frac{y}{a} + c\right)^2} \quad .$$

Integrating first over z and then numerically over y does not give good results when the slope of the ellipse goes to infinity. As seen in Figure 60, the sector can be better integrated first in y and then in z. The triangular section remaining in Figure 60a can be integrated analytically. We need to express y as a function of z in order to perform the numerical integration in the variable z.

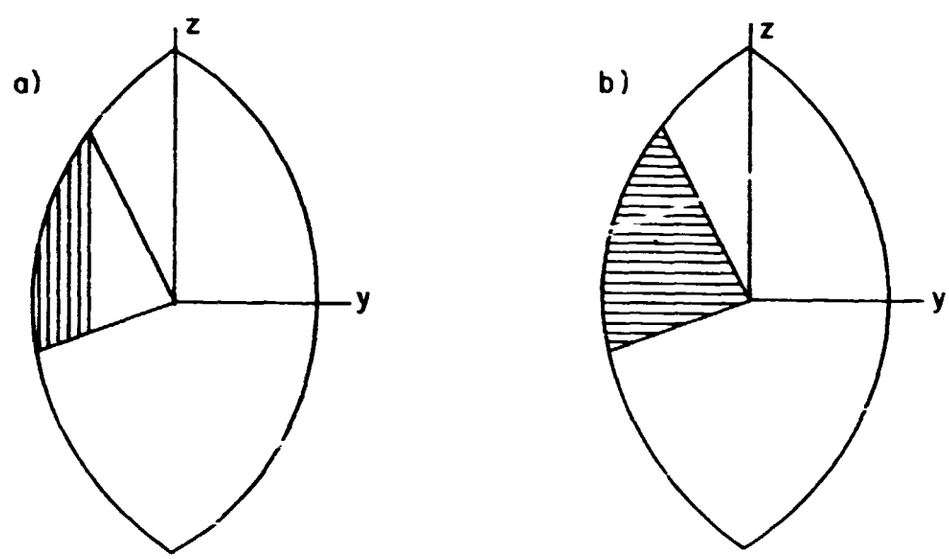

Figure 60. a) Normal order of integration; b) reverse order of integration.

Solving the equation

$$\left(\frac{y}{a} \mp c\right)^2 + z^2 = r^2$$

for y, we have

$$y = a\left(\pm c \mp \sqrt{r^2 - z^2}\right) \quad ,$$

where the upper signs refer to the left ellipse and the lower signs, to the right ellipse.

5.5.2.3 Intersection of a line and an ellipse

The active reflecting area of a circular retroreflector is divided into six sectors by the projection of the back edges onto the front face. In general, the diffraction integral must be done over each sector separately, since dihedral-angle offsets and polarization effects result in the field u being different in different sectors. Let the boundary line between two sectors be given by

$$z = Sy \quad ,$$

where S is the slope of the line (Figure 61). The intersection is given by the solution of the two equations

$$\left(\frac{y}{a} \mp c\right)^2 + z^2 = r^2$$

and

$$z = Sy \quad .$$

Substituting $z^2 = S^2y^2$ into the first equation gives

$$\left(\frac{y \mp ac}{a}\right)^2 + S^2y^2 = r^2 \quad ,$$

$$y^2 \mp 2acy + a^2c^2 + a^2S^2y^2 = a^2r^2 \quad ,$$

$$(1 + a^2S^2)\, y^2 \mp (2ac)y + a^2(c^2 - r^2) = 0 \quad ,$$

$$y = \frac{\pm 2ac \mp \sqrt{4a^2c^2 - 4(1 + a^2S^2)\, a^2(c^2 - r^2)}}{2(1 + a^2S^2)}$$

[eq. cont. on next page]

$$= \frac{\pm 2ac \mp 2a\sqrt{c^2 - (c^2 + a^2S^2c^2 - r^2 - r^2a^2S^2)}}{2(1 + a^2S^2)}$$

$$= a\left[\frac{\pm c \mp \sqrt{r^2 + a^2S^2(r^2 - c^2)}}{1 + a^2S^2}\right] .$$

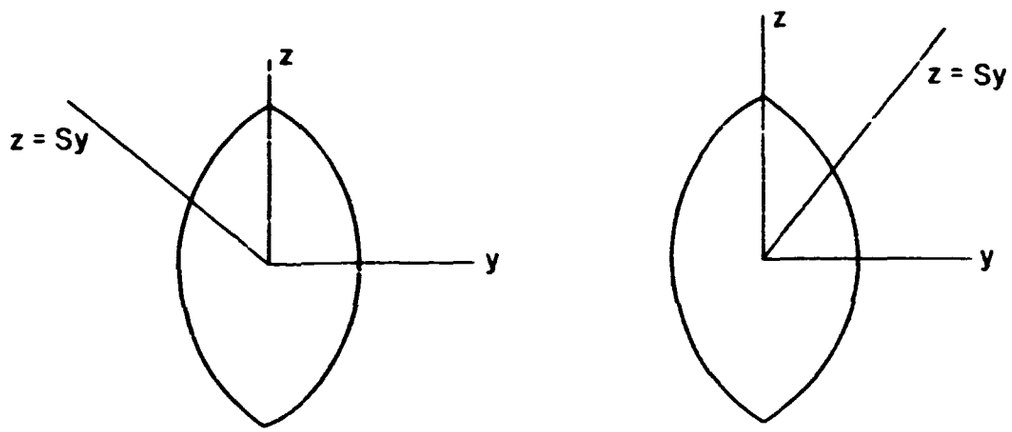

Figure 61. Intersection of a line and an ellipse.

In cases where the boundary of a sector is vertical, the y component of the vector defining the boundary line is zero and the slope S is infinite. In this case, the z coordinate of the intersection of the line and the ellipse is computed by

$$z = \pm\sqrt{r^2 - \left(\frac{y}{a} \pm c\right)^2}\Bigg|_{y=0} = \pm\sqrt{r^2 - c^2} .$$

The sign of the square root is chosen to be the same as that of the z component of the vector defining the boundary line.

5.5.2.4 Slope of an ellipse

The active reflecting area of a circular retroreflector is bounded by two ellipses, whose equation is

$$\left(\frac{y}{a} \mp c\right)^2 + z^2 = r^2 \quad .$$

The slope is given by differentiating

$$z^2 = r^2 - \left(\frac{y}{a} \mp c\right)^2$$

to give

$$2z\, dz = -\frac{2}{a}\left(\frac{y}{a} \mp c\right) dy \quad ,$$

$$\frac{dz}{dy} = -\frac{(y/a) \mp c}{az}$$

If $z = 0$, the slope is infinite. The value of the slope will be used in determining the best order of integration in order to obtain accurate numerical results.

5.5.2.5 Order of integration over y and z variables

The active reflecting area of a circular cube corner is divided into six sectors, each of which is bounded by two lines and one or two curves that are sections of an ellipse. The numerical integration used to calculate the diffraction pattern gives poor results when the slope of the curve as a function of the numerical-integration variable becomes very large or infinite. The problem can be avoided by integrating numerically over the other variable. A sector may be wholly contained in one quadrant of the coordinate system or may span two quadrants. If the latter situation occurs, the numerical integration is performed over the variable that changes sign over the sector. If the sector is in only one quadrant, the order of integration of the variables is chosen such that the maximum slope as a function of the numerical-integration variable is minimized. Since the slope is a monotonic function over a single quadrant, it can be computed at the ends of the elliptical arc as a function of both integration variables, and the variable having the smallest slopes (absolute magnitude) can be chosen.

5.5.2.6 Numerical and analytical parts of sector integration

If the boundary lines of a sector have slopes of the same sign, the integral can be broken into an analytical part bounded by straight lines and a numerical part bounded by two lines and a section of an ellipse, as shown in Figure 62a. If one of the sector boundaries is vertical, the integration is wholly numerical, as shown in Figure 62b. If the slopes are of different sign, the integration is numerical, and the curve has sections of two different ellipses if y changes sign over the sector (Figure 62c) or a single ellipse if z changes sign (Figure 62d). For Figures 62c and 62d, the numerical integration must be split into two sections, one for each of the boundary lines. The numerical integration is over the z variable in Figure 62d.

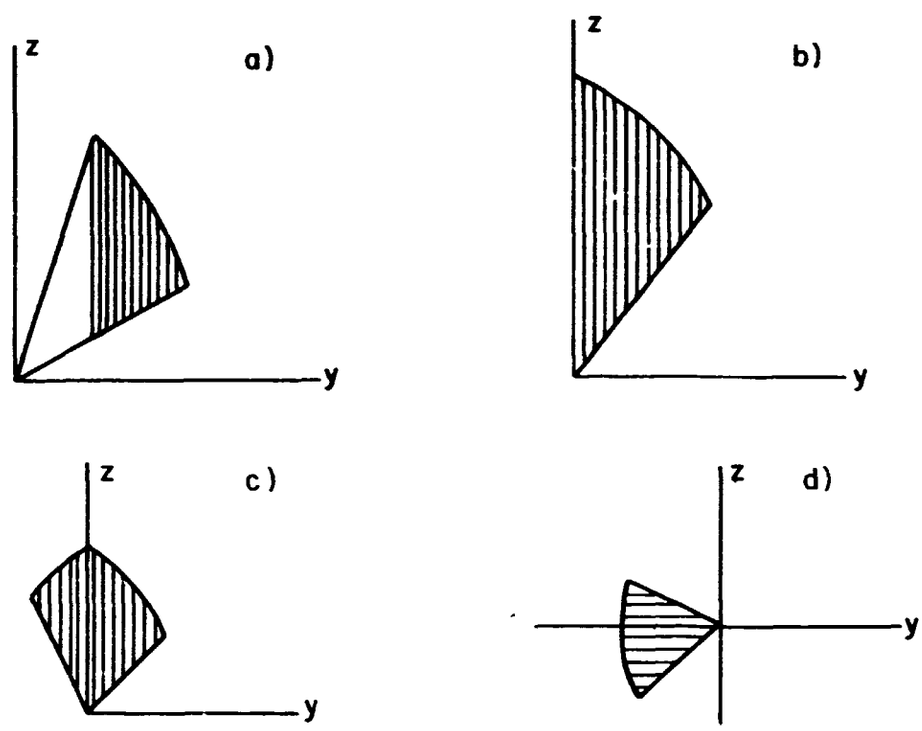

Figure 62. Analytical and numerical parts of sector integration.

5.5.2.7 Second-order numerical integration

The numerical part of the diffraction integral for a circular cube corner is done by means of a second-order technique. The interval is divided into equal pieces of length δ, and the value of the integrand f(y) is computed at each point to obtain a set of values f_i. Each set of three points is fitted with a quadratic, which can be integrated analytically. The result of the integration is Simpson's rule (Hildebrand, 1956, p. 73):

$$\int_{y_1}^{y_3} f(y)\, dy \approx \frac{\delta}{3} (f_1 + 4f_2 + f_3) \quad .$$

5.6 Symmetry of Cube-Corner Diffraction Patterns

The far-field diffraction pattern of a retroreflector is calculated by equation (5-21). Under certain conditions, the diffraction pattern has symmetry properties that are helpful in checking the accuracy of a diffraction calculation. If a retroreflector has perfect-metal reflecting faces, the polarization $\vec{E}_I$ of the reflected light is the same for all six sectors of the cube corner. In this case, the diffraction pattern has the symmetry property

$$E(\theta_1, \theta_2) = E(-\theta_1, -\theta_2) \quad , \tag{5-28}$$

which can be shown as follows. A ray incident at the point (-y, -z) in sector I′ emerges from the point (y, z) in the opposite sector I with a phase change $a_I y + b_I z$ due to dihedral-angle offsets. A ray incident at point (y, z) emerges from point (-y, -z) with a phase gradient

$$\begin{aligned} a_{I'}(-y) + b_{I'}(-z) &= (-a_I)(-y) + (-b_I)(-z) \\ &= a_I y + b_I z \quad . \end{aligned}$$

We have $a_{I'} = -a_I$ and $b_{I'} = -b_I$ because the rays travel virtually the same path in opposite directions for the I and the I′ sectors. The diffraction integral is the sum of pairs of points of the form

$$e^{i(a_I y + b_I z)} e^{-ik(\theta_1 y + \theta_2 z)} + e^{i(a_I y + b_I z)} e^{-ik(-\theta_1 y - \theta_2 z)}$$
$$= 2 e^{i(a_I y + b_I z)} \cos k(\theta_1 y + \theta_2 z) \quad .$$

Since the cosine function is symmetric with respect to a change in sign of the argument and since the diffraction integral is the sum of such symmetric terms, the diffraction pattern has the property given in equation (5-28).

Another symmetry property can be seen from the same argument. If all the dihedral-angle offsets are reversed in sign, the constants a and b change sign so that the integral is the sum of terms of the form

$$e^{i[(-a_I)y + (-b_I)z]} 2 \cos k(\theta_1 y + \theta_2 z) = e^{-i(a_I y + b_I z)} 2 \cos k(\theta_1 y + \theta_2 z) \quad .$$

Since the intensity is obtained by multiplying the integral by its complex conjugate, the diffraction pattern is unchanged when the sign of the dihedral-angle offsets is reversed.

6. RAYLEIGH DISTRIBUTION

The return signal from a satellite retroreflector array consists of reflections from a large number of cube corners. Since the laser beam is coherent and each reflection has a different phase, the reflections will interfere with each other. For a large number n of reflections each having unit amplitude, the normalized probability that the resultant amplitude will be A is (Rayleigh, 1945, pp. 35-42)

$$P(A)\,dA = \frac{2}{n} e^{-A^2/n} A\,dA \quad .$$

Since the energy E of the return signal is proportional to the square of the amplitude, the probability of a given energy is obtained by substituting

$$E = A^2 \quad ,$$

$$dE = 2A\,dA$$

into the above equation to give

$$P(E)\,dE = \frac{1}{n} e^{-E/n}\,dE \quad .$$

The mean energy $\overline{E}$ is given by

$$\overline{E} = \int_0^\infty P(E)\,E\,dE$$

$$= \int_0^\infty \frac{1}{n} e^{-E/n}\,E\,dE$$

$$= -E\,e^{-E/n}\Big|_0^\infty - \int_0^\infty -e^{-E/n}$$

[eq. cont. on next page]

PAGE 116 INTENTIONALLY BLANK

$$= 0 - \left(ne^{-E/n}\right) \Big|_{0}^{\infty}$$

$$= -(0 - n) = n \quad .$$

6.1 Factors Modifying the Rayleigh Distribution

Three factors that exist in actual retroreflector arrays make the probability distribution of the return energy somewhat different from the Rayleigh distribution:

A. The number of reflectors is finite.

B. The amplitudes of the reflections from individual reflectors may not be equal.

C. The transmitted pulse is of finite length, and thus the envelopes of individual reflections do not coincide exactly.

6.2 Guidelines for the Application of the Rayleigh Distribution

The following guidelines can be used to determine when the Rayleigh distribution is not appropriate:

A. The probability distribution for the resultant amplitude of a finite number of equal phasors (Slack, 1946; Jaffe, 1971) is quite different when N is 2, 3, or 4. For N = 5, the probability of E = 0 is about 15% lower than for the Rayleigh distribution. At N = 10, the difference is only about 5%. Therefore, anything over about N = 10 can be expected to give nearly a Rayleigh distribution.

B. If the amplitudes of the phasors are unequal, the probability distribution will still be a Rayleigh distribution as long as there is a large number of phasors of each amplitude (Rayleigh, 1945). Any number greater than about 10 is considered large for this purpose.

C. As long as the pulse length is long compared to the separation of the retroreflectors, the Rayleigh distribution will be applicable.

7. ARRAY TRANSFER FUNCTION

7.1 Retroreflector-Array Coordinate System

The coordinates of the center of the front face of each cube corner in an array are given in a system whose origin is at the center of mass of the satellite in the orbital configuration. If the array has a symmetry axis, let it coincide with the z axis. The direction of the x axis is chosen to be at some convenient angle in the plane normal to the symmetry axis. Let an x', y', z' coordinate system be set up parallel to the x, y, z system with its origin at the center of the front face of a cube corner (see Figure 63). The orientation of the cube corner is represented by the

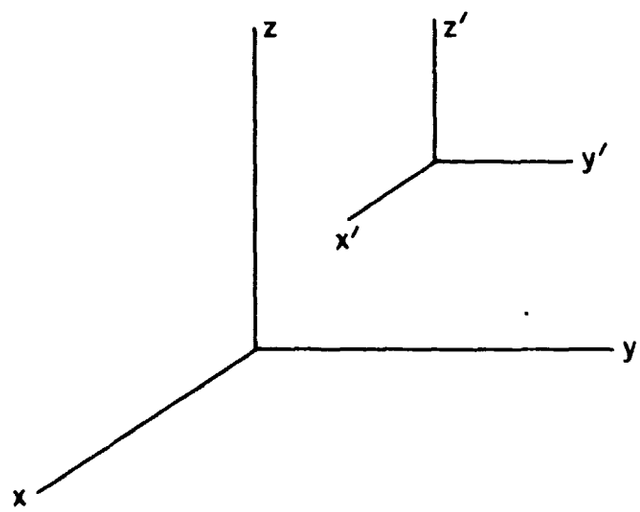

Figure 63. Array coordinate system.

three angles θ_R, ϕ_R, and α_R, the first two giving the direction of the normal to the front face of the cube corner in the x', y', z' system (see Figure 64).

To show the angle α_R, let an X', Y', Z' coordinate system be set up with its origin at the center of the front face, its X' axis normal to the front face, Y' in the direction of increasing θ_R, and Z' in the direction of decreasing ϕ_R. The orientation angle α_R

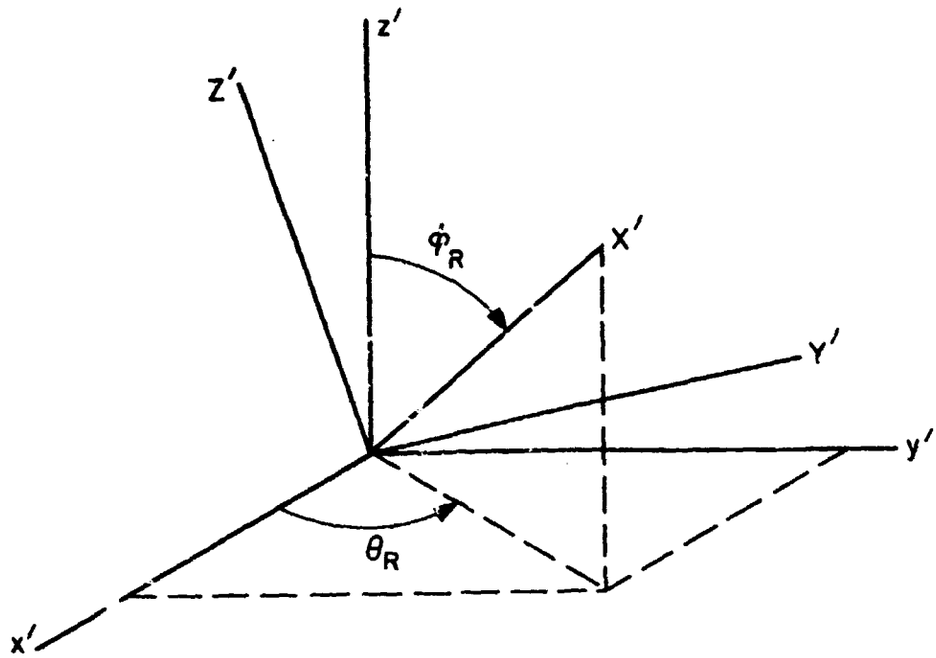

Figure 64. Coordinate system for cube-corner orientation.

is measured counterclockwise from the Z′ axis to the projection of one of the back edges of the cube corner onto the front face, as shown in Figure 65.

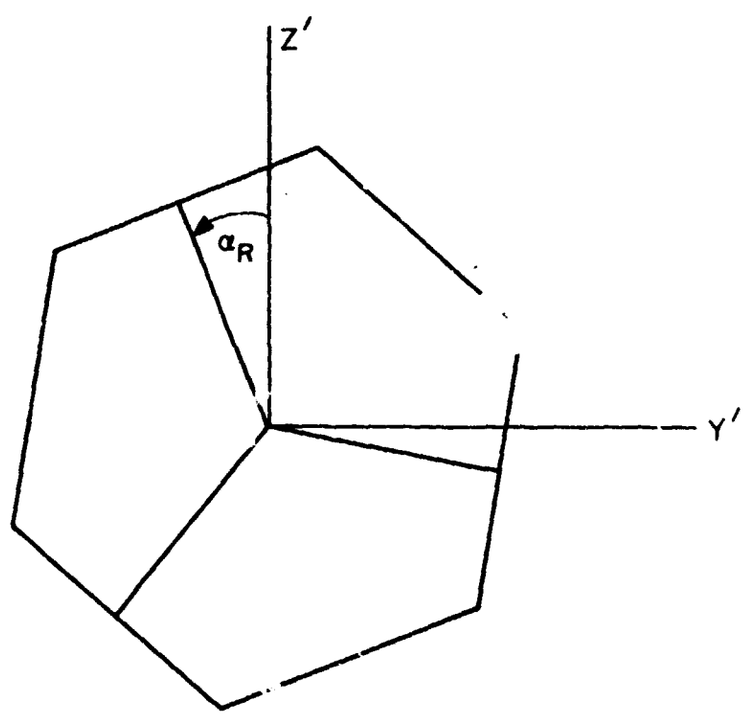

Figure 65. Cube-corner orientation angle α_R.

7.2 Coordinate System of the Incident Beam and the Observer

Let the direction to the illuminating source be given by the angles θ_S and ϕ_S related to the x, y, z coordinate system of the array (Figure 66). Let the complex vector $\vec{E}$ giving the polarization state of the incident beam be given in the x*, y*, z* coordinate system, defined as follows. The x* axis points toward the source and the y* and z* axes are in the direction of increasing θ_S and decreasing ϕ_S, respectively. This is the coordinate system of the observer and is the one in which the diffraction pattern of the array will be given.

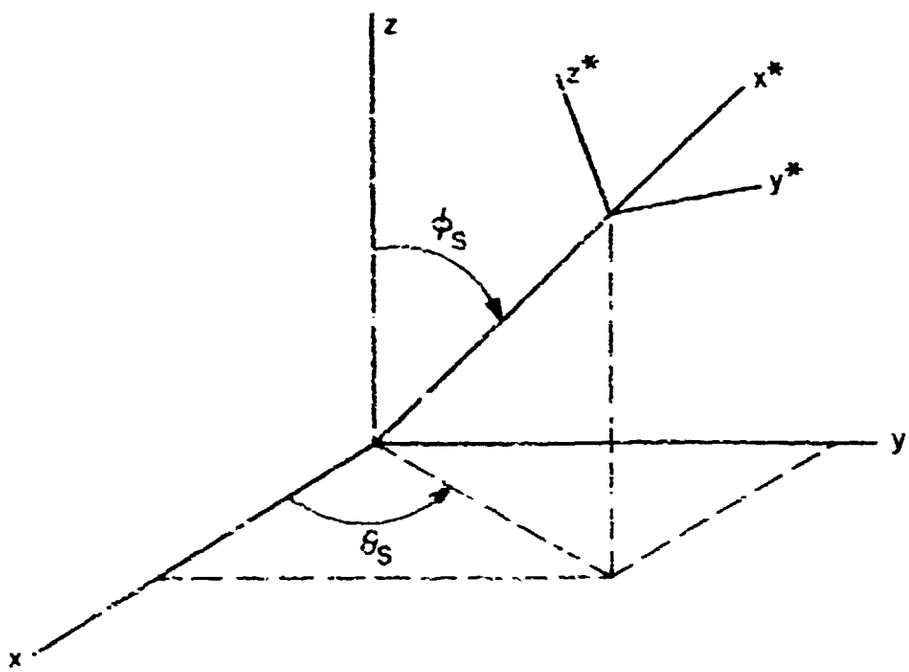

Figure 66. Coordinate system of an incident beam.

7.3 Coordinate System for the Diffraction Pattern of Cube Corners

The direction of the beam incident on a cube corner is specified by the two angles θ and ϕ, where ϕ is the angle between the normal to the front face and the incident beam. The azimuth angle θ is measured to the projection of the incident direction onto the front face, as shown in Figure 67. The coordinate system in which the

diffraction pattern of the cube corner is computed has its 1 axis pointing toward the source, its 2 axis in the plane of incidence pointing in the direction of increasing ϕ, and its 3 axis perpendicular to the plane of incidence in the direction of increasing θ.

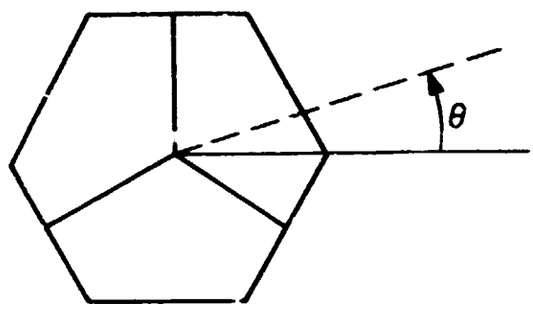

Figure 67. Projection of an incident beam onto the face of a cube corner.

7.4 Conversion between the Coordinate Systems of the Incident Beam and the Retro-reflector

Let $\hat{S}$ be the unit vector pointing toward the illuminating source and $\hat{R}$ be the unit normal to the front face of a cube corner in the array. In the coordinate system of the array, the components of the vectors are

$$S_x = \sin\phi_S \cos\theta_S \quad , \qquad R_x = \sin\phi_R \cos\theta_R \quad ,$$

$$S_y = \sin\phi_S \sin\theta_S \quad , \qquad R_y = \sin\phi_R \sin\theta_R \quad ,$$

$$S_z = \cos\phi_S \quad , \qquad R_z = \cos\phi_R \quad .$$

The incidence angle ϕ on the cube corner is given by

$$\cos\phi = \hat{S} \cdot \hat{R} \quad .$$

To compute the azimuth angle θ of the projection of the incident direction onto the cube corner face, the vector $\hat{S}$ must be expressed in the X′, Y′, Z′ coordinate system, in which the orientation angle α_R is given. This is accomplished by rotating the

coordinate system of $\hat{S}$ first about the z axis by the angle θ_R and then about the new y axis by the angle ϕ_R (Figure 68). The components of the vector $\hat{S}$ in the rotated coordinate system are

$$\begin{pmatrix} S_{x''} \\ S_{y''} \\ S_{z''} \end{pmatrix} = \begin{pmatrix} \cos\phi_R & 0 & -\sin\phi_R \\ 0 & 1 & 0 \\ \sin\phi_R & 0 & \cos\phi_R \end{pmatrix} \begin{pmatrix} \cos\theta_R & \sin\theta_R & 0 \\ -\sin\theta_R & \cos\theta_R & 0 \\ 0 & 0 & 1 \end{pmatrix} \begin{pmatrix} S_x \\ S_y \\ S_z \end{pmatrix} .$$

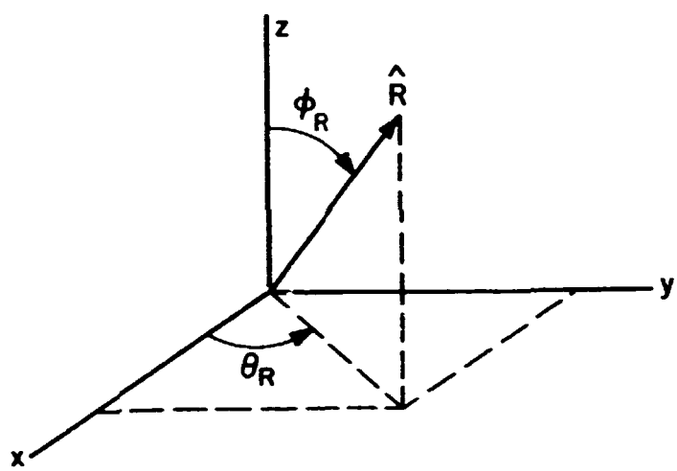

Figure 68. Direction of the normal to the cube-corner front face.

The relationship of the x'', y'', z'' coordinate system to that of X', Y', Z' is given in Figure 69. The components of the vector $\hat{S}$ in the X', Y', Z' coordinate system are

$$S_{X'} = S_{z''} \quad ,$$

$$S_{Y'} = S_{y''} \quad ,$$

$$S_{Z'} = -S_{x''} \quad ,$$

and the projection of the incident beam direction onto the $Y'Z'$ plane makes an angle

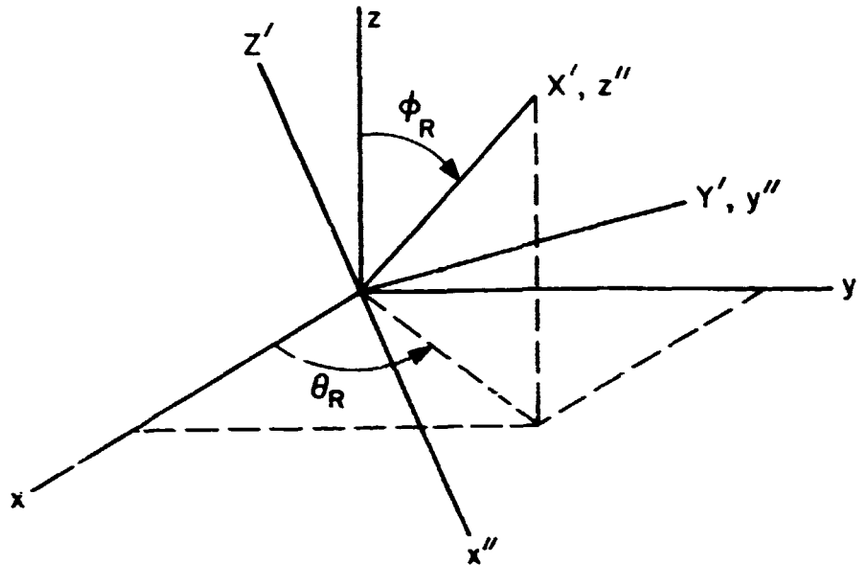

Figure 69. Relationship of X′, Y′, Z′ and x″, y″, z″ axes.

$$\theta' = \tan^{-1}\left(\frac{S_{Z'}}{S_{Y'}}\right)$$

with the Y′ axis, as shown in Figure 70. The desired azimuth angle θ is

$$\theta = \theta' - \alpha_R \quad .$$

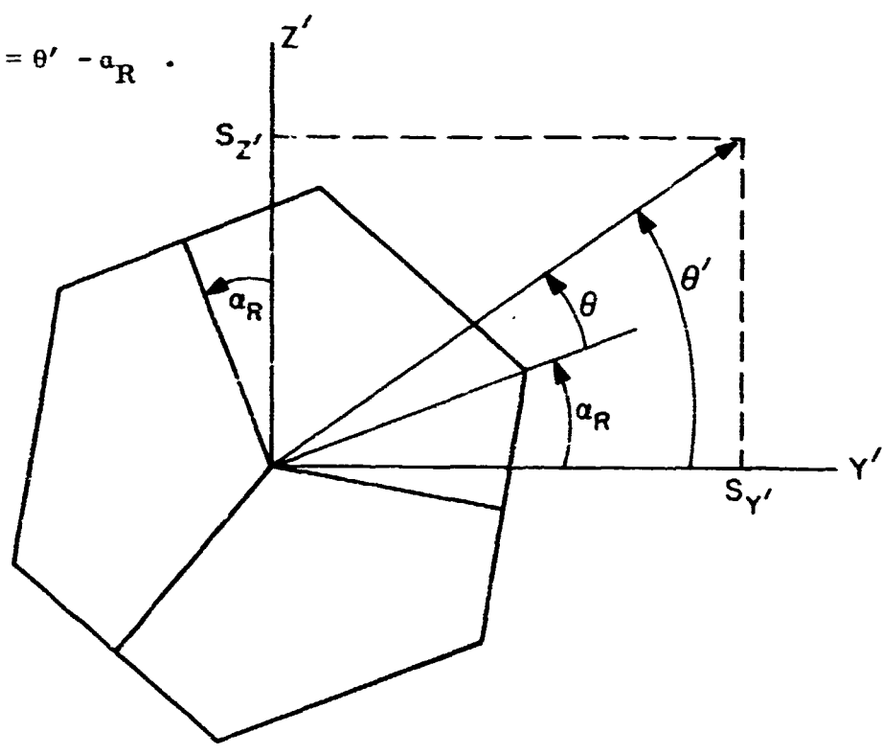

Figure 70. Diagram for computing the azimuth angle θ.

The complex vector $\vec{E}$ is in the x^*, y^*, z^* coordinate system of Figure 66. The diffraction pattern of a retroreflector is computed in the coordinate system defined in Section 7.3. The two coordinate systems are therefore related by a rotation about the x^* axis through a rotation angle γ, which can be computed by expressing the vector $\hat{R}$ in the x^*, y^*, z^* coordinate system of the observer. This is done by rotating the coordinate system of $\hat{R}$ about the z axis by the angle θ_S and then about the new y axis by the angle ϕ_S. The components of $\hat{R}$ in the rotated system are then

$$\begin{pmatrix} R_{x''} \\ R_{y''} \\ R_{z''} \end{pmatrix} = \begin{pmatrix} \cos\phi_S & 0 & -\sin\phi_S \\ 0 & 1 & 0 \\ \sin\phi_S & 0 & \cos\phi_S \end{pmatrix} \begin{pmatrix} \cos\theta_S & \sin\theta_S & 0 \\ -\sin\theta_S & \cos\theta_S & 0 \\ 0 & 0 & 1 \end{pmatrix} \begin{pmatrix} R_x \\ R_y \\ R_z \end{pmatrix} .$$

Figure 71 gives the relationship of the x'', y'', z'' coordinate system to that of x^*, y^*, z^*. The components of the vector $\hat{R}$ in the latter system are

$$R_{x^*} = R_{z''} ,$$

$$R_{y^*} = R_{y''} ,$$

$$R_{z^*} = -R_{x''} ,$$

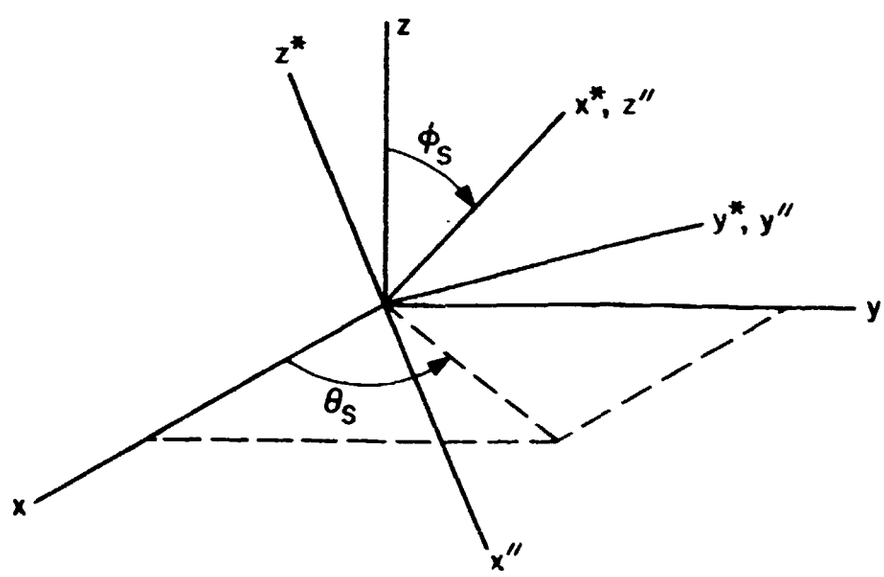

Figure 71. Relationship of x'', y'', z'' and x^*, y^*, z^* axes.

and the projection of the normal to the front face of the cube corner onto the y*z* plane makes an angle

$$\gamma' = \tan^{-1}\left(\frac{R_{z*}}{R_{y*}}\right)$$

with the y* axis, as shown in Figure 72. The direction of the 2 axis in the y*z* plane is opposite that from the projection of the vector $\hat{R}$ onto the y*z* plane (see Figure 73).

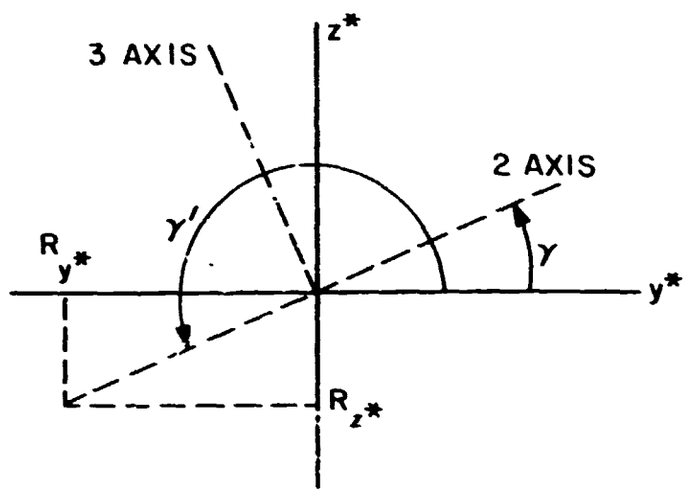

Figure 72. Diagram for computing the angle γ.

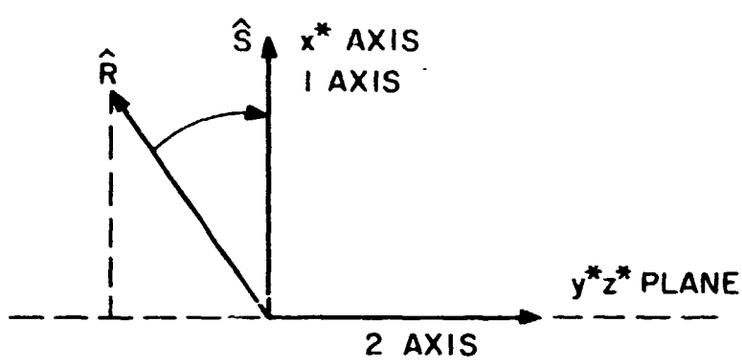

Figure 73. Relationship of the 2 axis to the unit vector $\hat{R}$.

The desired angle γ as shown in Figure 72 is

$$\gamma = \gamma' - \pi \quad .$$

Let E_{y*} and E_{z*} be the complex components of the incident polarization vector in the x^*, y^*, z^* coordinate system. The components E_2 and E_3 in the coordinate system used for the diffraction pattern of the cube corner are then

$$E_2 = E_{y*} \cos \gamma + E_{z*} \sin \gamma \quad ,$$

$$E_3 = -E_{y*} \sin \gamma + E_{z*} \cos \gamma \quad .$$

A point with the angular coordinates (θ_1', θ_2') in the coordinate system for the diffraction pattern of the array has the following angular coordinates in the coordinate system for the diffraction pattern of an individual cube corner:

$$\theta_1 = \theta_1' \cos \gamma + \theta_2' \sin \gamma \quad ,$$

$$\theta_2 = -\theta_1' \sin \gamma + \theta_2' \cos \gamma \quad .$$

7.5 Transmitted Pulse

The transmitted pulse is assumed to be a monochromatic wave with a gaussian envelope. The intensity across the retroreflector array is assumed to be uniform. In the x^*, y^*, z^* coordinate system, where the x^* axis points from the array to the source, the complex vector field incident on the array is

$$\vec{E} = (E_y \hat{y} + E_z \hat{z})\, e^{ik(x + ct)} \frac{1}{\sqrt{\sigma \sqrt{2\pi}}}\, e^{-(x + ct)^2/4\sigma^2} \quad , \tag{7-1}$$

where $k = 2\pi/\lambda$, λ is the wavelength, c is the velocity of light, and σ is the sigma of the transmitted pulse. For simplicity, we have dropped the asterisks on x, y, and z. The intensity I of the pulse is

$$I = (E_y E_y^* + E_z E_z^*) \frac{1}{\sigma\sqrt{2\pi}} \; e^{-(x + ct)^2/2\sigma^2} \quad .$$

If the width of the transmitted pulse is given as the distance ℓ between half-power points, σ is calculated from

$$e^{-(\ell/2)^2/2\sigma^2} = \frac{1}{2} \quad ,$$

which can be solved to give

$$-\left(\frac{\ell}{2}\right)^2 \frac{1}{2\sigma^2} = \ln\frac{1}{2} \quad ,$$

$$\frac{\ell}{2}\,\frac{1}{\sqrt{2}\sigma} = \sqrt{\ln 2} \quad ,$$

$$\sigma = \frac{\ell}{2}\,\frac{1}{\sqrt{2\ln 2}} = \frac{\ell/2}{\sqrt{\ln 4}} = \frac{\ell/2}{1.17741} = \frac{\ell}{2.35482} \quad .$$

7.6 Position of the Retroreflector along the Line of Sight

Let $\hat{S}$ be a unit vector pointing from the array toward the incident beam and $\vec{C}$ be the vector from the satellite center of mass to the center of the front face of a cube corner. The position of the cube corner along the line of sight is

$$\hat{S} \cdot \vec{C} \quad .$$

If we take the optical path length in the dielectric (Section 2.5) into account, the apparent position of the cube corner along the line of sight is

$$x = \hat{S} \cdot \vec{C} - L\sqrt{n^2 - \sin^2\phi} \quad ,$$

where L is the length of the cube corner from the vertex to the face, n is the index of refraction of the cube corner, $\phi = \cos^{-1}(\hat{S} \cdot \hat{R})$, and x is the distance to the satellite center of gravity minus the apparent distance to the cube corner.

7.7 Incoherent Return

The equations given in this section apply to situations in which the return signal is independent of the phase relationships among the reflections from individual cube corners. If the array is illuminated by an incoherent source containing many frequencies, the phase relationships are different for each frequency, so that averaging occurs over all possible phase relationships. The equations also apply to a laboratory experiment in which the total reflected energy is measured. The return pulse is the sum of the total reflected signals from each cube corner. The primary use of these equations is to compute the average behavior of a large number of returns measured at some point in the far-field pattern when the array is illuminated by a coherent source. In this situation, it is assumed that the phase relationships vary randomly from pulse to pulse as a result of changes in viewing angle to the array. The incoherent return is constructed by adding the intensities of the reflections from each cube corner at a point in the far field. In Section 7.8, it will be shown that this gives the average pulse shape of a large number of coherent returns.

The reflection from a cube corner has the same mathematical form as the incident pulse, except that the reflection is moving in the opposite direction. The displacement between the pulses reflected from two different cube corners is twice the difference in distance to the two reflectors. Let the return pulse be constructed in a coordinate system having its origin at the center of the reflection that would be received from a cube corner at the center of mass of the satellite. The positive direction will be taken as the direction to the observer. In this coordinate system, the intensity I_K of the reflection from the Kth cube corner is

$$I_K = \frac{S_K}{\sigma\sqrt{2\pi}} e^{-(x-d_K)^2/2\sigma^2} ,$$

where d_K is twice the distance of the apparent reflection point for the Kth retroreflector from the plane through the center of mass of the satellite perpendicular to the incident beam. The constant S_K giving the intensity of the reflection from the Kth cube corner is proportional to the active reflecting area, if the total reflected energy is being measured, or to the intensity of the diffraction pattern at the position of the observer, if the detector is located at a point in the far field. Depending on the method of detection, S_K is either the total intensity $(E_y E_y^* + E_z E_z^*)$ or the intensity of any component of polarization being measured.

The total intensity I of the incoherent return is

$$I(x) = \sum_K I_K$$

$$= \sum_K \frac{S_K}{\sigma\sqrt{2\pi}} e^{-(x-d_K)^2/2\sigma^2} ,$$

and the total energy of the return is proportional to

$$\int_{-\infty}^{\infty} I(x)\, dx = \sum_K S_K \int_{-\infty}^{\infty} \frac{1}{\sigma\sqrt{2\pi}} e^{-(x-d_K)^2/2\sigma^2} dx$$

$$= \sum_K S_K .$$

The mean position of the return pulse is

$$\bar{x} = \frac{\int_{-\infty}^{\infty} xI(x)\, dx}{\int_{-\infty}^{\infty} I(x)\, dx}$$

$$= \frac{\sum_K S_K \int_{-\infty}^{\infty} (x/\sigma\sqrt{2\pi})\, e^{-(x-d_K)^2/2\sigma^2} dx}{\sum_K S_K} . \qquad (7\text{-}2)$$

Substituting $x' + d_K = x$, $x' = x - d_K$, and $dx' = dx$, we get

$$\bar{x} = \frac{\sum_K S_K \int_{-\infty}^{\infty} [(x' + d_K)/\sigma\sqrt{2\pi}]e^{-x'^2/2\sigma^2}\, dx'}{\sum_K S_K}$$

$$= \frac{\sum_K S_K d_K}{\sum_K S_K} \quad . \tag{7-3}$$

A measure of the spreading of the pulse due to the array is obtained by computing the second moment V of the return:

$$V = \frac{\int_{-\infty}^{\infty} x^2 I(x)\, dx}{\int_{-\infty}^{\infty} I(x)\, dx}$$

$$= \frac{\sum_K S_K \int_{-\infty}^{\infty} (x^2/\sigma\sqrt{2\pi})\, e^{-(x-d_K)^2/2\sigma^2}\, dx}{\sum_K S_K} \quad . \tag{7-4}$$

If we make the same substitutions for x, $x-d_K$, and dx, the integral becomes

$$\int_{-\infty}^{\infty} \frac{x^2}{\sigma\sqrt{2\pi}} e^{-(x-d_K)^2/2\sigma^2}\, dx = \int_{-\infty}^{\infty} \frac{(x' + d_K)^2}{\sigma\sqrt{2\pi}} e^{-x'^2/2\sigma^2}\, dx'$$

$$= \int_{-\infty}^{\infty} \frac{x'^2}{\sigma\sqrt{2\pi}} e^{-x'^2/2\sigma^2}\, dx' + 2d_K \int_{-\infty}^{\infty} \frac{x'}{\sigma\sqrt{2\pi}} e^{-x'^2/2\sigma^2}\, dx'$$

[eq. cont. on next page]

$$+ d_K^2 \int_{-\infty}^{\infty} \frac{1}{\sigma\sqrt{2\pi}} e^{-x'^2/2\sigma^2} dx'$$

$$= \sigma^2 + 0 + d_K^2 \quad .$$

After we substitute this into equation (7-4),

$$V = \frac{\sum_K S_K (\sigma^2 + d_K^2)}{\sum_K S_K} \quad .$$

Defining $\sigma' = \sqrt{V}$, we have

$$\sigma' = \sqrt{\frac{\sum_K S_K(\sigma^2 + d_K^2)}{\sum_K S_K}} \quad ;$$

for $d_K \ll \sigma$, the incoherent return is nearly gaussian, with a sigma of σ'.

7.8 Coherent Return

The coherent return from an array is computed by adding the fields of the reflections from all the cube corners and squaring the sum to obtain the intensity. The field of the transmitted pulse is given by equation (7-1). Let the return pulse be constructed in a coordinate system whose origin is the center of the pulse that would be reflected from a cube corner at the center of mass of the satellite. Let d_K be twice the distance of the Kth cube corner from the plane through the center of mass of the satellite perpendicular to the incident beam. The quantity d_K is known with sufficient accuracy for use in positioning the envelope of the reflection from each cube corner. However, it is not known with enough precision to predict the relative phases among the reflections. We will therefore assume that the relative phases are random and vary randomly from pulse to pulse. Very small changes in aspect angle of the satellite are

sufficient to change the phase relationships completely. In the expressions below, the field strength E_K can be any component of polarization. The phase of the field component can be absorbed in the random phase factor $e^{i\theta_K}$. The field reflected from the Kth cube corner is

$$E_K = e^{ik(x-d'_K)} \sqrt{\frac{S_K}{\sigma\sqrt{2\pi}}}\, e^{-(x-d_K)^2/4\sigma^2}$$

$$= e^{ikx} e^{i\theta_K} \sqrt{\frac{S_K}{\sigma\sqrt{2\pi}}}\, e^{-(x-d_K)^2/4\sigma^2} \quad .$$

where $\theta_K = -kd'_K$ = a random phase between 0 and 2π.

The field of the whole array is

$$E = \sum_K E_K$$

$$= \sum_K e^{ikx} e^{i\theta_K} \sqrt{\frac{S_K}{\sigma\sqrt{2\pi}}}\, e^{-(x-d_K)^2/4\sigma^2} \quad ,$$

and the total intensity is

$$I(x) = EE^* = \sum_K e^{ikx} e^{i\theta_K} \sqrt{\frac{S_K}{\sigma\sqrt{2\pi}}}\, e^{-(x-d_K)^2/4\sigma^2}$$

$$\times \sum_L e^{-ikx} e^{-i\theta_L} \sqrt{\frac{S_L}{\sigma\sqrt{2\pi}}}\, e^{-(x-d_L)^2/4\sigma^2}$$

$$= \sum_{KL} e^{i(\theta_K-\theta_L)} \frac{\sqrt{S_K S_L}}{\sigma\sqrt{2\pi}} \exp\left[-\frac{(x-d_K)^2 + (x-d_L)^2}{4\sigma^2}\right] \quad .$$

Since EE^* is real, all imaginary terms cancel, resulting in

$$I(x) = \sum_{KL} \cos(\theta_K - \theta_L) \frac{\sqrt{S_K S_L}}{\sigma\sqrt{2\pi}} \exp\left[-\frac{(x-d_K)^2 + (x-d_L)^2}{4\sigma^2}\right] . \tag{7-5}$$

The mean value of $\cos(\theta_K - \theta_L)$ over a large number of coherent returns where the phases vary randomly is 0 for $K \neq L$ and 1 for $K = L$. Therefore, the mean return pulse shape is

$$\sum_K \frac{S_K}{\sigma\sqrt{2\pi}} e^{-(x-d_K)^2/2\sigma^2} , \tag{7-6}$$

which is the incoherent case derived previously.

In order to obtain the total energy by integration, the exponent can be transformed into a perfect square plus a constant:

$$\begin{aligned}
(x-d_K)^2 + (x-d_L)^2 &= x^2 - 2xd_K + d_K^2 + x^2 - 2xd_L + d_L^2 \\
&= 2x^2 - 2x(d_K + d_L) + \left(d_K^2 + d_L^2\right) \\
&= 2\left[x^2 - x(d_K + d_L) + \left(\frac{d_K + d_L}{2}\right)^2 - \left(\frac{d_K + d_L}{2}\right)^2\right] + \left(d_K^2 + d_L^2\right) \\
&= 2\left(x - \frac{d_K + d_L}{2}\right)^2 - \frac{1}{2}(d_K + d_L)^2 + \left(d_K^2 + d_L^2\right) \\
&= 2\left(x - \frac{d_K + d_L}{2}\right)^2 + \frac{-d_K^2 - 2d_K d_L - d_L^2 + 2d_K^2 + 2d_L^2}{2} \\
&= 2\left(x - \frac{d_K + d_L}{2}\right)^2 + \frac{d_K^2 - 2d_K d_L + d_L^2}{2} \\
&= 2\left(x - \frac{d_K + d_L}{2}\right)^2 + \frac{1}{2}(d_K - d_L)^2 .
\end{aligned}$$

Substituting this into equation (7- we get

$$I(x) = \sum_{KL} \cos(\theta_K - \theta_L)\, e^{-(d_K - d_L)^2/8\sigma^2} \frac{\sqrt{S_K S_L}}{\sigma\sqrt{2\pi}} \exp\left\{-\frac{\left[x - (d_K + d_L)/2\right]^2}{2\sigma^2}\right\} \quad . \tag{7-7}$$

The total energy is proportional to

$$\int_{-\infty}^{\infty} I(x)\, dx = \sum_{KL} \cos(\theta_K - \theta_L)\, e^{-(d_K - d_L)^2/8\sigma^2} \sqrt{S_K S_L} \quad .$$

If we substitute equation (7-7) into the first line of equation (7-2), the mean position of the return pulse, we have

$$\bar{x} = \frac{\int_{-\infty}^{\infty} x \sum_{KL} \cos(\theta_K - \theta_L)\, e^{-(d_K - d_L)^2/8\sigma^2} \left(\sqrt{S_K S_L}/\sigma\sqrt{2\pi}\right) e^{-\left[x - (d_K + d_L)/2\right]^2/2\sigma^2}\, dx}{\int_{-\infty}^{\infty} \sum_{KL} \cos(\theta_K - \theta_L)\, e^{-(d_K - d_L)^2/8\sigma^2} \left(\sqrt{S_K S_L}/\sigma\sqrt{2\pi}\right) e^{-\left[x - (d_K + d_L)/2\right]^2/2\sigma^2}\, dx} \quad . \tag{7-8}$$

Incorporating the following substitutions

$$x' = x - \frac{d_K + d_L}{2} \quad , \tag{7-9a}$$

$$dx' = dx \quad , \tag{7-9b}$$

$$x = x' + \frac{d_K + d_L}{2} \tag{7-9c}$$

into equation (7-8), we have

$$\bar{x} = \frac{\sum_{KL} \cos(\theta_K - \theta_L)\, e^{-(d_K - d_L)^2/8\sigma^2} \sqrt{S_K S_L} \int_{-\infty}^{\infty} \left\{\left[x' + (d_K + d_L)/2\right]/\sigma\sqrt{2\pi}\right\} e^{-x'^2/2\sigma^2}\, dx'}{\sum_{KL} \cos(\theta_K - \theta_L)\, e^{-(d_K - d_L)^2/8\sigma^2} \sqrt{S_K S_L} \int_{-\infty}^{\infty} (1/\sigma\sqrt{2\pi})\, e^{-x'^2/2\sigma^2}\, dx'}$$

$$= \frac{\sum_{KL} \cos(\theta_K - \theta_L)\, e^{-(d_K - d_L)^2/8\sigma^2} \sqrt{S_K S_L}\, [(d_K + d_L)/2]}{\sum_{KL} \cos(\theta_K - \theta_L)\, e^{-(d_K - d_L)^2/8\sigma^2} \sqrt{S_K S_L}} .$$

If we substitute equation (7-7) into the first line of equation (7-4), make the change of variables given in equation (7-9a, b) plus

$$x^2 = x'^2 + x'(d_K + d_L) + \left(\frac{d_K + d_L}{2}\right)^2 ,$$

and perform the integrations, the variance of the return pulse becomes

$$V = \frac{\sum_{KL} \cos(\theta_K - \theta_L)\, e^{-(d_K - d_L)^2/8\sigma^2} \sqrt{S_K S_L} \left\{\sigma^2 + [(d_K + d_L)/2]^2\right\}}{\sum_{KL} \cos(\theta_K - \theta_L)\, e^{-(d_K - d_L)^2/8\sigma^2} \sqrt{S_K S_L}} . \quad (7\text{-}10)$$

The square root of the variance is

$$\sigma' = \sqrt{V} .$$

7.8.1 Calculation shortcuts

The expression for the coherent reflected intensity was given above as a sum involving a double index. This form was necessary in order to obtain the total energy,

mean position, and second moment of the reflected pulse. For plotting the intensity, however, it is much more efficient to calculate the field involving a single index and square the result. Omitting the factor e^{ikx}, which disappears when E is multiplied by E^*, we have

$$E(x) \sim \sum_K e^{i\theta_K} \sqrt{\frac{S_K}{\sigma\sqrt{2\pi}}}\, e^{-(x-d_K)^2/4\sigma^2} \quad ,$$

from which the intensity is

$$I(x) = E(x)\, E^*(x) \quad .$$

In computing the total energy, the mean, and the variance of a coherent return, the following techniques can be employed to reduce computation time. The cosine factor can be expanded to give

$$\cos(\theta_K - \theta_L) = \cos\theta_K \cos\theta_L + \sin\theta_K \sin\theta_L \quad .$$

The terms on the right can be precomputed and saved, which requires 2N trigometric calculations, where N is the number of retroreflectors. Each value of $\cos(\theta_K - \theta_L)$ can then be computed with two multiplications and one addition, a much faster procedure than doing N^2 cosine calculations.

In all the expressions, the terms with index KL are equal to those with index LK, so we need to compute only about half the terms. Since terms with K = L are independent of the random phases used, their sum can be precomputed and saved when many coherent returns are being calculated for the same incidence angle on the array. The terms for K = L give the incoherent results.

7.8.2 Relation of coherence to diffraction

The calculation of coherent returns by use of a random-number generator to assign phases to the reflections from individual cube corners is a way of gaining some

statistical information despite the impossibility of knowing the actual phase relationships between the reflections. A coherent calculation is actually a diffraction calculation for the whole array at one point in the far field, based on assumed phases. If we have accurate enough information, we can perform the diffraction integral over the whole array, calculating the phases from the relative positions of the reflectors in the array. The characteristic width of the diffraction pattern of a single reflector is roughly λ/D_R, where D_R is the diameter of the cube corner. The basic physical reason for this is that the phase relationship between the opposite sides of the cube corner changes by 360° when the angular position of the observer changes by λ/D_R. The phase relationship between reflectors on opposite sides of an array changes by 360° when the viewing angle changes by λ/D_A, where D_A is the diameter of the array. Since D_A is generally much larger than D_R, we can expect the diffraction pattern of the whole array to vary within a characteristic angle λ/D_A, giving rise to a mottled appearance in the array diffraction pattern. It is these variations that are being studied statistically in a coherent calculation.

7.8.3 Coherent variations

Let x_i represent some property of the ith coherent return, such as the energy or mean position, and let W_i be the weighting factor for the return. The mean value of the quantity for a set of coherent returns is

$$\bar{x} = \frac{\sum_i W_i x_i}{\sum_i W_i} ,$$

and the variance of the quantity is

$$V = \frac{\sum_i W_i (x_i - \bar{x})^2}{\sum_i W_i}$$

$$= \frac{\sum_i (W_i x_i^2 - 2 W_i \bar{x} x_i + W_i \bar{x}^2)}{\sum_i W_i}$$

[eq. cont. on next page]

$$= \overline{x^2} - 2\overline{x}\,\overline{x} + \overline{x}^2$$

$$= \overline{x^2} - \overline{x}^2 \quad .$$

In cases where the average value $\overline{x}$ of a coherent quantity is substantially different from the incoherent value, the statistical significance of the differences Δx can be measured by the quantity $\Delta x/\sigma_{\overline{x}}$, where

$$\sigma_{\overline{x}} = \sqrt{\frac{V}{N}} \quad ,$$

N being the number of coherent returns.

7.8.4 Mean value of coherent quantities

It has already been pointed out that the mean value of the intensity, equation (7-5), averaged over many coherent returns is the incoherent intensity shown in equation (7-6). Since the total energy is the integral of the intensity, the mean value of the coherent energies is the incoherent energy. This result is also obtained from the expression

$$\text{energy} = \sum_{KL} \cos\,(\theta_K - \theta_L)\; e^{-(d_K - d_L)^2/8\sigma^2} \sqrt{S_K S_L} \quad .$$

Since the average value of $\cos\,(\theta_K - \theta_L)$ is 0 for $K \neq L$ and 1 for $K = L$, the mean value of the coherent energy is

$$\overline{\text{energy}} = \sum_{K} S_K \quad ,$$

which is the incoherent expression.

The situation is a little more complicated for the other quantities. The mean position of the return pulse is

$$\bar{x} = \frac{\sum_{KL} \cos(\theta_K - \theta_L)\, e^{-(d_K - d_L)^2/8\sigma^2} \sqrt{S_K S_L}\,(d_K + d_L)/2}{\sum_{KL} \cos(\theta_K - \theta_L)\, e^{-(d_K - d_L)^2/8\sigma^2} \sqrt{S_K S_L}} , \qquad (7\text{-}11)$$

in which the mean value of the numerator is

$$\sum_K S_K d_K .$$

The denominator is the energy of the return that has a mean value of $\sum_K S_K$. If it were true that the mean value of the quotient of the two quantities is the quotient of the mean values, then the mean value of $\bar{x}$ for the coherent returns would be the same as the value of $\bar{x}$ for the incoherent return. Calculations of large numbers of coherent returns for certain arrays have shown statistically significant differences between these two values of $\bar{x}$. The arrays used had unsymmetrical distributions of retroreflectors along the line of sight. Presumably, if both the incident pulse and the distribution of reflectors were symmetrical, there would be no mechanism for causing a bias.

A technique for removing the difference between the average $\bar{x}$ of the coherent returns and the $\bar{x}$ for the incoherent case is to weight each coherent $\bar{x}$ by the energy of the coherent return. This has the effect of canceling the denominator in equation (7-11), so that we need to average only the numerator, whose mean value has already been shown to be equal to the numerator in the incoherent expression for $\bar{x}$, equation (7-3). Computer runs on large samples of coherent returns have verified that this weighting technique works to within the statistical uncertainty due to the number of returns computed. These computer runs also show, however, that the whole sample must be used; excluding returns below a certain energy causes a bias. This is probably the result of the fact that a return's low energy puts constraints on the phases such that they are no longer random.

A similar situation exists with the variance given by equation (7-10), whose mean value of the numerator, $\sum_K S_K(\sigma^2 + d_K^2)$, is the same as in the incoherent case; the

denominator is the energy. Weighting by the mean energy removes any bias between the mean coherent value and the incoherent value.

7.8.5 Coherent variations versus pulse length

Computation of coherent returns for various arrays with different pulse lengths has shown that the variation of the mean position of the return pulse decreases as the pulse length decreases. A qualitative explanation of this phenomenon is the following: If the pulse length is much shorter than the spacing between the reflections from different reflectors, no interference occurs between the different reflections, because they do not overlap. In this case, the coherent return is identical to the incoherent return, and all properties of the coherent return, such as the energy and mean position, are constant. As the pulse length increases, both the degree of overlap between individual reflections and the variations in pulse shape increase. Therefore, the variations in energy, mean position, and other properties will increase as the pulse length increases.

7.9 Half-Maximum Range Correction

In a half-maximum detection system, the range to a retroreflector array is measured by recording the time interval between the half-maximum points on the leading edge of the transmitted and received pulses. If the received pulse is the same shape as the transmitted pulse, this will give the same range as a centroid detection system. However, if the pulse is broadened by the array, because of the fact that the cube corners are distributed in range from the observer, then the range measured by a half-maximum system will, in general, be shorter than that measured by a centroid detection system. The difference between the half-maximum range correction and the centroid range correction must be computed by plotting the return pulse and numerically finding the point on the leading edge where the intensity is half the maximum intensity. In cases where the half-intensity point is multivalued, the first point on the leading edge will be considered the half-maximum point $x_{1/2}$. The difference between the half-maximum point and the centroid on the transmitted pulse is $\sigma\sqrt{\ln 4}$, as shown in Section 7.5. The corresponding difference on the received pulse is $x_{1/2} - \bar{x}$, where $\bar{x}$ is the centroid of the received pulse. The difference between the half-maximum and the centroid range corrections is

$$\frac{1}{2}\left[(x_{1/2} - \bar{x}) - \sigma\sqrt{\ln 4}\right] .$$

The factor of 1/2 converts the result to a one-way correction.

7.10 Pulse Spreading by Array versus Pulse Length

Computer runs on various retroreflector arrays with different pulse lengths have shown that the amount of pulse spreading due to the array increases as the pulse length decreases. There is one particular array geometry where this result can be proved analytically. Let the array consist of a large number of reflectors whose density along the line of sight is approximately gaussian. Let the density of reflectors be

$$\mathscr{D}(2x'')(2\,dx'') = \frac{1}{\sigma_1\sqrt{2\pi}}\, e^{-(2x'')^2/2\sigma_1^2}\,(2\,dx'') \quad ,$$

and let the intensity of the incoming pulse be

$$I_0(x) = \frac{1}{\sigma_0\sqrt{2\pi}}\, e^{-(x+ct)^2/2\sigma_0^2} \quad .$$

The contribution $dI(x)$ to the incoherent return signal from an element of the array at the point x'' is a gaussian moving in the $+x$ direction reflected from point x'' at time $t = -x''/c$ and centered at $2x''$ at time $t = 0$. If we define $x' = 2x''$, we get at $t = 0$

$$dI(x) = \frac{1}{\sigma_1\sqrt{2\pi}}\, e^{-x'^2/2\sigma_1^2}\, dx' \, \frac{1}{\sigma_0\sqrt{2\pi}}\, e^{-(x-x')^2/2\sigma_0^2} \quad ,$$

and then we can integrate over x' to obtain the total incoherent intensity:

$$I(x) = \int_{-\infty}^{\infty} dI(x)$$

$$= \frac{1}{2\pi\sigma_1\sigma_0} \int_{-\infty}^{\infty} \exp\left\{-\frac{1}{2}\left[\frac{x'^2}{\sigma_1^2} + \frac{(x-x')^2}{\sigma_0^2}\right]\right\} dx' \quad .$$

The terms in the square brackets can be rewritten to form a perfect square plus a constant, as follows:

$$\frac{x'^2}{\sigma_1^2} + \frac{(x-x')^2}{\sigma_0^2} = \frac{x'^2}{\sigma_1^2} + \frac{x^2 - 2xx' + x'^2}{\sigma_0^2}$$

$$= x'^2\left(\frac{1}{\sigma_1^2} + \frac{1}{\sigma_0^2}\right) - x'\left(\frac{2x}{\sigma_0^2}\right) + \frac{x^2}{\sigma_0^2}$$

$$= \frac{\sigma_1^2 + \sigma_0^2}{\sigma_1^2\sigma_0^2}\left(x'^2 - \frac{\sigma_1^2 2x}{\sigma_1^2 + \sigma_0^2}\, x'\right) + \frac{x^2}{\sigma_0^2}$$

$$= \frac{\sigma_1^2 + \sigma_0^2}{\sigma_1^2\sigma_0^2}\left[\left(x' - \frac{\sigma_1^2 x}{\sigma_1^2 + \sigma_0^2}\right)^2 - \left(\frac{\sigma_1^2 x}{\sigma_1^2 + \sigma_0^2}\right)^2\right] + \frac{x^2}{\sigma_0^2}$$

$$= \frac{\sigma_1^2 + \sigma_0^2}{\sigma_1^2\sigma_0^2}\left(x' - \frac{\sigma_1^2 x}{\sigma_1^2 + \sigma_0^2}\right)^2 - \frac{\sigma_1^2 x^2}{\sigma_0^2\left(\sigma_1^2 + \sigma_0^2\right)} + \frac{x^2\left(\sigma_1^2 + \sigma_0^2\right)}{\sigma_0^2\left(\sigma_1^2 + \sigma_0^2\right)}$$

$$= \frac{\left\{x' - \left[\sigma_1^2 x/\left(\sigma_1^2 + \sigma_0^2\right)\right]\right\}^2}{\sigma_1^2\sigma_0^2/\left(\sigma_1^2 + \sigma_0^2\right)} + \frac{x^2}{\sigma_1^2 + \sigma_0^2}$$

$$= \frac{\left[x' - \left(\sigma_1^2 x/\sigma^2\right)\right]^2}{\sigma_1^2\sigma_0^2/\sigma^2} + \frac{x^2}{\sigma^2} \quad ,$$

where

$$\sigma^2 \equiv \sigma_1^2 + \sigma_0^2 \quad .$$

After we substitute this back into the exponent, the integral becomes

$$I(x) = \frac{1}{2\pi\sigma_1\sigma_0} e^{-x^2/2\sigma^2} \int_{-\infty}^{\infty} \exp\left\{-\frac{\left[x' - (\sigma_1^2 x/\sigma)\right]^2}{2(\sigma_1\sigma_0/\sigma)^2}\right\}$$

$$= \frac{1}{2\pi\sigma_1\sigma_0} e^{-x^2/2\sigma^2} \sqrt{2\pi}\, \frac{\sigma_1\sigma_0}{\sigma}$$

$$= \frac{1}{\sigma\sqrt{2\pi}} e^{-x^2/2\sigma^2} \quad .$$

The reflected pulse is a gaussian with $\sigma = \sqrt{\sigma_1^2 + \sigma_0^2}$. A measure of the amount of pulse spreading is the difference

$$\Delta\sigma = \sigma - \sigma_0 = \sqrt{\sigma_1^2 + \sigma_0^2} - \sigma_0 \quad .$$

For very long incident pulses,

$$\sqrt{\sigma_1^2 + \sigma_0^2} = \sigma_0\sqrt{1 + \frac{\sigma_1^2}{\sigma_0^2}} \approx \sigma_0\left(1 + \frac{\sigma_1^2}{2\sigma_0^2}\right) \quad ,$$

so that

$$\Delta\sigma \approx \left(\sigma_0 + \frac{\sigma_1^2}{2\sigma_0}\right) - \sigma_0 = \left(\frac{\sigma_1}{2\sigma_0}\right)\sigma_1 \quad .$$

Instead of having $\Delta\sigma$ on the order of σ_1, which we might have expected intuitively, the spreading is reduced by the factor $\sigma_1/2\sigma_0$, so that $\Delta\sigma \to 0$ as $\sigma_0 \to \infty$.

For very short pulses,

$$\sqrt{\sigma_1^2 + \sigma_0^2} = \sigma_1 \sqrt{1 + \frac{\sigma_0^2}{\sigma_1^2}} \approx \sigma_1 \left(1 + \frac{\sigma_0^2}{2\sigma_1^2}\right) ,$$

and thus

$$\Delta\sigma \approx \left(\sigma_1 + \frac{\sigma_0^2}{2\sigma_1}\right) - \sigma_0 = \sigma_1 + \sigma_0 \left(\frac{\sigma_0}{2\sigma_1} - 1\right) .$$

In the limit, as $\sigma_0 \to 0$, $\Delta\sigma \to \sigma_1 - \sigma_0 \approx \sigma_1$ as we would expect for a point reflector.

By taking the derivative of $\Delta\sigma$ with respect to σ_0, we can prove the statement made at the beginning of this section for the special case of a gaussian distribution of retro-reflectors. We have

$$\frac{d}{d\sigma_0}(\Delta\sigma) = \frac{d}{d\sigma_0}\left(\sqrt{\sigma_1^2 + \sigma_0^2} - \sigma_0\right)$$

$$= \frac{\sigma_0}{\sqrt{\sigma_1^2 + \sigma_0^2}} - 1 .$$

Since $\sigma_0/\sqrt{\sigma_1^2 + \sigma_0^2} \leq 1$, $d(\Delta\sigma)/d\sigma_0 \leq 1$, so that the pulse spreading increases as the pulse length decreases.

7.11 Range Equation and Gain Function

The range equation giving the received energy as a function of the transmitted energy can be written

$$E_r = ET_A \frac{dE/E}{d\Omega_S} \Omega_S T_S T_A \frac{dE_S/E_S}{d\Omega_r} \Omega_r \quad ,$$

where E_r is the received energy, E is the transmitted energy, T_A is the atmospheric transmission factor, Ω_S is the solid angle subtended by the active reflecting area of the satellite array, T_S is the transmission factor of the array, E_S is the energy reflected by the satellite, and Ω_r is the solid angle subtended by the receiving telescope. To calculate the number of photoelectrons, the equation must be divided by $h\nu$ and multiplied by $\mathscr{E}_r$, where h is Planck's constant, ν is the frequency of the laser, and $\mathscr{E}_r$ is the efficiency of the receiver in photoelectrons per photon.

The solid angles Ω_S and Ω_r are

$$\Omega_S = \frac{A_S}{R} \quad ,$$

$$\Omega_r = \frac{A_r}{R} \quad ,$$

where A_S is the active reflecting area of the array, A_r is the area of the receiving telescope, and R is the range. Introducing the definitions

$$G_t \equiv \frac{dE/E}{d\Omega_S} \quad ,$$

$$G_S \equiv \frac{dE_S/E_S}{d\Omega_r} \quad ,$$

we get the following equation for the number of photoelectrons N:

$$N = \frac{E}{h\nu} \frac{G_t A_S G_S A_r}{R^4} T_A^2 T_S \mathscr{E}_r \quad . \tag{7-12}$$

This definition of the gain functions G_t and G_S differs from standard usage, which includes a factor of 4π. Equation (7-12) can be converted to the standard definition of gain by adding $(4\pi)^2$ to the denominator.

The gain G_S of the array is proportional to the intensity of the diffraction pattern of the array in the direction of the receiver. In the incoherent case, the intensity of the whole array is the sum of the intensities of all the cube corners. In Section 5.1.2, we showed that the intensity I_p from each cube corner in terms of the dimensionless intensity F' is

$$I_p = \frac{S^2}{\lambda^2 D^2} F' I_0 \quad .$$

For an array of identical cube corners, the intensity is

$$\sum I_p = \frac{S^2}{\lambda^2 D^2} \sum F' I_0 \quad .$$

In order to facilitate comparison with the range equation, let us make the substitutions

$$D = R \quad ,$$

$$I_0 = \frac{dE}{dt} G_t \frac{1}{R^2} \quad ,$$

which results in

$$\sum I_p = \frac{S^2}{\lambda^2 R^2} \sum F' \frac{dE}{dt} G_t \frac{1}{R^2}$$

$$= \frac{dE}{dt} G_t \left(\frac{S^2}{\lambda^2} \sum F' \right) \frac{1}{R^4} \quad .$$

We can ignore the factors T_A, T_S, and $\mathscr{E}_r$ and write $\sum I_p$ in terms of the variables used in the range equation:

$$\sum I_p = \frac{dE}{dt} G_t (G_S A_S) \frac{1}{R^4} \quad .$$

Comparing the two expressions for $\sum I_p$, we see that

$$G_S A_S = \frac{S^2}{\lambda^2} \sum F' \quad ,$$

which gives

$$G_S = \frac{S}{\lambda^2} \left(\frac{S}{A_S} \sum F' \right) \quad .$$

For a single cube corner at normal incidence, $A_S = S$. If the cube corner is perfect, in the sense that the reflected field equals the incident field, then $F' = 1$ at the center of the far-field pattern, as shown in Section 5.1.2. The gain in this case is S/λ^2. The standard definition of gain for a perfect reflector of area S is $4\pi S/\lambda^2$.

7.12 Velocity Aberration

In the moving coordinate system of a retroreflector aboard a satellite, a laser beam incident on the cube corner is reflected back along the same line as the incident beam. In the coordinate system of the observer on the ground, the reflected beam makes an angle $2v/c$ with the incident beam, where v is the component of the satellite's velocity perpendicular to the line of sight. The position of the receiving equipment in the diffraction pattern of the array is therefore determined by the magnitude and direction of the tangential component of the satellite's velocity. Since the transfer function varies within the diffraction pattern, it can also vary with the amount and direction of the velocity aberration. In cases studied, fortunately, the variation is not too large and is reduced when the beam width is deliberately widened, such as by building dihedral-angle offsets into the cube corners.

7.13 Variation of the Transfer Function within the Diffraction Pattern

The light reflected from each cube corner in an array is initially a separate pencil of light antiparallel to the incident beam. At large distances from the array, the individual reflections spread, owing to diffraction, and overlap each other. It is assumed that the return is observed at a distance large enough so that the diffraction patterns of the individual cube corners are much larger than the size of the retroreflector array. Under these conditions, the difference in position of the centers of the individual diffraction patterns can be neglected. The incoherent intensity at a particular point in the far field is obtained by adding the intensity of the diffraction pattern of each cube corner at that point. Since cube-corner diffraction patterns can be rather lumpy, the incoherent return energy will vary at different points in the far field. The average position of the incoherent return pulse is calculated from equation (7-3). Although the values of d_K are essentially constant over the whole diffraction pattern, the intensities S_K of the individual reflections vary from point to point. Therefore, the mean position of the pulse varies at different points in the diffraction pattern. At each point, there will also be variations about the incoherent values as a result of coherent interference.

In cases where the information available on the optical specifications of the cube corners is insufficient to model the diffraction patterns, we can assume that the intensity due to each reflector is proportional to the active reflecting area of the cube corner. This is equivalent to assuming that the diffraction patterns of all cube corners are identical.

8. RETROREFLECTOR-POSITION CALCULATIONS

8.1 Calculation of Retroreflector Positions and Orientations

In Section 7.1, we described the coordinate system of the retroreflector positions and orientations, in which three coordinates and three angles were given for each cube corner.

The arrays carried by many of the retroreflector satellites now in orbit consist of several panels with cube corners arranged in rows and columns on each panel. The general procedure for computing the position of each cube corner is first to compute the position with respect to the panel and then, through a series of translations and rotations, to move the panel to its position on the satellite. The rotations performed define the direction of the normal to the front face of the cube corner.

Let the panel, row, and column indices of a cube corner be I, J, and K, respectively (see Figure 74). The position of a cube corner with respect to the supporting panel is

$$x_{IJK} = C_{x_{IJ}} + (K - 1)\, dx \quad ,$$

$$y_{IJK} = C_{y_I} + (J - 1)\, dy \quad ,$$

$$z_{IJK} = C_{z_I} \quad .$$

The constant C_{z_I} is the height of the cube-corner face above the hinge point of the panel.

PAGE 150 INTENTIONALLY BLANK

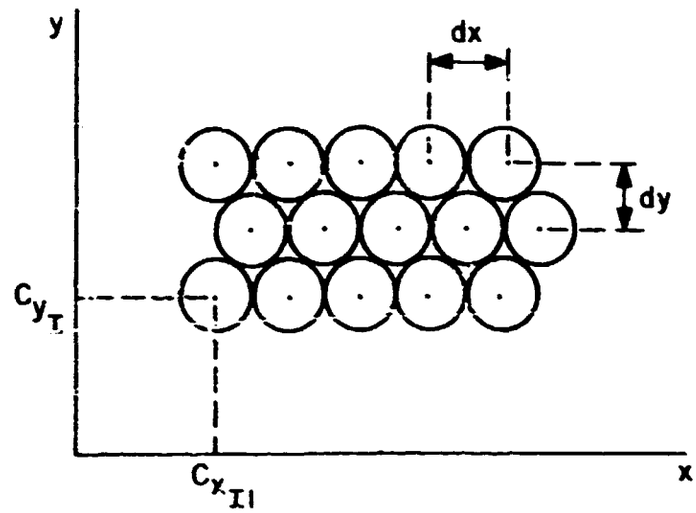

Figure 74. A panel of cube corners.

The arrangement of the panels on most satellite arrays is such that it is convenient to rotate the panel about the x and y axes by the angles β_I and ϕ_I, displace the panel by Δx_I, Δy_I, and Δz_I, and then rotate about the z axis by the angle θ_I. The result is

$$\begin{pmatrix} x'_{IJK} \\ y'_{IJK} \\ z'_{IJK} \end{pmatrix} = \begin{pmatrix} \Delta x_I \\ \Delta y_I \\ \Delta z_I \end{pmatrix} + \begin{pmatrix} \cos\phi_I & 0 & \sin\phi_I \\ 0 & 1 & 0 \\ -\sin\phi_I & 0 & \cos\phi_I \end{pmatrix} \begin{pmatrix} 1 & 0 & 0 \\ 0 & \cos\beta_I & -\sin\beta_I \\ 0 & \sin\beta_I & \cos\beta_I \end{pmatrix} \begin{pmatrix} x_{IJK} \\ y_{IJK} \\ z_{IJK} \end{pmatrix} ,$$

$$\begin{pmatrix} x''_{IJK} \\ y''_{IJK} \\ z''_{IJK} \end{pmatrix} = \begin{pmatrix} \cos\theta_I & -\sin\theta_I & 0 \\ \sin\theta_I & \cos\theta_I & 0 \\ 0 & 0 & 1 \end{pmatrix} \begin{pmatrix} x'_{IJK} \\ y'_{IJK} \\ z'_{IJK} \end{pmatrix} .$$

The double-primed coordinates are the positions of the center of the front face of each cube corner in the array coordinate system.

The direction (θ_R, ϕ_R) of the normal to the front face of the cube corner is obtained by performing the β_I, ϕ_I, and θ_I rotations successively on the vector (0, 0, 1) and then computing the angles of the vector, from which we get

$$\begin{pmatrix} x' \\ y' \\ z' \end{pmatrix} = \begin{pmatrix} \cos\phi_I & 0 & \sin\phi_I \\ 0 & 1 & 0 \\ -\sin\phi_I & 0 & \cos\phi_I \end{pmatrix} \begin{pmatrix} 1 & 0 & 0 \\ 0 & \cos\beta_I & -\sin\beta_I \\ 0 & \sin\beta_I & \cos\beta_I \end{pmatrix} \begin{pmatrix} 0 \\ 0 \\ 1 \end{pmatrix} ,$$

$$\theta_R = \theta_I + \tan^{-1}\left(\frac{y'}{x'}\right) ,$$

$$\phi_R = \tan^{-1}\left(\frac{\sqrt{x'^2 + y'^2}}{z'}\right) .$$

Let the orientation of the cube corner on the panel be α', as shown in Figure 75. The angle α' is the orientation with respect to the pole (θ_I, ϕ_I). The orientation α can be computed with respect to the pole of the array coordinate system $(\theta = \phi = 0)$, as described in Section 8.2, by using

$$\theta_p = \theta_I ,$$

$$\phi_p = \phi_I .$$

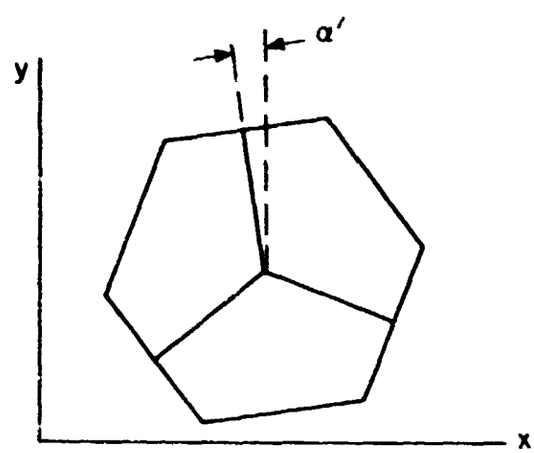

Figure 75. Orientation of a cube corner on a panel.

The above method was used to calculate retroreflector positions for the satellites analyzed in Weiffenbach (1973) and Arnold (1972, 1975a). The geometry of the Starlette array, whose transfer function is given in Arnold (1975a), is described in Centre National d'Etudes Spatiales (CNES, 1972). Photographs showing the construction of Starlette have also been published (CNES, 1975). The information used to compute retroreflector positions for Geos 3 can be found in Arnold (1975b).

8.2 Orientation with Respect to a New Pole

In computing the position and orientation of a cube corner in an array, the orientation α' can be given initially with respect to some local pole having angular coordinates θ_p and ϕ_p with respect to the z axis of the array coordinate system (see Figure 76). All such orientations must be expressed with respect to the z axis of the array ($\theta = \phi = 0$). Let the normal to the face of the reflector be given by the angles θ_R and ϕ_R. The orientation angle is measured left from the great circle joining the points (θ_R, ϕ_R) and (θ_p, ϕ_p) on a unit sphere, as shown in Figure 77. The plane in Figure 77

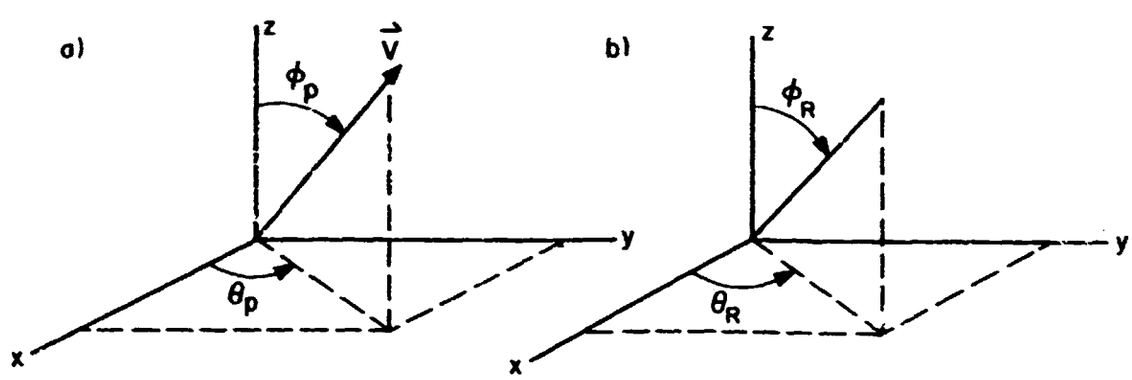

Figure 76. a) Direction of a local pole; b) direction of the normal to the front face of a cube corner.

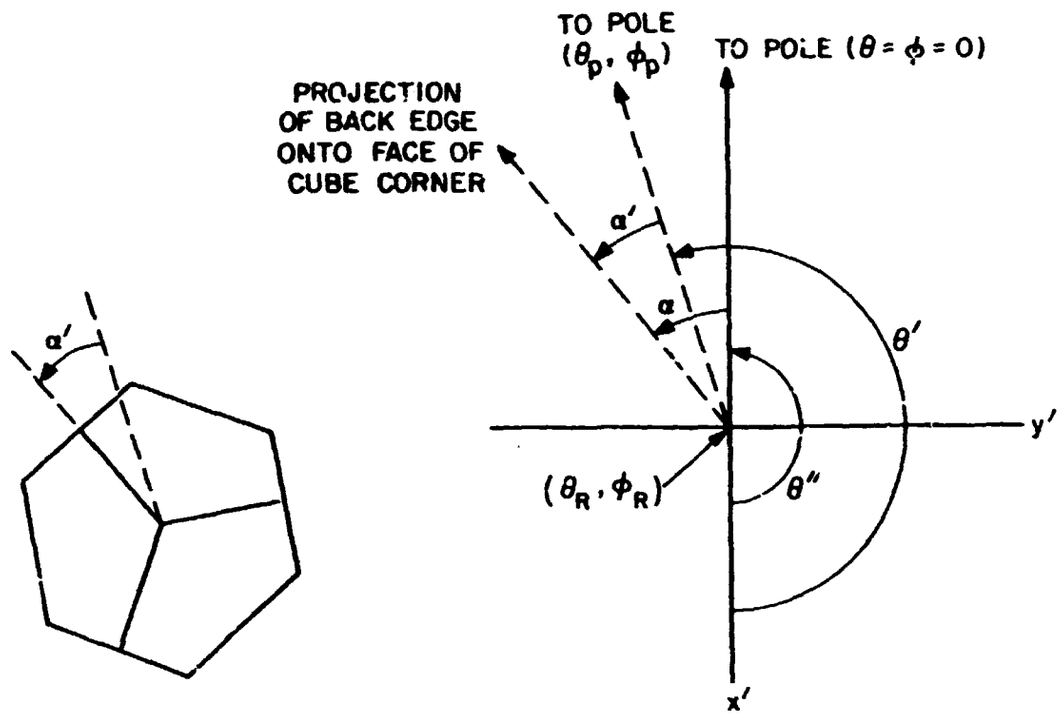

Figure 77. Diagram for computing the orientation of a cube corner with respect to a new pole $(\theta = \phi = 0)$.

is the front face of the cube corner. To express the orientation with respect to a new pole, we must compute the difference in direction to the two poles. Let $\vec{V}$ be a unit vector in the direction (θ_p, ϕ_p) with the following components:

$$V_x = \sin\phi_p \cos\theta_p \quad ,$$

$$V_y = \sin\phi_p \sin\theta_p \quad ,$$

$$V_z = \cos\phi_p \quad .$$

Let an x', y', z' coordinate system be defined with z' in the direction of the normal to the front face of the cube corner (θ_R, ϕ_R), the x' axis in the direction of increasing ϕ_R, and the y' axis in the direction of increasing θ_R. The components of $\vec{V}$ in the x', y', z' coordinate system can be obtained by rotating the x, y, z coordinate system about the z axis by the angle θ_R and then about the new y axis by the angle ϕ_R. The result is

$$\begin{pmatrix} V_{x'} \\ V_{y'} \\ V_{z'} \end{pmatrix} = \begin{pmatrix} \cos\phi_R & 0 & -\sin\phi_R \\ 0 & 1 & 0 \\ \sin\phi_R & 0 & \cos\phi_R \end{pmatrix} \begin{pmatrix} \cos\theta_R & \sin\theta_R & 0 \\ -\sin\theta_R & \cos\theta_R & 0 \\ 0 & 0 & 1 \end{pmatrix} \begin{pmatrix} V_x \\ V_y \\ V_z \end{pmatrix} .$$

The angle to the pole ($\theta = \phi = 0$) in the $x'y'$ plane is $\theta'' = \pi$, while the angle to the pole (θ_p, ϕ_p) in the $x'y'$ coordinate system is

$$\theta' = \tan^{-1}\left(\frac{V_{y'}}{V_{x'}}\right) .$$

The desired orientation α from Figure 77 is

$$\alpha = \alpha' + \theta' - \pi .$$

8.3 Condensing Large Arrays for Coherent Calculations

The amount of computer time required to compute the energy and mean position of a coherent return from a satellite retroreflector array is roughly proportional to the square of the number of active retroreflectors. Satellites such as Geos 1 and Geos 2 have a very large number of reflectors, all of which are generally active since they all face the same direction. The variations in energy and mean position are largely independent of the number of reflectors as long as the number is reasonably large. Guidelines regarding what is considered a reasonably large number of reflectors were given in Section 6. Considerable savings in computer time can be accomplished by averaging groups of neighboring reflectors and representing each group by a single reflector at the mean position, weighted by the number of cube corners averaged. All reflectors averaged must have the same orientation.

8.4 Shadowing

8.4.1 Geos

Both Geos 1 and Geos 2 have a hemispherical structure in the center of the side containing the retroreflector panels (see Figure 78). At large incidence angles, some of the cube corners may be shadowed by its structure. Let x, y, and z be the coordinates of a cube corner, and let the center of the hemisphere of radius R be located on the symmetry axis of the satellite a distance z_c from the satellite center of mass (CM). The position of the cube corner in a coordinate system with its origin at the center of the sphere is

$$x' = x \quad , \tag{8-1a}$$

$$y' = y \quad , \tag{8-1b}$$

$$z' = z - z_c \quad . \tag{8-1c}$$

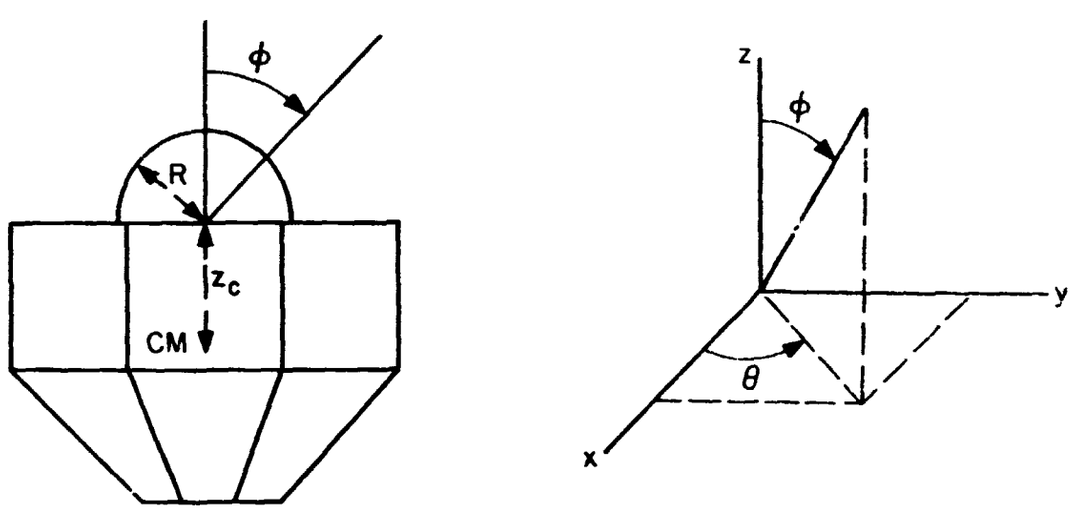

Figure 78. a) Geos 1 and 2 satellites; b) direction of incident beam on Geos 1 and 2.

Let the direction of the incident beam be (θ, φ), as shown in Figure 78. We can rotate the x′, y′, z′ coordinate system about the z′ axis by θ and about the new y′ axis

by ϕ so that the final z'' axis points toward the source. The coordinates of the cube corner become

$$\begin{pmatrix} x'' \\ y'' \\ z'' \end{pmatrix} = \begin{pmatrix} \cos\phi & 0 & -\sin\phi \\ 0 & 1 & 0 \\ \sin\phi & 0 & \cos\phi \end{pmatrix} \begin{pmatrix} \cos\theta & \sin\theta & 0 \\ -\sin\theta & \cos\theta & 0 \\ 0 & 0 & 1 \end{pmatrix} \begin{pmatrix} x' \\ y' \\ z' \end{pmatrix} \quad . \tag{8-2}$$

The cube corner will be shadowed if both

$$z'' < 0$$

and

$$\sqrt{x''^2 + y''^2} < R \quad .$$

The values of R and z_c for the two Geos satellites are as follows:

Satellite	R (m)	z_c (m)
Geos 1	0.3048	0.423
Geos 2	0.3048	0.444 .

8.4.2 Peole

The Peole satellite has a frustrum of a cone extending from the satellite in the positive z direction. The axis of the cone is the z axis. Let R_1 and R_2 be the radii of the bottom and the top of the cone, respectively, and let z_c be the z coordinate of the base and H be the height. The position of a cube corner with respect to the center of the bottom of the cone is given by equations (8-1), where x, y, and z are the coordinates of the cube corner with respect to the center of mass of the satellite. Let the direction of the incident beam be (θ, ϕ). Rotating the primed coordinate system so that the z'' axis points in that direction, we get the coordinates given by equation (8-2). The frustrum of a cone in the double-primed coordinate system has the shape shown in Figure 79.

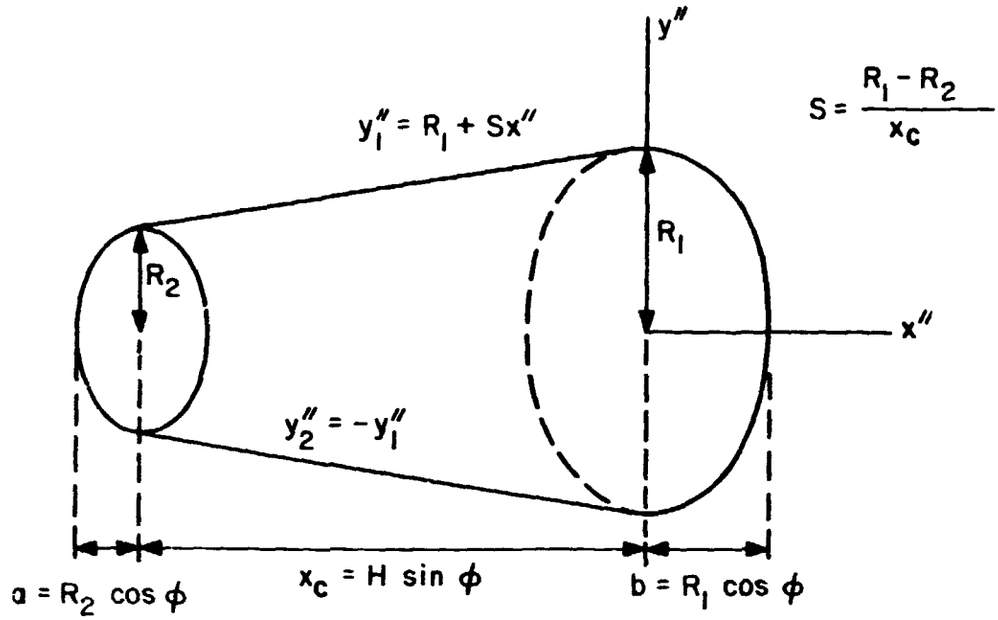

Figure 79. Shape of Peole cone.

The cube corner will be shadowed if the following four conditions are met:

$$x'' < 0 \quad ,$$

$$y'' < y_1'' \quad ,$$

$$y'' < -y_1'' \quad ,$$

$$x'' > -x_c \quad ;$$

or if

$$\left(\frac{y''}{R_1}\right)^2 + \left(\frac{x''}{b}\right)^2 < 1 \quad ;$$

or if

$$\left(\frac{y''}{R_2}\right)^2 + \left(\frac{x'' + x_c}{a}\right)^2 < 1 \quad .$$

The values of the parameters, in meters, are

$$z_c = 0.831 \quad , \qquad H = 0.561 \quad , \qquad R_1 = 0.151 \quad , \qquad R_2 = 0.051 \quad .$$

9. ACKNOWLEDGMENTS

The author wishes to express his appreciation to all those who have helped with this work and particularly to Dr. George C. Weiffenbach, Dr. Michael R. Pearlman, and Mr. Carlton G. Lehr for their guidance and assistance.

PAGE 160 INTENTIONALLY BLANK

10. REFERENCES

ARNOLD, D. A.

1972. Calculation of retroreflector array transfer functions. Final Tech. Rep., NASA Grant NGR 09-015-196, December.

1974. Optical transfer function of NTS-1 retroreflector array. Tech. Rep. RTOP 161-05-02, Grant NGR 09-015-002, Supplement No. 57, October.

1975a. Optical transfer function of Starlette retroreflector array. Tech. Rep. RTOP 161-05-02, Grant NGR 09-015-002, Supplement No. 57, February.

1975b. Optical and infrared transfer function of the Geos 3 retroreflector array. Tech. Rep. RTOP 161-05-02, Grant NGR 09-015-002, Supplement No. 57, October.

1978. Optical and infrared transfer function of the Lageos retroreflector array. Grant NGR 09-015-002, Supplement No. 57, May.

CENTRE NATIONAL D'ETUDES SPATIALES

1972. Project STARLET - Etude Geometrique de la Structure Porteuse de Reflecteurs Laser. CNES Publ. No. 645, October.

1975. STARLETTE. CNES, Groupe de Recherches de Geodesie Spatiale, February.

CHANDLER, K. N.

1960. On the effects of small errors in the angles of corner cube reflectors. Journ. Opt. Soc. Amer., vol. 50, pp. 203-206.

CHANG, R. F.

1970. Possible failure of total reflection in an uncoated solid retroreflector. University of Maryland Tech. Rep. 70-130, NASA Contract NAS 9-7809, June.

CHANG, R. F., CURRIE, D. G., and ALLEY, C. O.

1971. Far field diffraction pattern for corner reflectors with complex reflection coefficients. Journ. Opt. Soc. Amer., vol. 61, pp. 431-438.

ECKHARDT, H. D.

1971. Simple model of corner reflector phenomena. Appl. Opt., vol. 10, pp. 1559-1566.

PAGE 162 INTENTIONALLY BLANK

FELSENTREGER, T. L.

1972. Geos-1 laser pulse return shape analysis. Goddard Space Flight Center X-553-72-354, September.

FITZMAURICE, M. W., MINOTT, P.O., ABSHIRE, J. B., and ROWE, H. E.

1977. Prelaunch testing of the laser geodynamic satellite (LAGEOS). NASA Tech. Paper 1062, October.

HILDEBRAND, F. B.

1956. Introduction to Numerical Analysis. McGraw-Hill Book Co., New York, 511 pp. (see especially p. 73).

JAFFE, R. M.

1971. Signal strength fluctuations in a laser ranging system due to optical interference between the many reflectors on a satellite. JPL Tech. Memo. 391-218, July.

JULIAN, R. S., HIESER, G., and MAGILL, A. A.

1970. Evaluation of solid cube corner reflectors. GE Doc. No. 70SD4218, Sci. Rep. No. 2, Project No. 7600, July.

LANDAU, L. D., and LIFSHITZ, E. M.

1962. The Classical Theory of Fields. Rev. 2nd ed., Pergamon Press, Oxford, 404 pp. (see especially pp. 167-168).

MAHAN, A. I., BITTERLI, C. V., and CANNON, S. M.

1964. Far-field diffraction patterns of single and multiple apertures bounded by arcs and radii of concentric circles. Journ. Opt. Soc. Amer., vol. 54, pp. 721-732.

MINOTT, P. O.

1972. Analysis of requirements for Geos-C laser cube corner reflector panels. Goddard Space Flight Center X-524-72-33, January.

1974a. Design of retrodirector arrays for laser ranging of satellites. Goddard Space Flight Center X-723-74-122, March.

1974b. Measurement of the lidar cross sections of cube corner arrays for laser ranging of satellites. Goddard Space Flight Center X-722-74-301, September.

1976. Reader's guide to the "RETRO" program output. Goddard Space Flight Center X-722-76-267, September.

MINOTT, P. O., FITZMAURICE, M. W., ABSHIRE, J. B., and ROWE, H. E.

1978. Prelaunch testing of the Geos-3 laser reflector array. NASA Tech. Paper 1138, January.

PECK, E. R.

1972. Polarization properties of corner reflectors and cavities. Journ. Opt. Soc. Amer., vol. 52, pp. 253-257.

PLOTKIN, H. H.

1964. Geos-1 laser retroreflector design and preliminary signal calculations. Goddard Space Flight Center X-524-64-205, July.

RAYLEIGH, J. W. S.

1945. The Theory of Sound, Vol. I. Dover Publ., New York, 480 pp. (see especially pp. 35-42).

REGARDIE, M. L., KIRK, J. G., and ZIMMERMAN, J. J.

1976. Cube corner retroreflector (RETRO) program functional design description and user's guide, revision 1. Computer Science Corporation CSC/TM-76/6009.

RITYN, N. E.

1967. Optics of corner cube reflectors. Soviet Journ. Opt. Tech., vol. 34, pp. 198-201.

SCHULZ, L. G.

1954. The optical constants of silver, gold, copper, and aluminum. Journ. Opt. Soc. Amer., vol. 44, pp. 357-368.

SLACK, M.

1946. The probability distributions of sinusoidal oscillations combined in random phase. IEE Proc., vol. 93, pp. 76-86.

SMITH, R. C., and MARSH, J. S.

1974. Diffraction patterns of simple apertures. Journ. Opt. Soc. Amer., vol. 64, pp. 798-803.

STRATTON, J. A.

1941. Electromagnetic Theory. McGraw-Hill Book Co., New York, 615 pp. (see especially pp. 494-506).

WEIFFENBACH, G. C.

1973. Use of a passive stable satellite for earth-physics applications. Final Report, NASA Grant NGR 09-015-164, April.

YODER, P. R., Jr.

1958. Study of light deviation errors in triple mirrors and tetrahedral prisms. Journ. Opt. Soc. Amer., vol. 48, pp. 496-499.